STOCHASTIC GEOMETRIC ANALYSIS OF ENERGY EFFICIENCY IN TWO-TIER HETEROGENEOUS NETWORKS

RAUL HERNANDEZ AQUINO

Submitted in accordance with the requirements for the degree of

Doctor of Philosophy

School of Electronic & Electrical Engineering,

University of Leeds.

31st December 2015

DECLARATION

The candidate confirms that the work submitted is his/her own, except where work which has formed part of jointly authored publications has been included. The contribution of the candidate and the other authors to this work has been explicitly indicated below. The candidate confirms that appropriate credit has been given within the thesis where reference has been made to the work of others. It is to assert that the candidate has contributed solely to the technical part of the joint publication under the guidance of his academic supervisors. Detailed breakdown of the publications is presented in the first chapter of this thesis.

Raul Hernandez Aquino

This thesis is dedicated to my parents, Araceli & Raul.

ACKNOWLEDGEMENTS

First and foremost, I would like to thank God for providing me with the privilege of being born and for all the blessings and happiness I have had in my life.

I would like to thank Dr. Des McLernon for all his support in my PhD programme from day one. Thank you for all the knowledge transferred to me and all the confidence you put in me, which motivated my evolution in the PhD. But above all things, thank you for caring about your students' well-being even before their work. Your kindness will always be appreciated and remembered.

My gratitude goes to Professor Mounir Ghogho for his support and guidance. Thank you very much for the constructive talks that helped me improve my work and ensure that it was going in the right direction. I owe a great deal of my success to you.

My appreciation and admiration goes also to Dr. Syed Ali Raza Zaidi for his very helpful advice. His valuable discussions, expert and guidance helped me find new ideas and enhance my work.

I would like to thank my parents Araceli and Raul for their endless love and support. I would not have been able to take any steps in my life without your motivation and support. Thank you for teaching me the way towards academic excellence but beyond that, for being a life example for me. My gratitude goes to you for having as my constant motivation the will to honour you and follow your steps to the best of my ability. My gratitude also goes to my sister Araceli for teaching me the true meaning of loyalty between sibillings and for her unconditional support and care even in times when I could have been a better brother. I would also like to thank my niece Fanny for coming to our lives to light them up with her beautiful being.

I would also like to thank the rest of my family, my auntie Elvia, my grandmothers Ita and Ina, my grandfathers Papaul and Arcadio, my uncle

Armando and his family. Thank you for being a supportive family and for being with me through thick and thin.

I would like to thank Samane for all her support and caring which made my PhD experience way easier and enjoyable. Thank you also to all my friends who provided me with a great support in difficult times.

Finally, a huge thanks you to all my colleagues from the I3S research group and to all the people I met throughout my PhD studies which made it a wonderful experience that opened my eyes to many great things that the world has to offer. I am truly grateful with you.

ABSTRACT

The exponential growth in the number of users of cellular mobile networks (and their requirements) has created a massive challenge for network operators to cope with demands for coverage and data rates. Among the possible solutions for the ever increasing user needs, the deployment of Heterogeneous Networks (HetNets) constitutes both a practical and an economical solution. Moreover, while the typical approach for network operators has been to consider the coverage and data rates as design parameters in a network, a major concern for next generation networks is the efficiency in the power usage of the network. Therefore, in recent years the energy efficiency parameter has gathered a great deal of attention in the design of next generation networks.

In the context of HetNets, while the densification of the network in terms of the number of base stations deployed can potentially increase the coverage and boost the data rates, it can also lead to a huge power consumption as the energy used escalates with the number of base stations deployed. To this end, the purpose of this thesis is to investigate the energy efficiency performance of different deployment strategies in a HetNet consisting of macro- and femtocells. We make use of well established tools from stochastic geometry to model the different strategies, as it provides a theoretical framework from which the scalability of the network in terms of the design parameters can be taken into account. Those strategies consisted first, on the analysis of the effect of using multiple antennas and diversity schemes on both, the throughput and the energy efficiency of the network. The optimum diversity schemes and antenna configurations were found for an optimal energy efficiency while keeping constraints on the quality of Service of both tiers. Then, the effect of the vertical antenna tilt was analyzed for both, a traditional macrocell only network and a two-tier network. The optimum antenna tilt in terms of energy efficiency was found while keeping constraints on the Quality of Service required. Finally, an energy efficient deployment of femtocells was proposed where

the smart positioning of femtocells derived into improvements of coverage probability, effective throughput and energy efficiency of the network. The proposed model also improved in general the performance of the cell edge user which in turn resulted in a more balanced network in terms of the overall performance.

NOTATION

$\mathbf{a}$	small bold-faced letter defines a vector
$\mathbf{A}$	capital bold-faced letter defines a matrix
$\mathbf{A}^H$	conjugate transpose of matrix $\mathbf{A}$
$\|\mathbf{A}\|$	denotes the determinant of matrix $\mathbf{A}$
$\|\|\mathbf{A}\|\|_F$	denotes the Frobenius norm of matrix $\mathbf{A}$
a_l	lower case normal letter denotes the l-th entry of vector $\mathbf{a}$
$(\mathbf{A})_{l,n}$	denotes the (l,n)-th entry of matrix $\mathbf{A}$
$\mathbb{P}(A)$	denotes the probability of event A
$\mathbb{E}[X]$	denotes the expected value of random variable X
f	subscript f denotes the femtocell tier
m	subscript m denotes the macrocell tier
$\mathbf{H}_{j,k}$	denotes the channel matrix between the j-th transmitter and the k-th receiver for a MIMO case
$\mathbb{R}$	denotes the set of real numbers
$h_{j,k}$	denotes the channel gain between the j-th transmitter and the k-th receiver
M_i^t	denotes number of available antennas at the transmitter side in the i-th tier
M_i^r	denotes number of available antennas at the receiver side in the i-th tier

$\mathrm{Exp}(\frac{1}{\mu})$	represents an exponential random variable with mean μ
$\mathrm{Pois}(\mu)$	represents a Poisson random variable with mean μ
Φ_i	denotes the point process in the i-th tier
λ_i	denotes the density of a point process in the i-th tier
$x_j \in \Phi_i$	denotes the position of the j-th point belonging to Φ_i
x_0	denotes the origin in $\mathbb{R}^2$
$j \in \Phi_i$	denotes the index of the j-th point belonging to Φ_i
$\mathcal{L}_{I_{\Phi_i}}(.)$	denotes the Laplace transform of the point process in the i-th tier
β_i	denotes the SIR threshold for the i-th tier
α_i	denotes the path loss exponent in for the i-th tier
N_S	denotes the number of MBS antenna sectors
P_i^{tx}	denotes the transmitted power for BSs in the i-th tier
P_i^{sleep}	denotes the power used by BSs in the i-th tier with sleep mode capabilities
P_i^{RF}	RF transceiver power consumption in the i-th tier
$P_i^{RF_{sleep}}$	Sleep mode RF transceiver power consumption in the i-th tier
$P_i^{RF,tx}$	RF transceiver power consumption used for transmission in the i-th tier
$P_i^{RF,rx}$	RF transceiver power consumption used for reception in the i-th tier
P_i^{BB}	Base band interface power consumption in the i-th tier
P_i^{BB}	Base band interface power consumption in the i-th tier
$P_i^{BB_{sleep}}$	Sleep mode base band interface power consumption in the i-th tier

$P_i^{BB,rx/tx}$	Base band reception/transmission radio power consumption in the i-th tier
$P_i^{BB,LTE}$	Base band LTE turbo encoding power consumption in the i-th tier
$P_i^{BB,processors}$	Base band processors power consumption in the i-th tier
a_i	denotes the power component related to the transmitted power used by BSs in the i-th tier
b_i	denotes the constant power component related to signal processing, site cooling, etc., used by BSs in the i-th tier
W_i	denotes the wall partition loss in the i-th tier
$\mathcal{P}_i^c$	denotes the coverage probability of the i-th tier
T_i	denotes the throughput of the i-th tier
R_f	denotes the typical coverage radius of a femtocell
R_c	denotes the macrocell user guard zone
EE	denotes the energy efficiency
EE_{sleep}	denotes the energy efficiency with sleep mode capabilities
ϕ	denotes the angle between the MBS antenna and receiver's antenna
ϕ_{tilt}	denotes the antenna tilt angle below the horizontal
ϕ_{3dB}	denotes the MBS antenna half beamwidth
η_i^{PA}	Efficiency of the power amplifier in the i-th tier
P_i^{RF}	RF transceiver power in the i-th tier
P_i^{BB}	Baseband interface power in the i-th tier
$P_i^{RF_{sleep}}$	Sleep mode RF transceiver power in the i-th tier

$P_i^{BB_{sleep}}$	Sleep mode baseband interface power in the i-th tier
σ_i^{DC}	Loss factor of the DC-DC power supply in the i-th tier
σ_i^{COOL}	Loss factor of the cooling of site in the i-th tier
σ_i^{MS}	Loss factor of the main supply in the i-th tier
σ_i^{feed}	Loss factor of the feeder in the i-th tier
H_a	denotes the MBS antenna height
H_{ue}	denotes the user equipment antenna height
$v_d(B)$	denotes the Lebesgue measure of the bounded region B

Note: This is a set of basic variables, used throughout this thesis. Notations specific to an individual chapter are defined inside that chapter.

ABBREVIATIONS

BF-SC	Beamforming - selection combining
BS	Base station
CAPEX	Capital expenditure
CDF	Cumulative distribution function
CCDF	Complementary cumulative distribution function
CSI	Channel state information
CSG	Closed subscriber group
EE	Energy efficiency
ECR	Energy consumption ratio
FAP	Femtocell access point
HetNet	Heterogeneous network
HSG	Hybrid subscriber group
ICT	Information and Communication Technology
JAS	Joint antenna selection
LTE	Long term evolution
MBS	Macro base station
MIMO	Multiple input multiple output
MRC	Maximum ratio combining
MRT	Maximum ratio transmission
NGN	Next Generation Networks

OPEX	Operating expenditure
OSG	Open subscriber group
PDF	Probability density function
PGF	Probability generating functional
PHP	Poisson Hole Process
PPP	Poisson Point Process
QoS	Quality of Service
RAN	Radio Access Network
SC	Selection combining
SIR	Signal to interference ratio
SINR	Signal to interference plus noise ratio
SNR	Signal to noise ratio
SISO	Single Input, Single Output
UE	User equipment

Contents

List of Figures

1 Introduction

IN THIS CHAPTER:

The overview of the motivation behind this work is presented. Moreover, we elaborate on the justification of the study carried out in this thesis. The background and motivation behind the need to deploy Heterogeneous Networks is presented and the potential gains in performance for future network deployments is identified. Additionally, the energy efficiency challenge is introduced. Finally, the direction and focus of the work carried out are presented along with the organization of the thesis.

1.1 Motivation

In recent years, the world has witnessed an exponential growth in the number of cellular mobile subscribers. This growth has been sustained by the amount and variety of newly developed devices with internet connection, which ranges from laptops, PDA's, tablets and smart-phones. As a direct result, the amount of mobile data traffic has reached unprecedented levels. According to a recent analysis carried out by Cisco, the monthly global mobile data traffic is expected to surpass 24.3 exabytes by 2019, which represents a tenfold increase between 2014 and 2019, [1]. Moreover, the annual global

IP traffic will reach 2 zettabytes (10^{21} bytes) per year from 2019 [2]. Furthermore, as both academia and industry prepare for the evolution towards 5G, an increase in the capacity by about 1000x in comparison with 4G is visualized [3–6]. This creates a challenge for mobile network operators to cope with the ever increasing user demands as new paradigms in network design are needed to meet these requirements.

In the context of cellular networks, the traditional deployment which consists in the placement of macro base stations (MBSs), will be unable to provide the required Quality of Service (QoS). This is due to the increase in the number of users and the environmental conditions of the network which impose a limit on the service performance of MBSs. Additionally, the deployment of MBSs has high cost implications, as deploying and operating a high tower can add up to $\$60,000$/macrocell/year plus around $\$1000$ per month due to site lease [7]. Thus, the common approach of adding MBSs either to increase the coverage area, or to handle the user increase by means of cell splitting, represent a very costly strategy.

A promising solution to cope with the demands for better coverage and higher data rates for Next Generation Networks (NGNs) resides in the concept of heterogeneous networks (HetNets) [8]. HetNets consist of the deployment of several tiers of smaller, cheaper and less energy consuming base stations (BSs) overlaid with the traditional MBS network. While BSs belonging to the same tier have the same operational parameters, both the power and the coverage area vary between different tiers. Thus, a HetNet is constituted by cells of different sizes, with each one belonging to a particular tier. Figure 1.1 depicts a HetNet deployment, with 4 tiers of BSs, namely, macrocells, microcells, picocells and femtocells. The typical cell radii of smaller cells range from less than 30 m for a femtocell, less than 100 m for a picocell and less than 500 m for a microcell. This is in contrast with MBSs which can cover typical radii up to 2 km [9].

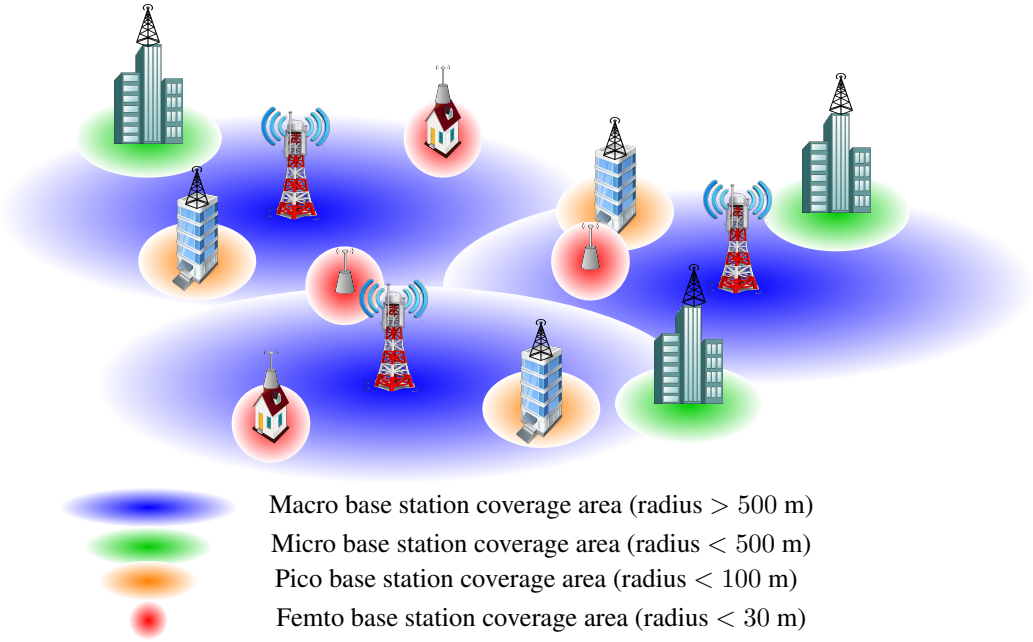

Figure 1.1: A 4-tier heterogeneous network, composed of macro-, micro-, pico- and femtocells.

The advantage of HetNets deployments resides in the fact that depending on the size of the area which needs to be covered or the number of users which need to be served, placing a smaller cell can increase both the coverage and the data rates of the users in places where the MBSs fail to provide the required service. Additionally, deploying small cells represents economic savings from an network operator perspective, as both the CAPEX and OPEX of small cells are considerably smaller than those of a big, and expensive MBS [7]. Moreover, as the coverage regions of the small cells will have reduced dimensions, their distances to their designated users will be small. Therefore, there is a decrease in the path loss experienced by small cell users, in comparison with an MBS, which results in a direct increase in the performance of the users.

Among the available types of smaller cells, the deployment of femtocells has gained a lot of attention due to their practicality and cost. Visually, femtocell access points

(FAPs) look not much different than Wi-fi access points and they operate with a transmission power of under 100 mW. Due to their range, femtocells are an ideal solution to provide users with the required coverage and data rate in an indoor environment such as offices, stores or houses. Along the same lines, users can directly acquire a FAP, place it, turn it on and off, etc., effectively relieving the operator from operating the FAP. Moreover, average users spend around 50 to 60% of their time in an indoor environment [10], while 50% of the calls and more than 80% of data traffic are also generated indoors [7, 11]. These numbers highlight the importance of placing small cells to provide service to indoor environments where a good portion of the total cellular traffic is generated. Additionally, when dealing with indoor environments, the walls play a particularly important role in the received signal power from a given BS. This is due to the power factor which is lost when a signal trespasses a wall. This is the effect commonly referred as wall partition loss. The wall partition loss is a deterrent from traditional macrocell-only networks to provide service to indoor environments, due to the MBSs' outdoor locations which results in the signal having to transverse a wall to reach the intended user. However, in the case of an indoor femtocell, the wall partition loss becomes an ally for the femtocell user performance. This is because the wall partition loss acts as a blockage from the signal in two constructive ways: on one hand, it attenuates the interfering signal from outdoor BSs, and on the other hand, the signal generated by the indoor FAPs is also blocked from leaking outside, effectively reducing the interference with outdoor users.

While (as previously described) the advantages of an indoor deployment are many, the use of femtocells is not only limited to indoor environments. This is due to the flexibility and the costs related to the placement of femtocells (and small cells) in limited areas where the installation of a bigger BS is not justified. This is the reason why

the user-deployed femtocells perspective has shifted over the last years to an operator-deployed panorama, in which network operators position and operate the FAPs in a planned manner. This deployment of femtocells follows the trends in the user growth and behaviour, i.e. femtocells can be planned in hotspots where a given number of users congregate in particular areas of the network.

Similar to other small cells, FAPSs have a backhaul connection to the core network which in the case of femtocells is normally via DSL, cable modem or a separate RF backhaul channel [7]. This represents a very attractive characteristic from a network operator's point of view due to the potential traffic offloading from the MBSs to the FAPs. This is a critical issue due to the increase in the traffic associated with the growth in the number of users. In this thesis we focus on a two-tier network consisting of femtocells and macrocells due to the flexibility and the interesting interactions between them previously stated, such as the cost reduction associated with the placement and operation of femtocells, the considerable path loss reduction as a result of the user to FAP distance, the easiness of placement and setup of FAPs, and the additional advantage of FAP performance in indoor areas where 80% of the data is generated. The addition of other tiers of interference is then left out as future work. As it will be evident from the analysis presented in the following chapters, this can be achieved in a straightforward manner thanks to the stochastic geometry theory.

Despite the many advantages of deploying HetNets, a critical issue arises when considering the high densification of the network in terms of the number of BSs deployed. This issue comes in the form of the energy efficiency of the network, which is properly addressed in the next section.

1.2 Energy efficiency

For decades, the focus of the development of wireless systems has been to improve the coverage and increase the offered data rates. While this approach has resulted in the evolution of a major number of techniques and algorithms, one important aspect has not been given the attention that it deserves, i.e., power consumption. Over recent years, the power consumption of the network has started to receive an important consideration for the sustainable planning of future wireless systems due to its both economic and environmental implications. From an economical point of view, the power constitutes an expensive resource of the wireless communication system, and hence the importance of limiting its consumption. From an environmental perspective, it is estimated that around 2% of the global CO_2 emissions come from the Information and Communication Technology (ICT) [12]. Within this, mobile communications accounts for about 10% of the ICT total emissions. While both figures are expected to increase in the following years, the mobile communication share is predicted to more than triple from 2007 to 2020 [13]. This CO_2 footprint is directly related to the power consumed in the network. In particular, in the case of the cellular system, about 80% of the energy used is consumed in the radio access network (RAN). Therefore, there is a potential to reduce the energy consumption by deploying more energy-aware signal processing algorithms.

As a result of these findings, there have been an increasing number of organizations that have devoted their efforts in creating new paradigms for future energy efficient wireless networks. This in turn has created a whole new area of research found in the concept of *green wireless networks* [12]. The implementation of green wireless networks comprises several sub-areas in the deployment of energy efficient systems,

such as the architecture of the network, the system design and the network planning. Along these lines, the study of green cellular networks has identified future directions and potential areas for the development of energy efficient wireless networks. Among these, the deployment of HetNets has been highlighted as a promising solution due to the direct effect of deploying small BSs with reduced power consumption. However, a large scale planning of HetNets requires an in-depth study of the intricacies associated with this deployment.

In section 1.1 the advantages of HetNets deployments were addressed in detail. However, these advantages do not come for free when considering a large scale deployment. With the increase in the number of users, the amount of smaller cells which need to be deployed also increases. This leads to the emergence of several challenges to cope with the densification of the network in terms of the number and types of BSs deployed. While an increase in the number of BSs has the potential to generate benefits in terms of coverage and data rate improvements, it can also lead to an unwanted increase in the power consumed by the added BSs. Moreover, an increase in the number of deployed BSs is directly related to an increase in the interference of the network. This is a particularly critical aspect of future cellular networks in which the noise is no longer the main impairment of the communication system, with interference taking its place [14, 15]. Interference does not only limit the performance of the cellular system, but also creates a challenge in the design of HetNets, as the operating parameters need to be carefully selected for an efficient use of the available resources. Therefore, an accurate model of the energy efficiency of HetNets deployments needs a correct characterization of the interference in the network. To this end, the concept of stochastic geometry becomes a promising approach to effectively model HetNets. The next section elaborates the theory and contribution of stochastic geometry.

1.3 Stochastic geometry for the modelling of wireless networks

As stated in section 1.2, interference becomes a predominant factor in the performance of HetNets. Hence, a point to point link characterization of the communication channel is not accurate for the modelling of HetNets, and a more holistic perspective is needed to model the interference generated by the multiple types and numbers of BSs in the network. Moreover, another factor arises while considering the interference in the context of HetNets, namely, the position of the BSs in the network. A characteristic of traditional macrocell networks is that they possess a more structured arrangement of the MBSs in the service area as a direct result of network planning. However, this is not the case in HetNets, where the smaller base stations are placed in areas where MBSs cannot provide the users with the required QoS, which is highly dependant on the environment, the presence of buildings or other sources of signal blockage, etc., which results in more irregular topologies for the small cells. A more severe scenario is the case of user-deployed femtocells, in which FAPs are placed in different locations depending on the users' needs and/or preferences.

This dependency on the position and number of BSs increases the complexity of the network. Therefore, the traditional approach to model HetNets is to assume either that the location of the BSs are known a priori, or that they are randomly placed while making use of time and resource consuming simulations to characterize the performance of the network. This in turn complicates the development of an analytical framework to obtain an in-depth insight of the impact that the design parameters have on the performance of the network.

To this end, the concept of *stochastic geometry* has emerged as a viable and effective solution to provide an analytical support in the modelling of wireless networks. A

book that has become the main reference on the area of stochastic geometry is to be found in reference [16]. Stochastic geometry is not a new concept in the mathematical world. Typically, it has been used to characterize physical phenomena in which the number of elements and their locations are uncertain, such as the positioning of seeds in a given field, the number and location of stars, the imperfections in textiles, etc. However, until recent years, its application has extended to the modelling of wireless networks. This is due to the intricacies associated with the infrastructure-less nature of HetNets resulting from the environmental conditions of the network, as well as the growth in the number of users and their demands.

An essential concept that arises from stochastic geometry is the point process theory, which is particularly useful in the modelling of wireless networks. Informally, a point process refers to a random collection of points deployed in a given area. The number of points in a particular sub-area follows a given distribution, given rise to, for example, a binomial point process (BPP) if the number of points follows a binomial distribution or a Poisson point process (PPP) if the number of points follows a Poisson distribution. On the other hand, the points are uniformly distributed all across the area. The point process theory allows among other things to model the expected value of a given function applied to each point of the process taking into consideration their location. Therefore, in the context of wireless networks, a point process can be defined, where the points correspond to BSs, and the (location dependent) path loss function can be applied to all BSs in the system, effectively modelling the interference perceived. Very useful references on the use of stochastic geometry for the modelling of wireless networks can be found in [17–20].

In this thesis we have made use of tools from stochastic geometry and point process theory to model the locations of a two-tier HetNet under different deploying scenarios

and constraints.

1.4 Large scale deployment challenges

The deployment of HetNets (and in particular of femtocell networks) has many challenges for large scale planning. We have encompassed these challenges in Figure 1.2. The focal point of this thesis touches on some of these challenges from an energy efficient point of view, in particular, the access modes of femtocells and the interference management, which are described next. A detailed discussion on the other challenges can be found in [8, 21–23].

1.4.1 Access modes

Depending on the users which are allowed to connect to a given FAP, there are 3 defined access modes for a femtocell, namely open subscriber group (OSG), closed subscriber group (CSG) and hybrid subscriber group (HSG).

In the case of OSG all users within the coverage region of a nearby femtocell are allowed to freely connect to the FAP. This access mode is preferred from an operator perspective as it can extend the coverage, increase the data rates of the users and also offload some of the traffic from the MBS to the femtocell tier.

In a CSG only the users approved by the owner of a FAP are allowed to connect to it whenever they are in the vicinity of a femtocell. This is a preferred access mode for a user-deployed femtocell due to the fact that the owners who paid for a FAP will of course not be willing to compromise their service by sharing their FAPs with other users.

The case of HSG can be considered as a midpoint between OSG and CSG. In HSG

users are allowed to connect to a nearby FAP only if they belong to an FAP access list. Different charges for users outside the CSG are expected in this case.

In this thesis we have analysed a CSG case in chapters 2 and 3 for indoor femtocell users and outdoor macrocell users. On the other hand, in chapter 4, an OSG scenario is considered in a non-uniform deployment for outdoor users.

1.4.2 Interference management

As explained in section 1.2, interference is a major concern for NGN due to the high increase in the number of users. The effect of interference in HetNets is even more critical due to the high densification of the network in terms of the number of different tiers of BSs deployed. In a HetNet, with the increase of BSs of different types, there is not only inter-tier interference (such as in the case of a macrocell-only network) but also intra-tier interference between the different BSs in the network. This heterogeneity associated with the different properties of BSs belonging to different tiers creates an important challenge in the use of the available resources to cope with the interference. Therefore, it is imperative to consider both, an accurate characterization of the interference and an interference management strategy for the large scale modelling of HetNets.

In [23] the different interference management approaches are classified into three broad categories along with their representative techniques, namely, interference cancellation, interference avoidance and distributed interference management.

As discussed in section 1.2, the energy efficiency is a paramount metric for the deployment of NGN. However, the energy efficiency is a broad concept that covers several areas where potential improvements can be identified towards green sustainable wireless networks. Therefore, in this thesis, we have alluded to some of these

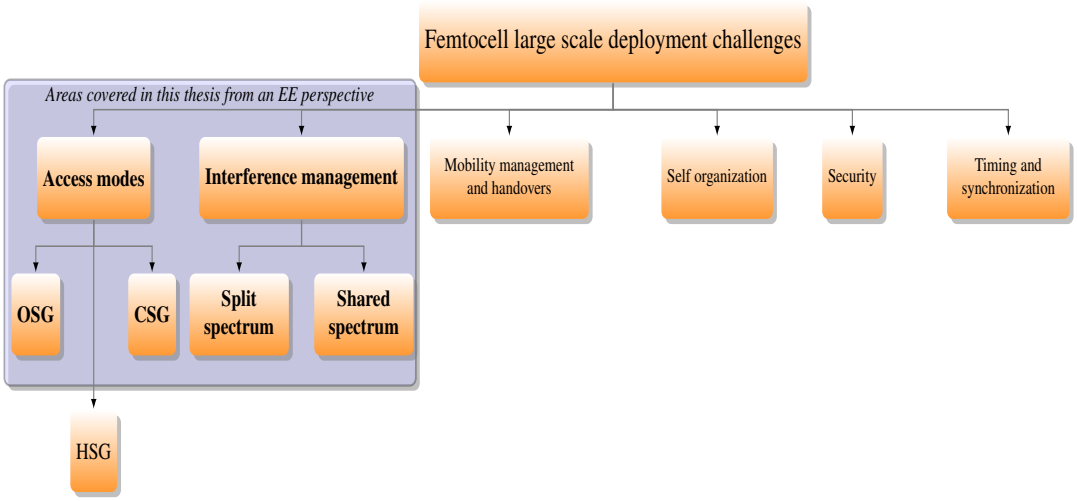

Figure 1.2: Challenges for large scale deployment and scope of the thesis.

challenges in a direct manner.

We have considered both cases of deployment strategies, namely a split spectrum and a shared spectrum in the scenarios studied. In chapter 2 a split spectrum strategy is considered, while chapters 3 and 4 deal with a co-channel deployment.

In the next section we address the extent and the scope of this thesis.

1.5 Objectives and scope of this thesis

In Figure 1.2 we have identified the areas that we have touched on from an energy efficiency perspective. The main objective of this thesis is to analyse the EE of a two-tier HetNet consisting of macrocells and femtocells. We have focused on design parameters and deployment strategies that will allow us to achieve the required QoS for NGN, while keeping an energy efficient perspective. To this end, we have addressed the inherent trade-off existing in HetNets between the spectrum efficiency and the power consumption in different deployment scenarios, namely analysing the impact of MIMO diversity schemes, antenna tilt angle design and femtocell strategic deployment on the

energy efficiency of the network.

The specific objectives of this thesis are:

1. To develop an accurate characterization of MIMO diversity schemes in a two-tier network.

2. To investigate the effect of the densification of femtocells on the EE of a two-tier MIMO network with antenna diversity schemes.

3. To obtain the optimum diversity scheme combination used for both MBSs and FAPs for the purpose of increasing the EE of the network while keeping constraints on the QoS requirements.

4. To obtain the optimum antenna configuration in terms of EE for the diversity schemes used.

5. To develop an accurate, yet tractable analytical framework for a 3D antenna pattern in a two-tier network.

6. To investigate the effect of the antenna tilt angle on the performance of both, a traditional macrocell-only network and a HetNet consisting of macro- and femtocells.

7. To obtain the optimum values of antenna tilt angle that maximize the EE of the two-tier network, while providing a minimum QoS.

8. To propose an energy efficient deployment model of femtocells towards areas where the expected QoS provided from a serving BS is low (towards the edge of the macrocell).

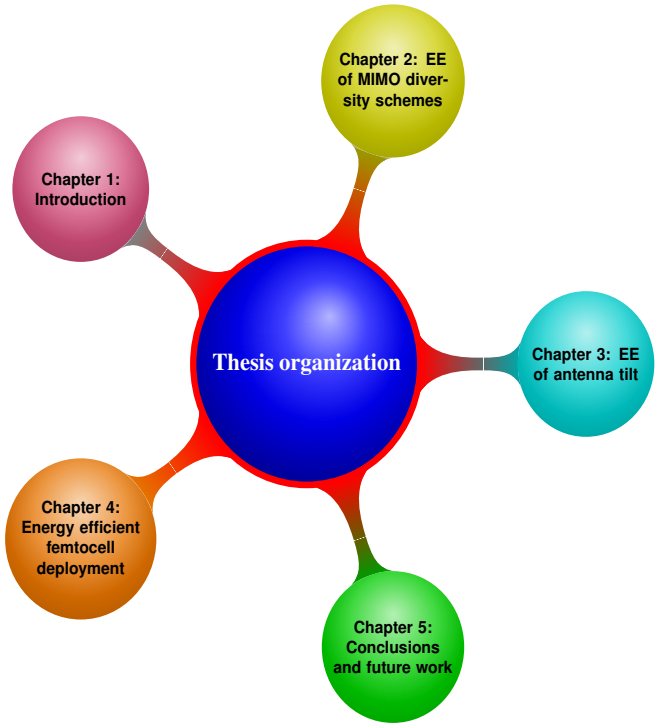

Figure 1.3: Thesis organization

9. To improve the cell edge user performance with a cell edge-oriented deployment of femtocells. The objective of this deployment is to obtain a network with a more balanced performance all across the service area.

10. To improve the coverage, data rates and EE of the network by only utilizing femtocells in areas with poor signal strength from the serving MBS.

1.6 Outline of the Thesis

In this thesis, an analysis of different deploying scenarios is considered for a two-tier HetNet consisting of macro- and femtocells. The strategic parameter design constitutes the focus of the different scenarios analysed. The general outline of the thesis is presented in Figure 1.3. Chapter 2 studies the EE of MIMO antenna diversity schemes.

For the two-tier network analysed, a femtocell tier is overlaid with a traditional MBS tier and it is assumed that femtocells provide service to indoor users. Additionally, femtocells are assumed to operate in CSG mode, and so they will only serve their designated indoor users. The focus of this chapter is to analyse the effect of diversity schemes and antenna configurations in the energy efficiency of the system and how it is affected by deploying several femtocells in the coverage area.

In chapter 3 the antenna tilt design for EE improvements is addressed. In this chapter, the effect of the antenna tilt is quantized in terms of the coverage and energy efficiency improvements for both a traditional (MBS only network) and two-tier networks (consisting of MBS and FAPs). Femtocells are assumed to be deployed by indoor users and again, they operate in CSG mode. The effect of antenna tilt on the coverage, data rates and the EE of the network are evaluated.

Chapter 4 analyses an EE efficient deployment of femtocells. By making use of the advantages associated with the use of FAPs, an energy efficient deployment of femtocells towards the edge of macrocells is assumed. In contrast with chapters 2 and 3 it is assumed an operator deployed scenario in which femtocells operate in an OSG mode where users can freely connect to a nearby FAP. The focus of this chapter is on the modelling and characterization of the improvements in performance of the network obtained by placing femtocells only in areas where the expected signal strength from a macrocell is not enough to provide the desired QoS.

The conclusions and final remarks of the thesis are given in chapter 5.

1.7 Contributions of the Thesis

As stated in section 1.6, the study carried out in this thesis focuses on different deployment design parameters with an EE perspective of two-tier networks consisting of macro- and femtocells. As a result of the analysis carried out, several contributions have been attained and they are summarized as follows.

Chapter 2: MIMO diversity schemes

1. **Energy efficiency of MIMO diversity schemes**: The performance of different MIMO diversity schemes were analysed from an EE perspective. The schemes analysed in chapter 2 are: Joint Antenna Selection (JAS), Beamforming - Selection Combining (BF-SC) and MRT. Depending upon the number of antennas used, these schemes cover a wide range of other diversity schemes such as selection combining, maximum ratio combining or beamforming. We have carried out an in depth study on the role of the density of femtocells in the EE of the different diversity schemes analysed.

2. **Optimum diversity schemes and antenna configurations**: We obtained the optimum diversity schemes and antenna configurations which yield the best performance in terms of EE for a given density of femtocells deployed in the area. From this, we address network design issues such as how the EE of the network is coupled with the number of antennas. Additionally, we deal with aspects such as whether it is more energy efficient to implement the same diversity schemes in both tiers and what antenna configuration will improve the EE metric in each case.

3. **Adaptive modulation with MIMO**: We have considered the use of adaptive

modulation in combination with MIMO spatial diversity schemes to add a more realistic flavour to the model, motivated by the fact that practical systems use a finite number of modulation schemes each of which corresponds to a fixed number of possible constellation points.

4. **Sleep mode**: We have analysed the savings when femtocells are assumed to be able to go into sleep mode when they are not transmitting in combination with MIMO diversity schemes. This way, the average energy used in the femtocell tier is efficiently reduced while achieving the same throughput, thus enhancing the EE.

   Chapter 3: Antenna tilt design

5. **Stochastic approach with full antenna pattern**: In chapter 3 we proposed a simplified 3D model that takes into account both the horizontal and the vertical patterns of an MBS antenna with a stochastic geometry approach. This is in contrast with previous works where stochastic geometry has been a common thread and in which the directive nature of sectorized antennas has been taken into account only from a horizontal pattern perspective. On the other hand, previous works that have considered a full 3D antenna pattern lack of an analytical framework, as they resort to simulations to obtain optimum values. In this thesis, we have used the properties of stochastic geometry to simplify the modelling of the antenna pattern. As a result, we have developed a full 3D antenna pattern model while providing an analytical framework from which the impact of the scalability of the network's parameters can be quantized.

6. **Optimum tilt angle for a traditional (macrocell only) network**: We focused on the impact of the vertical antenna pattern on the system performance. We

derived coverage and EE formulas for the case of a traditional network. In this scenario, the optimum tilt is the one that provides the best performance in terms of the coverage probability and EE. The dependency of the optimum tilt angle on the density of the macrocells was addressed with the developed analytical framework while avoiding long time and resource consuming simulations.

7. **Optimum tilt angle for a two-tier network in a co-channel deployment with QoS constraints**: For a two-tier co-channel HetNet consisting of FAPs and MBSs we have proposed the use of a guard zone around each macrocell user to protect it from the interfering FAPs. From there, we developed an optimization problem in which the energy efficiency of the system is maximized over the antenna tilt and the guard zone, while keeping QoS in both tiers.

   Chapter 4: Energy efficient femtocell deployment

8. **Introduction of Stienen's model for performance improvements**: In chapter 4 we propose the use of Stienen's model for a non-uniform deployment where femtocells are deployed in areas towards the edge of the macrocell coverage regions. In this model, the users located inside a disc (Stienen cell) surrounding each MBS will be served by that MBS, while users outside the disc will be restricted to being served by a neighbouring FAP.

9. **Improved edge user performance**: With the proposed model, the edge user performance which constitutes the bottleneck of cellular systems can be greatly increased with the deployment of femtocells, while the macrocell user performance is not considerably reduced by the addition of interfering FAPs. Therefore a more balanced network has been achieved.

10. **Characterization of coverage, throughput and EE of users in both tiers**: The characterization of the coverage, user throughput and the overall EE of the system is obtained by means of tools from stochastic geometry. With the tractable framework developed, the scalability of the network as a function of different design parameters can be addressed.

11. **Improved coverage, throughput and EE**: In the proposed model the performance in terms of coverage, throughput and EE was improved in both tiers in comparison with a typical uniform deployment. This is supported by the strategic positioning of femtocells which allows macrocell users to be located closer to the serving MBS and femtocell users to be served by areas where interfering signal power from an interfering MBS is not very high.

List of Publications

The work undertaken in this thesis has resulted in the the following publications.

- R. Hernandez-Aquino, D. McLernon, M. Ghogho, and S. A. R. Zaidi, “Energy efficiency in MIMO large scale two-tier networks with beamforming and adaptive modulation", Proceedings of the 21st European Signal Processing Conference (EUSIPCO), pp. 1-5, IEEE, Marrakesh 2013.

- R. Hernandez Aquino, S. Zaidi, D. McLernon, and M. Ghogho,“Energy efficiency analysis of two-tier MIMO diversity schemes in poisson cellular networks", IEEE Transactions on Communications, vol. pp, no. 99, pp. 1-13, 2015.

- R. Hernandez Aquino, S. Zaidi, D. McLernon, M. Ghogho, and Ali Imran,“Tilt

angle optimization in two-tier cellular networks - a stochastic geometry approach", IEEE Transactions on Communications, vol. pp, no. 99, pp. 1-16, 2015.

- R. Hernandez Aquino, S. Zaidi, D. McLernon, and M. Ghogho,"Modelling and performance evaluation of non-uniform two-tier Cellular Networks through Stienen Model", Proceedings of the IEEE International Conference on Communications (ICC), pp. 1 - 6, IEEE, Kuala Lumpur 2016.

- R. Hernandez Aquino, S. Zaidi, D. McLernon, M. Ghogho and A. Swami,"Stochastic Geometric Modeling & Analysis of Non-Uniform Two-tier Networks: A Stienen Model Base Approach", submitted to IEEE Transactions on Wireless Communications.

For all of the above publications, the contributions of the authors were the following:

Author: Raul Hernandez Aquino
Contributions: Conceived and implemented the models designed for both theory and simulations. Wrote first draft of the manuscripts.

Co-Author: Dr. Syed Ali Raza Zaidi
Contributions: Helped conceive the implemented models. Provided feedback on technical analyses.

Co-Author: Dr. Des McLernon

Contributions: Provided overall supervision of the implemented models development. Supported the project with field expertise and feedback from early to final drafts of the manuscripts.

Co-Author: Professor Mounir Ghogho

Contributions: Supported the project with field expertise and technical feedback for the development of the implemented models.

Co-Author: Dr. Ali Imran

Contributions: Provided field expertise and funding. Provided feedback on final drafts of the manuscript.

Co-Author: Dr. Ananthram Swami

Contributions: Provided field expertise and funding. Provided feedback on final drafts of the manuscript.

1.8 Notation

Throughout the thesis the following notation is used. Boldface capital and lower case letters represent matrices and vectors respectively. $\mathbb{E}[X]$ stands for the expected value of the random variable X. $\mathbf{A}^H$ represents the conjugate transpose of the matrix $\mathbf{A}$. A random variable X following a complex Gaussian distribution with mean μ and variance σ^2 is expressed as $X \sim \mathcal{CN}(\mu, \sigma^2)$. $|\mathbf{A}|$ denotes the determinant of matrix $\mathbf{A}$, a_l denotes the l-th entry of vector $\mathbf{a}$ and $(\mathbf{A})_{l,n}$ denotes the (l,n)-th entry of

matrix $\mathbf{A}$. An exponential distribution with mean μ is written as $\mathrm{Exp}\left(\frac{1}{\mu}\right)$, while a Poisson distribution with mean μ is expressed as $\mathrm{Pois}(\frac{1}{\mu})$. CDF $(F_X(x))$ and CCDF $(F_X^c(x) = 1 - F_X(x))$ stand respectively, for the cumulative and complementary cumulative distribution function of the random variable X. Finally $\mathcal{B}(x, D)$ represents the ball of radius D centered at x.

2 EE of MIMO diversity schemes

IN THIS CHAPTER:

The EE of different MIMO diversity schemes is analysed for the downlink of a two-tier network consisting of both macro- and femtocells. The locations of the BSs in both tiers are modeled by PPPs. The EE of the system in b/J/Hz is obtained for different antenna configurations under various diversity schemes. Adaptive modulation is employed to maximize both the throughput and the EE across both tiers. Borrowing well established tools from stochastic geometry, we obtain closed-form expressions for the coverage, throughput and power consumption for a two-tier, rate adaptive cellular network. Building on the developed analytical framework, we formulate the resource allocation problem for each diversity scheme with the aim of maximizing the network-wide EE while satisfying a minimum QoS in each tier. We consider that both the number of antennas and the spectrum allocated to each tier constitute the network resource which must be efficiently selected for both tiers to maximize network-wide performance. The best performance in terms of the EE was found to be provided by the schemes which strike a good balance between the achievable maximum throughput and the consumed power (both increasing with the number of RF chains used). In addition, the potential savings in EE by using femtocells with sleeping mode capabilities are analysed. It is observed that when the density of active co-channel femtocells exceeds a certain threshold, the EE of the system can be significantly improved by sleep scheduling.

2.1 Introduction

2.1.1 Motivation

As discussed in chapter 1, there has been an exponential increase in both the number of users of cellular systems and their bandwidth requirements, and the typical approach of network designers has been to increase the data rates that the system can handle and improve the coverage where it is needed. However, until very recently designing for EE has not received the importance that it deserves in the development of techniques and algorithms for future wireless networks deployments. According to recent studies, around 2% of the CO_2 emissions to the atmosphere comes from the Information and Communication Technology (ICT) industry [12]. In particular, the share for telecommunications is around 1%, and this is directly related to the energy used in the cellular system. Moreover, about 80% of this energy is consumed by the Radio Access Network (RAN). So reducing the energy consumption in cellular networks has therefore both environmental and economical implications.

A promising solution for Next Generation Networks (NGNs) to cope with the demands for better coverage and higher data rates is through the deployment of heterogeneous networks (HetNets) which consist of smaller, cheaper and less energy consuming base stations (BSs) overlaid with the traditional MBS network [8]. The use of HetNets has the potential to provide both the required coverage and increase the data rates of the users. However, realising such a potential may incur a significant energy penalty if the EE is not used as a metric to design the HetNet, mainly due to the increased co-channel interference.

Now, the use of MIMO technologies to improve communications performance has become a requirement for NGNs and it also has the potential to improve EE [24, 25].

However, the EE of the different MIMO techniques has not yet been analysed in depth, particularly beyond a point-to-point link. The use of multiple antennas has the direct benefit of increasing the average throughput. Nevertheless, the energy consumed also increases with the number of antennas, and this leads to a trade-off between throughput gains and the energy consumption. Additionally, the densification of the network to deal with traffic growth creates challenges for the efficient management of the available spectrum. While a co-channel deployment seems to be the appropriate choice when dealing with a relatively sparse network to avoid an underutilization of the spectrum, a disjoint channel assignment appears to be the best option for ultra dense deployment. Disjoint channel deployment of small cells has attracted support from 3GPP, whose Release 11 clearly identifies potential gains. Non co-channel deployment not only protects the users from the inter-tier interference but also provides a certain QoS guarantee. Such a deployment has been proposed by both academia [26] and industry [27]. NTT DOCOMO proposed the *phantom cell* concept, which advocates a deployment in which macro-cells manage the entire control plane, while the user plane is split between macro- and femtocells [27]. Thus, users with high throughput requirements and low mobility can be served by femtocells. While disjoint spectrum sharing between tiers seems to be the way ahead, the amount of spectrum shared across the tiers must be investigated. The optimal split of spectral resources is a function of various PHY layer parameters. Thus, the optimal allocation requires a characterization of the network wide performance in terms of these design parameters. To this end, the objective of this chapter is to investigate the design space of two-tiered cellular networks where macro and femtocells are deployed in non co-channel mode. Adaptive modulation is employed in each tier to maximize the attainable performance. BSs are equipped with multiple antennas to further enhance the downlink performance by exploiting the in-

herent diversity gain. The key objective of this study is to dimension the network-wide resource such that both EE and throughput can be maximized while satisfying some minimum desired QoS at each tier.

In order to characterize the performance of a large scale network, Poisson Point Processes (PPPs) [16] have frequently been used to model infrastructure-less networks such as ad-hoc [28–30] or femtocell networks [31–34]. In these networks the randomness is an intrinsic ingredient of the network topology. Thus PPPs are a natural choice to capture the spatial dynamics. Furthermore, the use of PPPs has also been extended to model macro-cells [14, 15, 26], since the traditional hexagonal lattice based models only provide an upper bound on the performance of actual networks. Moreover the upper-bound comes at the cost of time consuming and tedious simulations and/or numerical integrations. By contrast, PPPs can accurately provide a lower bound on the network performance with an analytically tractable model. Therefore, in this chapter we make use of stochastic geometry tools to characterize the performance of various diversity schemes in terms of EE for a two-tier network to find the diversity scheme and antenna configuration which provides the best performance. In order to characterize the coverage probability of each tier, the analysis carried out in [14, 35] is generalized and expanded. The optimum diversity scheme combinations along with the number of antennas are then obtained via a simple greedy search. We study both the case where only the energy related to the transmission is considered and the case which includes the total energy consumption (i.e., the energy used for signal processing, cooling, etc.). Finally, the impact of implementing sleep scheduling in the femto-tier is also investigated.

2.1.2 Related Work

There have been several works devoted to the study of the EE in heterogeneous networks, most of which consider an hexagonal grid for the modelling of the macro-cells positions. These provide an upper bound on the actual network performance but are unable to effectively produce a tractable framework from which aspects such as the scalability of the network can be evaluated. In [36] the EE gains were analysed by deploying micro-cells with fixed positions at the edge of a macro-cell network placed under the hexagonal lattice model. The area power consumption (defined as the amount of power used per unit area) was obtained as a function of the inter-site distance and it was found that there is an optimum value that minimizes this metric. A more general case was investigated in [37] where system throughput, area power consumption and EE were compared between a homogeneous network (only macro-cells deployed) and a heterogeneous network (consisting of both macro and micro-sites). In this case, the micro-cells were uniformly positioned near the border of each macro-cell, which accounts for a more realistic scenario, as the micro-cells will serve particular areas where the capacity or coverage needs to be improved, which will not necessarily only be at the edge of a macro-cell. In the case of femtocell deployments, [38] addressed the compromise between spectral efficiency (or throughput) and EE for a two-tier network consisting of macro-cells and a given number of femtocells which are uniformly distributed inside the area of each macro-cell. Both tiers are assumed to operate with maximum ratio combining (MRC) as a diversity scheme and they share the same sub-channels for transmission. The results obtained show the degradation of the macro-cell throughput and the EE increment with an increasing number of femtocells. Although the works described make use of realistic assumptions, the results were obtained mainly though

simulations without providing an analytical framework.

Another trend found in recent works regarding the EE of wireless networks has been to make use of tools from stochastic geometry to characterize the performance of the networks with a tractable approach. The EE of a single-input single-output (SISO) two-tier network consisting of both macro- and pico-cells was analysed in [39] where both tiers were modelled with independent PPPs. Analytical results on the coverage probability, data rates and EE (in bps/m $^{-2}$/J) were obtained as a function of the base station densities. Also, by considering independent PPPs, [40] evaluated the EE in a scenario consisting of micro-cells and pico-cells. An optimization problem was formulated to obtain the density of pico-cells that maximized the EE of the network with constraints on the outage probabilities of both tiers. The study of EE with the use of PPPs was extended to the multi-antenna case in [33], where a scenario consisting of a single macro-cell overlaid with a tier of femtocells modelled with a PPP was analysed. The authors examined the throughput and the EE of a MIMO system with an opportunistic interference alignment scheme in order to mitigate interference. These works efficiently make use of PPP theory to obtain an analytical framework from which the EE of the network was evaluated. However, an open issue still remains when considering the EE aspects of antenna diversity schemes in the context of heterogeneous networks. In particular, the schemes which provide the highest gains in throughput may not necessarily be the ones which attain the highest EE, and so this is the focus of this chapter.

2.1.3 Contributions

In this chapter we explore the design issues related to the large scale deployment of a two-tier network with MIMO diversity schemes. In particular, the main contributions

of the chapter are stated as follows.

- *EE of MIMO diversity schemes*: In this chapter, the EE of different MIMO diversity schemes is analysed for a two-tier network. In [41], the EE aspect of Maximum Ratio Transmission (MRT) was considered. However, as the power used in the RF chains has a great impact in the overall EE of the network when multiple antennas are used (even more so than the power used for transmission) [42], in this chapter we explore and analyse the EE of other diversity schemes where only some of the available antennas are used for transmission. The main contributions of the chapter can now be summarized as follows.

- *Energy efficiency of MIMO diversity schemes*: The key aspect of this chapter is to analyse the performance of different MIMO diversity schemes from an EE point of view (in terms of bits/J/Hz). The schemes analysed in this chapter are: Joint Antenna Selection (JAS), Beamforming - Selection Combining (BF-SC) and MRT. Depending upon the number of antennas used, these schemes cover a wide range of other diversity schemes such as selection combining, maximum ratio combining or beamforming. In this regard, we address how the density of the femtocells deployed in the network affects the EE for the different diversity schemes. It is worthwhile mentioning that diversity schemes with interferers modelled via a PPP were first analysed for ad-hoc networks in [35]. However, the authors focused on the scalability of the network in terms of transmission capacity and node density. Additionally, in the case of MRT the authors considered a bound on the maximum eigenvalue (of $(\mathbf{H}_{j,k})^H \mathbf{H}_{j,k}$ - see later in this chapter) in terms of the Frobenius norm. Here, we follow the approach in [43]

which provides precise characterization[1].

- *Optimum diversity schemes and antenna configurations*: We obtain the optimum diversity schemes and antenna configurations which yield the best performance in terms of EE for a given density of femtocells deployed in the area. From this, we can address network design issues such as how the EE of the network is coupled with the number of antennas. Moreover, we deal with aspects such as whether it is more energy efficient to implement the same diversity schemes in both tiers and what antenna configuration will improve the EE metric in each case.

- *Adaptive modulation with MIMO*: We consider the use of adaptive modulation in combination with MIMO spatial diversity to provide a model for practical systems which use a finite number of modulation schemes each of which corresponds to a finite number of possible constellation points.

- *Sleep mode*: The effect of sleep mode with MIMO diversity schemes has not been investigated thoroughly in the context of two-tier networks. In this chapter we analyse the savings when femtocells are assumed to be able to go into sleep mode when they are not transmitting, thus effectively reducing the average energy used in the femtocell tier while obtaining the same throughput, i.e. this enhances the EE.

[1]Notice that the link success probability computed in [35] is a function of the transmitter-receiver association model. More specifically, in [35] the authors considered the well known bi-polar network model. However, for small cellular networks the performance must be averaged over the spatial distribution of the user.

2.1.4 CHAPTER ORGANIZATION

The rest of the chapter is organized as follows. Section 2.2 introduces the system model. The EE metric and its optimization are described in section 2.3. The expected throughput in each tier is derived in section 2.4. Section 2.5 describes the analysis of the coverage for both tiers for the diversity schemes studied in this chapter: JAS, BF-SC and MRT. The power consumption in the network is derived in section 2.6. The simulation results are presented in section 2.7. Finally, conclusions are given in section 2.8.

2.2 System model

Consider the downlink of an interference limited OFDMA (such as LTE) two-tier network consisting of femtocell access points (FAPs) and macro-cell base sations (MBSs). The effect of noise will be neglected as interference dominates the overall performance of the network. This is the normal case for most modern cellular networks, where interference is the main performance limiting factor. This is due to the fact that in the interior of a cell the noise is very small compared to the desired SNR, while at the edge of a cell the interference power is much larger than the noise [14]. We focus on a highly dense scenario where both macro- and femtocells always have a user to serve. We also assume that the total number of available subchannels (S) is divided between tiers, assigning orthogonal sub-channels to each one in a given time slot. So we will have $S_m < S$ sub-channels assigned to the macro-cell tier and $S_f = S - S_m$ sub-channels assigned to the femtocell tier, such that the inter-tier interference is completely avoided, as the only sources of interference are base stations belonging to the same tier. As we are assuming a reuse factor of 1, all the cells in the network use the

same sub-channels for transmission. As explained in section 2.1, the assumption of orthogonal subchannnel allocation is justified due to the highly dense scenario. However, if that was not the case, a co-channel allocation should be implemented to avoid miss-utilization of the spectrum. If the orthogonal subchannel assumption did not hold, this would result in an increase of interference at both tiers which would reduce the performance specially at the macrocell tier. This is due to the larger distances (and associated path loss) between a MBS and its user in comparison with a FAP and its user. Therefore, an interesting future work would be to investigate the tradeoffs associated with the use of orthogonal and non-orthogonal performances for a different density of users in the network.

The propagation model is assumed to be a composite of Rayleigh flat-fading and path loss. For the flat fading component, a MIMO system is assumed where the base stations in tier i use M_i^t antennas for transmission and M_i^r antennas for reception. So, let $\mathbf{H}_{j,k}$ denote the $M_i^r \times M_i^t$ channel matrix between the j-th base station and the k-th user. As we consider a Rayleigh environment, each entry of $\mathbf{H}_{j,k}$ follows a complex Gaussian distribution with zero mean and variance 1, i.e., $(\mathbf{H}_{j,k})_{l,n} \sim \mathcal{CN}(0,1)$, with $l = 1, 2, ..., M_i^r$ and $n = 1, 2, ..., M_i^t$. We will model the path loss as $l(r_{j,k}) = (r_{j,k})^{-\alpha_i}$, where $r_{j,k}$ is the distance from the j-th transmitter to the k-th user and α_i is the path loss exponent in the i-th tier ($i \in \{f, m\}$), where "f" and "m" refer to "femto" and "macro", respectively. In the femtocell tier we use different values for the path loss exponent of the desired link (α_0) and the path loss exponent of an interferer link (α_f), as the latter can experience different propagation scenarios [44]. The mean total transmitted power of a base station in tier $i \in \{f, m\}$ is denoted as P_i^{tx}. It is assumed that when a complex symbol $(s_{j,k})$ from the j-th transmitter to the k-th user is sent, then $\mathbb{E}\left[|s_{j,k}|^2\right] = 1$. This assumption is used in order to normalize the power used in the symbols transmitted

and to provide a base from which different models can be compared. It is worthwhile pointing out that we use "$j = 0$" to refer to the "desired transmitter" and "$k = 0$" to refer to the "desired user".

Femtocells are assumed to operate in CSG [7], and so they will only serve their subscribed users. As femtocell users are assumed to be located indoors, so a wall partition loss (W_i, $i \in \{f, m\}$) must be considered. This corresponds to the power which is lost when the RF signal passes through a wall (for the macro-cell tier the users are assumed to be located outdoors, and so we consider $W_m = 1$). The tiers are modeled by two independent homogeneous PPPs (Φ_i, $i \in \{f, m\}$) where the number of macro- and femtocells in each tier are random variables following a Poisson distribution with positions uniformly distributed across the total area of the network. The intensity characterizing the number of base stations per unit area is λ_i. In the case of femtocells, a Medium Access Probability (MAP) ρ_f is considered, where in the current time slot, each femtocell decides whether to transmit (with probability ρ_f) or not. Therefore, the *effective intensity* of the transmitting femtocells is given by $\rho_f \lambda_f$. The use of the MAP derives from the fact that the coexistence of femtocells in the area of the network creates a need to control the co-channel interference, and this can be implemented by a MAP. It is worthwhile noting that a scenario in which femtocells operate in CSMA/CA mode can be modelled by simply letting ρ_f be a function of a carrier sensing region, as in [45, 46]. To reduce interference, as in practical scenarios, macro-cells are assumed to be sectorized with N_S sectors and so the effective intensity of the interferers in this tier is considered to be $\frac{\lambda_m}{N_S}$[2]. In a highly dense scenario such as the one described, all sectors in a macro-cell are considered to be active but all of them use different

[2]This holds for the downlink under the assumption that the front to back ratio of the sectorized antennas is high. In this case, the power radiated to a user in another sector can be neglected.

subchannels, in order to effectively reduce the interference.

In the femtocell tier each femtocell user is assumed to be associated with a FAP, and its position randomly (uniformly) located in the coverage area of the femtocell, which is assumed to the inside of a circle with radius R_f. Therefore, the distance of the user to its serving FAP (r_f) is a random variable with PDF $f_{r_f}(r_f) = \frac{2r_f}{R_f^2}$, for $0 < r_f \leq R_f$ [31]. On the other hand, in the macro-cell tier a user is associated with the closest BS, and this is the so called “closest association scheme" [14]. This means that the distance (r_m) from the user to its serving MBS is a random variable following the distribution of the distance to the closest base station, which for a homogeneous PPP was shown in [14] to be Rayleigh, i.e., $f_{r_m}(r_m) = 2\lambda_m \pi r_m e^{-\lambda_m \pi r_m^2}$, for $r_m \geq 0$. The scenario just described is depicted in Figure 2.1(a) where both tiers can be observed. Note that under the closest association scheme used for the macro-cell tier, the cells form a Voronoi tesselation. In Figure 2.1(b) the typical users of each tier are depicted, along with the distances to their associated base stations.

In the next section, the EE metric used is described and the main problem is clearly formulated.

2.3 Energy Efficiency

To characterize the EE of the system, we make use of the common metric defined in the Energy Consumption Rating (ECR) initiative [47], as

$$EE = \frac{T}{P} \text{ b/J} \tag{2.1}$$

where T is the effective throughput of the network in bps/Hz and P is the total power consumption in Watts. In order to obtain the EE of the diversity schemes studied in

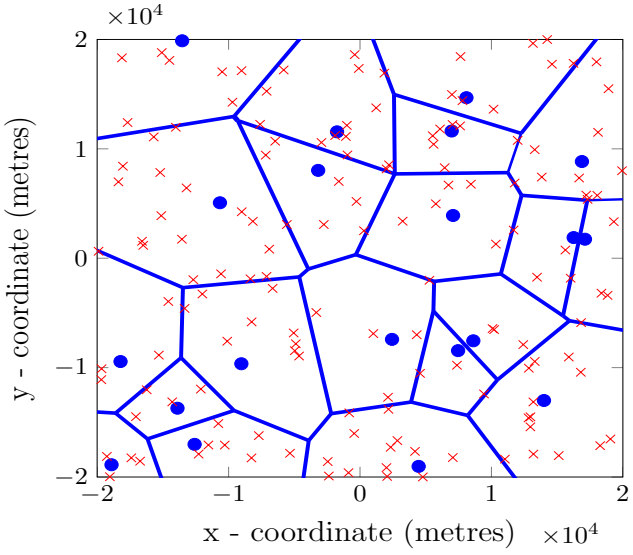

(a)

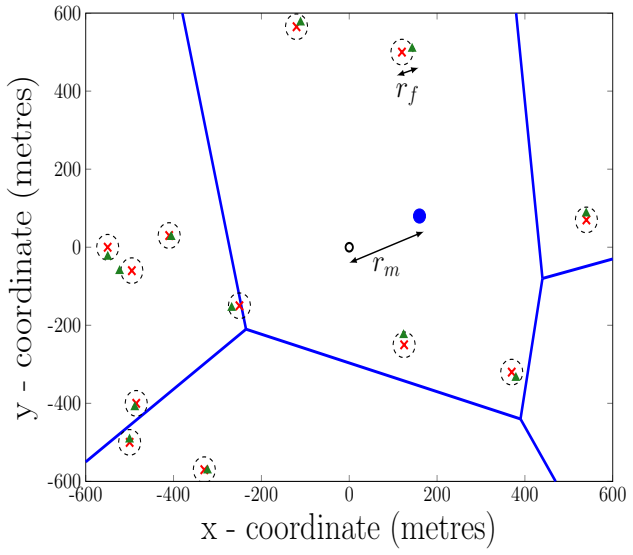

(b)

Figure 2.1: (a) two-tier network consisting of femtocells (red crosses) and macro-cells (blue dots). (b) the distance (r_m) of the macro typical user (black line circle) associated with its closest BS (blue dot) and the distance (r_f) of a femto user (green triangle) to its serving FAP (red cross). Note that each femtocell is associated with a femto user which is considered to be uniformly distributed inside a circular area of radius R_f (dotted line) of the femtocell.

this chapter, we need to characterize both the total expected throughput of the network as well as the total power used.

The problem to be addressed in this chapter is an optimization problem where the optimum diversity scheme, as well as antenna configuration, is obtained for a given density of femtocells deployed in the area, with QoS contraints. Note that the focus of this thesis resides in the energy efficiency optimization of the network. A multi-objective optimization problem is left out as a possible future work, as described in chapter 5. So, for each diversity scheme, the problem is defined as

$$M_i^{t\star}, M_i^{r\star}, S_m^{\star} = \arg \max_{M_i^t, M_i^r, S_m} \underbrace{\frac{S_m \lambda_m T_m + (S - S_m)\lambda_f T_f(\rho_f^{\star})}{\lambda_m P_m + \lambda_f P_f}}_{EE \text{ as in } (2.1)}$$

$$\text{s.t.} \tag{2.2}$$

$$S_m\, T_{m,u} \geq (S - S_m)\, q\, T_{f,u}\left(\rho_f^{\star}\right), \quad \text{if } T_{f,u}\left(\rho_f^{\star}\right) > T_{m,u}$$

$$(S - S_m)\, T_{f,u}\left(\rho_f^{\star}\right) \geq S_m q\, T_{m,u}, \quad \text{if } T_{f,u}\left(\rho_f^{\star}\right) \leq T_{m,u}$$

where T_m and T_f stand for (respectively) the expected throughput per base station in the macro- and femtocell tier; $\rho_f^{\star}$ is the MAP value which maximizes the throughput in the femtocell tier (see sections 2.4 and 2.5); u_i ($i \in \{f, m\}$) is the number of users served by each base station; $T_{m,u} = \frac{T_m}{u_m}$, $T_{f,u} = \frac{T_f(\rho_f^{\star})}{u_f}$ are (respectively) the expected throughput experienced by a user in the macro- and femtocell tier; P_m and P_f represent (respectively) the power consumed per MBS and FAP; and S_m is the number of subchannels assigned to the macro-cell tier. Additionally, $q \in [0, 1]$ is a quality of service requirement ensuring that a user in the tier with a smaller throughput experiences at least a fraction (q) of the throughput of a user in the tier providing the highest throughput. The expression in (2.2) can be solved for $S_m^{\star}$ as a function of the other

optimization variables ($M_i^{t\star}$, $M_i^{r\star}$) using the fact that the spectrum allocation is a linear combination with constraints on the minimum throughput requirement. Therefore, the EE would be maximized by assigning the maximum portion of the spectrum to the tier providing the highest EE, but the constraints set a limit on the spectrum allocated to the tier which experiences the lower expected throughput per user. In other words, there is a tradeoff between the EE and the spectral efficiency which depends on both, the diversity schemes and antenna configurations. Therefore, with the optimization problem proposed in (2.2) an optimal tradeoff is achieved due to the constraints set on the minimum QoS. The optimum value is then found when the constraints are met with equality, and is given by

$$S_m^\star = \begin{cases} S\left(1+\frac{T_{m,u}}{q\,T_{f,u}\left(\rho_f^\star\right)}\right)^{-1} & \text{if } T_{f,u}\left(\rho_f^\star\right) > T_{m,u} \\ S\left(1+\frac{qT_{m,u}}{T_{f,u}\left(\rho_f^\star\right)}\right)^{-1} & \text{if } T_{f,u}\left(\rho_f^\star\right) \leq T_{m,u}. \end{cases} \tag{2.3}$$

Now, both, the expected throughput and the power consumed depend on the diversity schemes and the number of antennas used in each case. These parameters need to be estimated in order to obtain the EE of the network in (2.2). We proceed to find expressions for the total expected throughput in section 2.4, which is a function of the coverage probability ($\mathcal{P}_i^c(\beta_i) = F_{SIR_i}^c(\beta_i)$, see section 2.5). Then, we investigate the total power consumed in each tier in section 2.6.

2.4 Network Throughput

In most modern wireless communication systems, the use of adaptive modulation according to the channel conditions has been used to maximize the throughput [49]. To the best of our knowledge no previous papers have studied adaptive modulation of

Table 2.1: SIMULATION PARAMETERS (Similar to [36] and [48])

Parameter	Value	Description
R_f	30 m	Femtocell coverage radius
α_m	4	Path loss exponent for the macro-cell tier
α_0	3	Path loss exponent for the femtocell tier in the desired link
α_f	3.5	Path loss exponent for the femtocell tier in an interference link
W_f	$2, 4$ dB	Wall partition loss for the femtocell tier,
W_m	0 dB	Wall partition loss for the macro-cell tier
G_s	3 dB	Shannon gap
C	8	Number of constellations available
N_S	3	MBS antenna sectors
q	0.5	Quality of Service factor
u_m	30	Number of macro users per cell
u_f	2	Number of femto users per femtocell
P_f^{tx}	100 mW	Femtocell transmission power
P_m^{tx}	20 W	Macro-cell transmission power
a_f	4	Femtocell power component dependent of transmitted power
a_m	3.77	Macro-cell power component dependent of transmitted power
b_f	9.6	Femtocell constant power component
b_m	68.73	Macro-cell constant power component
P_{UE}^1	0.94 W	Power used at the receiver's UE when 1 RF chain is used for reception
P_{UE}^2	1.27 W	Power used at the receiver's UE when 2 RF chains are used for reception

MIMO diversity schemes with BSs deployed following a PPP. In this chapter, we will further develop this scenario and study the performance of the diversity techniques

under an adaptive modulation scheme for a two-tier network. So, depending on the channel conditions, the symbols to be transmitted are chosen from a finite set of different constellations. Assuming C modulation schemes, in a given transmission then the normalized data rate that this system handles is given by $t_i^o = \log_2\left(1 + \frac{\beta_i^o}{G_s}\right)$ bps/Hz if $\beta_i^o \leq SIR_i < \beta_i^{o+1}$, with $o = 1, 2, ..., C$, $i \in \{f, m\}$ and G_s is the Shannon gap for un-coded QAM. In an adaptive modulation scheme, the average throughput per base station in each tier can be expressed as [49]

$$T_i = \sum_{o=1}^{C-1} t_i^o \, \mathbb{P}\left(\beta_i^o < SIR_i \leq \beta_i^{o+1}\right). \tag{2.4}$$

Therefore, the total throughput in each base station for each tier is given by

$$\begin{aligned} T_m &= \sum_{o=1}^{C-1} t_m^o \left(F^c_{SIR_m}(\beta_m^o) - F^c_{SIR_m}(\beta_m^{o+1})\right) + F^c_{SIR_m}(\beta_m^C)C \\ &= \sum_{o=0}^{C-1} \left(t_m^{o+1} - t_m^o\right) F^c_{SIR_m}(\beta_m^{o+1}) \quad \text{bps/Hz/m}^2 \end{aligned} \tag{2.5}$$

$$T_f\left(\rho_f\right) = \rho_f \sum_{o=0}^{C-1} \left(t_f^{o+1} - t_f^o\right) F^c_{SIR_f}(\beta_f^{o+1}) \text{ bps/Hz/m}^2 \tag{2.6}$$

where $F^c_{SIR_i}(x) = \mathbb{P}(SIR_i > x)$ is the cumulative complementary distribution function (CCDF) of the SIR_i, and $t_m^0 = t_f^0 = 0$. Note that for the femtocell tier, we have added the value of ρ_f, which accounts for the MAP of the femtocell tier. This is due to the fact that ρ_f represents the percentage of time in which a femtocell will be transmitting. The selection of MAP as the MAC strategy is justified given the fact that the femtocells are limited in power, and so simpler algorithms are expected. Also, by having a MAP assigned, no power is expended for cooperation in the femtocell tier.

As is clear from (2.5) and (2.6), we need to compute $F^c_{SIR_i}(\beta_i)$, defined as the cov-

erage probability (which is formally described in the next section), in order to obtain the total throughput for each tier. The expression for the coverage probability is different between tiers and for different diversity schemes. In the next section, we examine the coverage probability for each of the schemes addressed in this chapter.

2.5 Coverage

The coverage probability of each tier $\mathcal{P}_i^c(\beta_i) = F_{SIR_i}^c(\beta_i), i \in \{f, m\}$ is defined as the probability that the received SIR is above a certain threshold (β_i), which depends on the required QoS (i.e., $\mathcal{P}_i^c(\beta_i) = \mathbb{P}(SIR_i > \beta_i)$). Next, the coverage is presented for the diversity schemes analysed in this chapter. For convenience of notation, in the rest of the chapter we drop the subscripts in the desired link, i.e. $\mathbf{H} = \mathbf{H}_{0,0}$, and $s = s_{0,0}$.

2.5.1 Joint Antenna Selection (JAS)

We first analyse the case of transmit antenna selection at the transmitter and selection combining at the receiver side, i.e., the transmitter and the receiver jointly select the link with the best instantaneous channel and so, only one antenna RF chain remains turned on (i.e., using energy) at both transmitter and receiver sides. In this scenario, there are $M_i^r M_i^t$ channels available, where each channel $(h(l, n))$ corresponds to each entry of the flat fading channel matrix, i.e. $h(l, n) = (\mathbf{H})_{l,n}$, with $l \in \{1, 2..., M_i^r\}$ and $n \in \{1, 2..., M_i^t\}$. The best channel ($h^\star$) is selected in this scheme, that is, it satisfies $h^\star = \max_{l,n} |h(l, n)|^2$. Using Slivnyak's theorem [14], without loss of generality we place a typical user at the origin and obtain its statistics. In this case, the received

signal in the optimum link is given by

$$y_i = \sqrt{P_i^{tx}\, l\left(r_i\right)}\;\; h^{\star} s + \sum_{j \in \Phi_i} \sqrt{P_i^{tx}\;\; l\left(r_{j,0}\right) W_i^2}\, h_{j,0}\, s_{j,j} \tag{2.7}$$

where $h_{j,0}$ is the interfering channel coefficient corresponding to the link between the j-th transmitter and the desired user, for $i \in \{f, m\}$. From (2.7), the SIR can be computed as

$$SIR_i = \frac{|h^{\star}|^2\, r_i^{-\alpha_i}}{\sum\limits_{j \in \Phi_i} |h_{j,0}|^2\, W_i^2\, l\left(r_{j,0}\right)} = \frac{|h^{\star}|^2\, r_i^{-\alpha_i}}{I_{\Phi_i}}, \;\; i \in \{f, m\} \tag{2.8}$$

where I_{Φ_i} corresponds to the interference due to the PPP Φ_i and $|h_{j,0}|^2 \sim \mathrm{Exp}(1)$ represents the power of the channel between the j-th interferer and the desired user. The CCDF of $|h^{\star}|^2$ is obtained by using the fact that the CDF for an exponential random variable with mean equal to 1 is given by $F_X(x) = 1 - e^{-x}$, for $x \geq 0$. Thus, the CCDF $\left(F^c_{|h^{\star}|^2}\right)$, of the random variable $|h^{\star}|^2$, corresponding to the maximum value of $M_i^r M_i^t$ independent random variables, each one distributed as $\mathrm{Exp}(1)$, is given by

$$F^c_{|h^{\star}|^2}(y) = 1 - \left(1 - e^{-y}\right)^{M_i^r M_i^t} = \sum_{p=1}^{M_i^r M_i^t} \binom{M_i^r M_i^t}{p} (-1)^{p+1} e^{-py} \tag{2.9}$$

where binomial expansion notation is used. Using (2.9) in (2.8), the coverage probability can be expressed as

$$\mathcal{P}_i^c(\beta_i) = F_{SIR_i}^c(\beta_i) = \mathbb{E}_{I_{\Phi_i}, r_i}\left[\sum_{p=1}^{M_i^r M_i^t} \binom{M_i^r M_i^t}{p} (-1)^{p+1} e^{-s\, r_i^{\alpha_i} I_{\Phi_i}}\right]\Bigg|_{s=p\beta W_i^2}$$
$$= \sum_{p=1}^{M_i^r M_i^t} \binom{M_i^r M_i^t}{p} (-1)^{p+1}\, \mathbb{E}_{r_i}\left[\mathbb{E}_{I_{\Phi_i}}\left[e^{-s\, r_i^{\alpha_i} I_{\Phi_i}}\right]\right]$$
$$= \sum_{p=1}^{M_i^r M_i^t} \binom{M_i^r M_i^t}{p} (-1)^{p+1} \underbrace{\mathbb{E}_{r_i}\left[\mathcal{L}_{I_{\Phi_i}}\left(s\, r_i^{\alpha_i}\right)\right]}_{\mathcal{K}_i(s, r_i)}, \quad i \in \{f, m\} \tag{2.10}$$

where $\mathcal{L}_{I_{\Phi_i}}\left(s\, r_i^{\alpha_i}\right)$ corresponds to the Laplace transform of I_{Φ_i}. The resulting expressions for $\mathcal{K}_i\left(s, r_i\right)$ in each tier are given in appendix B. The following theorem defines the coverage probabilities for both tiers.

Theorem 2.1. *The coverage probabilities for a JAS diversity scheme in a two-tier network are given as*

$$\mathcal{P}_m^c(\beta_m) = \sum_{p=1}^{M_m^r M_m^t} \binom{M_m^r M_m^t}{p} (-1)^{p+1}$$
$$\times \quad \left(1 + \left(\frac{p\beta_m \delta_m}{N_S\left(1-\delta_m\right)}\, {}_2F_1\left(1, 1-\delta_m; 2-\delta_m; -p\beta_m\right)\right)\right)^{-1} \tag{2.11}$$

$$\mathcal{P}_f^c(\beta_f) = \sum_{p=1}^{M_f^r M_f^t} \binom{M_f^r M_f^t}{p} (-1)^{p+1} \frac{\gamma\left(\frac{\alpha_f}{\alpha_0}, R_f^{\alpha_0 \delta_f} \frac{\rho_f \lambda_f \pi^2 \delta_f}{\sin\left(\pi\delta_f\right)} \left(p\beta_f W_f^2\right)^{\delta_f}\right)}{R_f^2\, \frac{\alpha_0}{\alpha_f} \left(\left(\frac{\rho_f \lambda_f \pi^2 \delta_f}{\sin\left(\pi\delta_f\right)}\right)^{\alpha_f} \left(p\beta_f W_f^2\right)^2\right)^{1/\alpha_0}} \tag{2.12}$$

where $\delta_f = \frac{2}{\alpha_f}$, $\delta_m = \frac{2}{\alpha_m}$, *and* ${}_2F_1(a, b; c; x)$ *is the hypergeometric function.*

Proof. Substituting the expressions for $\mathcal{K}_i\left(s, r_i\right)$ into (2.10), then the expressions in (2.11) and (2.12) are found. □

Note that when $M_i^t = 1$ or $M_i^r = 1$, the expressions in (2.11) and (2.12) reduce (respectively) to the scenarios of a SIMO system performing selection combining at the receiver, or a MISO system selecting the best antenna at the transmitter.

2.5.2 BEAMFORMING - SELECTION COMBINING (BF-SC)

In this scheme, beamforming is performed at the transmitter, while selection combining is performed at the receiver. The receiver selects the antenna, $\hat{l}$, with the largest value of $\|\mathbf{h}(l)\|^2$, out of the M_i^r possible branches, i.e., $\hat{l} = \arg\max_l \|\mathbf{h}(l)\|^2, l \in \{1, 2, ..., M_i^r\}$, where $\mathbf{h}(l)$ corresponds to the l-th row vector of $\mathbf{H}$, and only its corresponding RF chain remains turned on. Now, $\|\mathbf{h}(l)\|^2$ is a random variable which follows a χ^2 distribution with $2M_i^t$ degrees of freedom. We will denote as $\tilde{h} = \max_l \|\mathbf{h}(l)\|^2$, the random variable that corresponds to the maximum value among M_i^r random variables, each one χ^2 distributed and having $2M_i^t$ degrees of freedom. The information about the selected antenna at the receiver's side is fed back to the transmitter so that it can perform beamforming. Therefore, all RF chains remain on at the transmitter side, while at the receiver only one RF chain is used. On the transmitter side, the complex symbol to be sent, s, is precoded before transmission with an $M_i^t \times 1$ beamforming vector, to give $\mathbf{v}\left(\hat{l}\right) s = \frac{\mathbf{h}^H\left(\hat{l}\right)}{\|\mathbf{h}\left(\hat{l}\right)\|} s$. So the received signal (at the receiver's single antenna which remains turned on) is given by

$$y_i = \sqrt{P_i^{tx}\, l\left(r_i\right)}\ \mathbf{h}\left(\hat{l}\right) \mathbf{v}\left(\hat{l}\right) s_i + \sum_{j \in \Phi_i} \sqrt{P_i^{tx}\ l\left(r_{j,0}\right) W_i^2}\ \mathbf{h}_{j,0}\, \mathbf{v}_{j,j}\, s_{j,j} \tag{2.13}$$

where $\mathbf{h}_{j,0}$ and $\mathbf{v}_{j,j} = \frac{\mathbf{h}_{j,j}}{||\mathbf{h}_{j,j}||}$ represent the j-th interference link channel vector and the beamforming vector in the j-th link, respectively. From (2.13), the SIR can be obtained as

$$\begin{aligned} SIR_i &= \frac{\|\mathbf{h}(\hat{l})\|^2 \, r_i^{-\alpha_i}}{\sum\limits_{j\in\Phi_i} |h_{j,0}|^2 \, W_i^2 \, l\,(r_{j,0})} \\ &= \frac{\tilde{h}\, r_i^{-\alpha_i}}{I_{\Phi_i}}, \;\; i \in \{f, m\}. \end{aligned} \tag{2.14}$$

We use the fact that a linear combination of Gaussian random variables is also Gaussian, and so the power fading coefficients of the interferers $|h_{j,0}|^2$ follow an exponentially distributed random variable [35]. Now, the cumulative complementary density function, of the random variable $\tilde{h}$, can be expressed as [35]

$$\begin{aligned} F_{\tilde{h}}^c(y) &= 1 - \left(1 - e^{-y} \sum_{p=0}^{M_i^t-1} \frac{y^p}{p!}\right)^{M_i^r} \\ &= \sum_{w=1}^{M_i^r} e^{-wy} \sum_{p=0}^{M_i^r(M_i^t-1)} a_{wp}\, y^p \end{aligned} \tag{2.15}$$

where $a_{wp} = (-1)^{M_i^r+w}\binom{M_i^r}{w} \sum\limits_{\substack{p_1,p_2,\ldots,p_w \le M_i^t-1 \\ p_1+p_2\cdots+p_w=p}} \prod\limits_{v=1}^{w} (p_v!)^{-1}$ and the sum runs over all ordered w-tuples of positive integers (including zero) less than $M_i^t - 1$ which add to p. Using (2.15), and the expression in (2.14), then the coverage can be expressed as

$$\begin{aligned} \mathcal{P}_i^c(\beta_i) &= F_{SIR_i}^c(\beta_i) \\ &= \mathbb{E}_{I_{\Phi_i}, r_i}\left[\sum_{w=1}^{M_i^r} \sum_{p=0}^{M_i^r(M_i^t-1)} a_{wp}\; e^{-w\beta_i W_i^2 \, r_i^{\alpha_i} I_{\Phi_i}} (\beta_i W_i^2 \, r_i^{\alpha_i} I_{\Phi_i})^p\right] \\ &= \sum_{w=1}^{M_i^r} \sum_{p=0}^{M_i^r(M_i^t-1)} a_{wp}\,(-1)^p \frac{\partial^p}{\partial w^p} \mathbb{E}_{r_i}\left[\mathbb{E}_{I_{\Phi_i}}\left[e^{-s\, r_i^{\alpha_i} I_{\Phi_i}}\right]\right]\Big|_{s=w\,\beta_i W_i^2} \end{aligned}$$

$$= \sum_{w=1}^{M_i^r} \sum_{p=0}^{M_i^r (M_i^t - 1)} a_{wp} \, (-1)^p \, \frac{\partial^p}{\partial w^p} \underbrace{\mathbb{E}_{r_i} \left[\mathcal{L}_{I_{\Phi_i}} \left(s \, r_i^{\alpha_i} \right) \right]}_{\mathcal{K}(s, r_i)}. \tag{2.16}$$

The coverage probabilities for both tiers are defined in the following theorem.

Theorem 2.2. *The coverage probabilities for a BF-SC diversity scheme in a two-tier network are given as*

$$\mathcal{P}_m^c(\beta_m) = \sum_{w=1}^{M_m^r} \sum_{p=0}^{M_m^r (M_m^t - 1)} a_{wp} \, (-1)^p \times \frac{d^p}{dw^p} \left(1 + \left(\frac{w \, \beta_m \, \delta_m}{N_S \, (1 - \delta_m)} \, {}_2F_1 \left(1, 1 - \delta_m; 2 - \delta_m; -w\beta_m \right) \right) \right)^{-1} \tag{2.17}$$

$$\mathcal{P}_f^c(\beta_f) = \sum_{w=1}^{M_f^r} \sum_{p=0}^{M_f^r (M_f^t - 1)} a_{wp} \, (-1)^p \, \frac{\partial^p}{\partial w^p} \frac{\gamma \left(\frac{\alpha_f}{\alpha_0}, R_f^{\alpha_0 \delta_f} \frac{\rho_f \lambda_f \pi^2 \delta_f}{\sin(\pi \delta_f)} \, (w \beta_f W_f^2)^{\delta_f} \right)}{R_f^2 \, \frac{\alpha_0}{\alpha_f} \left(\left(\frac{\rho_f \lambda_f \pi^2 \delta_f}{\sin(\pi \delta_f)} \right)^{\alpha_f} (w \beta_f W_f^2)^2 \right)^{1/\alpha_0}}. \tag{2.18}$$

Proof. Substituting the expressions for $\mathcal{K}(r_i, s)$ presented in appendix B into (2.16), the coverage probabilities for both tiers are obtained. □

Note that by substituting M_i^t for M_i^r and vice-versa, the formulas obtained apply to a scenario now with antenna selection at the transmitter and MRC at the receiver (AS - MRC). Also, when $M_i^r = 1$, a pure beamforming scenario is addressed.

2.5.3 MAXIMUM RATIO TRANSMISSION (MRT)

MRT consists of beamforming at the transmitter and MRC at the receiver [50]. Thus, in the MRT scheme, all RF chains remain on at both transmitter, and receiver. The complex symbol to be sent, s_i, is first precoded at the transmitter with an $M_i^t \times 1$ beamforming vector $\mathbf{v}_i$, which is the eigenvector corresponding to the maximum eigenvalue (Λ_{max}) of the Wishart matrix $(\mathbf{H})^H \mathbf{H}$. The received signal vector is then given by

$$\mathbf{y}_i = \sqrt{P_i^{tx}\, l\left(r_i\right)}\ \mathbf{H}\,\mathbf{v}\,s + \sum_{j\in\Phi_i}\sqrt{P_i^{tx}\ l\left(r_{j,0}\right)W_i^2}\ \mathbf{H}_{j,0}\,\mathbf{v}_{j,j}\,s_{j,j}, \quad i \in \{f,m\}. \tag{2.19}$$

where $\mathbf{v}_{j,j}$ represents the eigenvector corresponding to the maximum eigenvalue of the Wishart matrix $(\mathbf{H}_{j,j})^H \mathbf{H}_{j,j}$. At the receiver, MRC is used and a $1 \times M_i^r$ weight vector $(\mathbf{w})^H$ is applied to the received signal before decoding the symbols, i.e., the signal to be decoded is given by $y_i = (\mathbf{w})^H \mathbf{y}_i$, where $\mathbf{w} = \mathbf{H}\mathbf{v}$. The SIR in this case is given by

$$\begin{aligned} SIR_i &= \frac{\Lambda_{max,i}\, r_i^{-\alpha_i}}{\sum\limits_{j\in\Phi_i} |h_{j,0}|^2\, W_i^2\, l\left(r_{j,0}\right)} \\ &= \frac{\Lambda_{max,i}\, r_i^{-\alpha_i}}{I_{\Phi_i}}, \quad i \in \{f,m\} \end{aligned} \tag{2.20}$$

where $|h_{j,0}|^2 \sim \mathrm{Exp}(1)$ represents the fading power coefficient for the link between the desired user and the $j\text{-}th$ source of interference. The SIRs in (2.20) follow from the fact that with MRC, the resulting interference is a weighted combination of complex Gaussian random variables, which is again Gaussian. This makes the power of the interference a sum of exponential random variables, just as in the case of a SISO system [43].

Now, from (2.20), this coverage probability is related to the CDF of the maximum eigenvalue ($\Lambda_{max,i}$) of a Wishart matrix in the i-th tier, which was originally obtained in [51] as $F_{\Lambda_{max,i}}(x) = \frac{|\mathbf{\Psi}(x)|}{\prod_{k=1}^{c_i}(c_i-k)!\prod_{k=1}^{u_i}(u_i-k)!}$, where $c_i = \min(M_i^t, M_i^r)$, $u_i = \max(M_i^t, M_i^r)$ and $\mathbf{\Psi}(x)$ is a Hankel matrix whose elements are given by $(\mathbf{\Psi}(x))_{i,j} = \gamma(i+j-1, x)$ with $\gamma(a,b)$ being the lower incomplete Gamma function. In [43] an alternative expression was found as a sum of exponential functions. Using this alternative expression ([43], eq. (15)) and applying the definition in (2.20), the coverage probability is given as

$$\begin{aligned}
\mathcal{P}_i^c(\beta_i) &= F_{SIR_i}^c(\beta_i) \\
&= \mathbb{E}_{I_{\Phi_i},r_i}\left[\sum_{p=1}^{c_i}\sum_{w=u_i-c_i}^{(u_i+c_i)p-2p^2}\sum_{z=0}^{w} d_{p,w}\,\frac{e^{-p\beta_i W_i^2\, r_i^{\alpha_i} I_{\Phi_i}}(p\beta_i W_i^2\, r_i^{\alpha_i} I_{\Phi_i})^z}{z!}\right] \\
&= \sum_{p=1}^{c_i}\sum_{w=u_i-c_i}^{(u_i+c_i)p-2p^2}\sum_{k=0}^{w} d_{p,w}\,\frac{(-p)^z}{z!}\frac{\partial^z}{\partial p^z}\,\mathbb{E}_{r_i}\left[\mathbb{E}_{I_{\Phi_i}}\left[e^{-s\, r_i^{\alpha_i} I_{\Phi_i}}\right]\right]\Big|_{s=p\,\beta_i W_i^2} \\
&= \sum_{p=1}^{t_i}\sum_{w=u_i-t_i}^{(u_i+t_i)p-2p^2}\sum_{z=0}^{w} d_{p,w}\,\frac{(-p)^z}{z!}\frac{\partial^z}{\partial p^z}\underbrace{\mathbb{E}_{r_i}\left[\mathcal{L}_{I_{\Phi_i}}(s\, r_i^{\alpha_i})\right]}_{\mathcal{K}(s,r_i)}
\end{aligned} \tag{2.21}$$

where $d_{p,w}$ is a coefficient which can be obtained from $|\mathbf{\Psi}(x)|$ [43]. The coverage probabilities for both tiers are presented in the following theorem.

Theorem 2.3. *The coverage probabilities for a MRT diversity scheme in a two-tier network are given as in (2.22) and (2.23).*

Proof. Substituting the expressions for $\mathcal{K}(r_i, s)$ presented in appendix B into (2.21), the coverage probabilities for each tier are obtained. □

$$\mathcal{P}_m^c(\beta_m) = \sum_{p=1}^{c_m} \sum_{w=u_m-c_m}^{(u_m+c_m)p-2p^2} \sum_{z=0}^{w} d_{p,w} \frac{(-p)^z}{z!} \times \frac{d^z}{dp^z} \left(1 + \frac{p\,\beta\,\delta_m}{N_S\,(1-\delta_m)}\, {}_2F_1\,(1, 1-\delta_m; 2-\delta_m; -p\beta) \right)^{-1} \tag{2.22}$$

$$\mathcal{P}_f^c(\beta_f) = \sum_{p=1}^{c_f} \sum_{w=u_f-c_f}^{(u_f+c_f)p-2p^2} \sum_{z=0}^{w} d_{p,w} \frac{(-p)^z}{z!} \frac{d^z}{dp^z} \frac{\gamma\left(\frac{\alpha_f}{\alpha_0}, R_f^{\frac{2\alpha_0}{\alpha_f}} \frac{\rho_f \lambda_f \pi^2 \delta_f}{\sin(\pi\delta_f)} (p\beta W_f^2)^{\delta_f}\right)}{R_f^2 \frac{\alpha_0}{\alpha_f} \left(\left(\frac{\rho_f \lambda_f \pi^2 \delta_f}{\sin(\pi\delta_f)} \right)^{\alpha_f} (p\beta W_f^2)^2 \right)^{1/\alpha_0}}. \tag{2.23}$$

By substituting the appropriate expressions for the coverage probability in each tier (as stated in the previous section) into (2.5) and (2.6) respectively, the throughput for each tier can be obtained. Depending upon the particular scenario there is an optimal MAP value $\left(\rho_f^\star\right)$ which maximizes the throughput of femtocells, i.e., $\rho_f^\star = \arg\max_{\rho_f} T_f(\rho_f)$. The expressions for the coverage probability in the femtocell tier preserve the exponentially decreasing shape as a function of ρ_f (because of the Gamma function), while the multiplication by the linear increasing factor ρ_f means that the resulting expressions have an ALOHA like shape. This is shown in Figure 2.2 of section 2.7, where, depending upon the density of femtocells, there is an optimum value for ρ_f. Unfortunately, the optimum MAP cannot be obtained in closed form expression, given the fact that the summations in (2.12), (2.18) and (2.23) are not known in theory. However, the MAP value can be computed by extending the summations for each configuration of antennas, then taking the derivative of (2.6), equating to zero and solving for $\rho_f = \rho_f^\star$, with the restriction that the resulting value is between 0 and 1. This can be carried out with the aid of a symbolic software program like Maple.

2.6 Network power

We make use of the power consumption model presented in [36,37,52] for both macro and femtocells: $P_i = a_i P_i^{tx} + b_i, i \in \{f, m\}$. Here a_i is a parameter dependent on the transmitted power of the base station (P_i^{tx}), which is related to the efficiency of the power amplifier, and b_i is a parameter independent of the transmission power which deals with the power used for signal processing, cooling effects of the site and battery backup. A power penalty for the CSI acquisition is not considered, as the transmitters in both tiers only require the channel information of the desired link which needs only a small number of bits to be fed back to the transmitter. We also assume typical values for the components of the power consumption model ([36, 48]) as presented in Table 2.1.

Most of the works related to EE, only consider the power consumed at the transmitter side when analysing the downlink of a communication system [39, 40, 53, 54]. However in this chapter, we also consider the power consumed at the User Equipment (UE), given the fact that not taking this power into consideration would result in an unfair comparison of the models when different numbers of antennas are assumed at the receiver. In [55], an analysis was carried out for the case of a system using the 802.11n standard for transmission (which is also used by several smartphones) and the mean power consumed was obtained using a Network Interface Card (NIC) when up to 3 antennas were used for reception. These values are presented in Table 2.1, under the parameter $P_{UE}^{M_i^r}, i \in \{f, m\}$. Note that "$UE$" stands for User Equipment. By using the models previously described, the macro- and femto- tier total power consumption

models per base station are given by

$$P_m = N_S \left(a_m P_m^{tx} + \bar{M}_m^t b_m \right) + P_{UE}^{\bar{M}_m^r} \quad \text{W} \tag{2.24}$$

$$P_f = \rho_f^\star a_f P_f^{tx} + \bar{M}_f^t b_f + P_{UE}^{\bar{M}_f^r} \quad \text{W} \tag{2.25}$$

where $\bar{M}_i^t$ and $\bar{M}_i^r$ represent the effective number of antennas (RF chains) used depending upon the diversity scheme. That is, we have for MRT $\bar{M}_i^t = M_i^t, \bar{M}_i^r = M_i^r$, for BF-SC $\bar{M}_i^t = M_i^t, \bar{M}_i^r = 1$, and for JAS $\bar{M}_i^t = \bar{M}_i^r = 1$. Note that $a_i, i \in \{f, m\}$ in (2.24) and (2.25) are not scaled by the number of antennas, given that the total power radiated from all the antennas is equal to P_i^{tx}.

By substituting the values for T_i and P_i ($i \in \{f, m\}$) into (2.2) we can obtain the EE metric for each diversity scheme analysed. Now, from the expressions for coverage probability previously derived, the optimization problem in (2.2) is intractable for different values of M_i^t and M_i^r ($i \in \{f, m\}$). However, as we are dealing with a finite search space, we resort to an extensive search over the optimizing variables (diversity schemes and antenna configurations) to obtain the results.

2.6.1 Sleep Mode

One of the techniques from which further improvements can be obtained in the power savings of a communications system is through the use of sleeping modes, as highlighted in [12, 53, 56]. In a sleeping mode, a component of the communication system can be partially or completely shut down when its full operation is not justified. The use of sleeping modes in this chapter fits naturally in the context of the femtocell MAP. Before sending information, each FAP decides individually whether to transmit (with probability ρ_f) or not (with probability $1 - \rho_f$). If a FAP decides that it is not going

to transmit in the current time slot, then there is a potential saving in the power used if this femtocell can shut down its operation during the duration of the time slot.

Considering FAPs with sleep mode capabilities and neglecting the power consumed in a FAP when it goes into sleep mode (perfect sleep mode), then (2.25) becomes

$$P_f^{sleep} = \rho_f^{\star}\left(a_f P_f^{tx} + \bar{M}_f^t b_f\right) + P_{UE}^{\bar{M}_f^r} \quad \text{W}. \tag{2.26}$$

2.7 Results

Simulation results are now presented in Figs. 2.2 to 2.7 for both Monte Carlo simulations (i.e., circles, with 2×10^4 runs for each point) and the analytical plots (i.e., the lines). Note that the simulations lie (almost exactly) on the analytical plots. In general, the MonteCarlo simulations where carried out from a bit level as follows: i) A random number of MBSs and FAPs are deployed following a Poisson distribution, ii) the BSs are uniformly distributed in the area, iii) the typical user is located in the origin (as a result of Slivyank's theorem previously described) and it is associated to the its respective BS, iv) a random Rayleigh channel is simulated for all links, v) a random message to be sent is generated, vi) the received signal at the receiver is decoded depending on the diversity scheme and considering the path loss, vii) finally, this process is repeated for each simulation. From the results of the simulations, the SIR, coverage probability, effective throughput and energy efficiency can be obtained by following their respective definitions. This general process is carried out throughout the thesis to simulate the different scenarios.

The parameters used for the simulations are given in Table 2.1 and we deliberately chose them similar to other publications [36], [31]. Given the fact that the user equip-

Table 2.2: DIVERSITY SCHEMES ANALYSED

Macro-cell scheme	**Femtocell scheme**
MRT	MRT
JAS	JAS
MRT	BF - SC
BF - SC	MRT
BF - SC	JAS
JAS	BF - SC
MRT	JAS
JAS	MRT
BF - SC	BF - SC
JAS - MRC	JAS - MRC

ment is comprised of battery limited devices, the scenarios simulated in this chapter consider a maximum of $M_i^r = 2$ antennas per user, whereas the number of antennas in the BSs can be up to $M_m^t = 4$ in the macro-cell tier, and $M_f^t = 3$ for FAPs. In the simulations, we analysed different combinations of the diversity schemes previously described in each tier to obtain the optimum values of EE in each case. For all the diversity schemes and configurations we allocated the optimum portion of spectrum ($S_m^\star$) and for femtocells we use the optimum value of the MAP ($\rho_f^\star$) in order to obtain the higher gains in throughput. Without loss of generality, in the simulations we have assumed that there are $C = 8$ integer available data rates (i.e., $t_i^1 = 1$, $t_i^2 = 2$,...,$t_i^8 = 8$, $i \in \{f, m\}$). All the combinations of the diversity schemes analysed are presented in Table 2.2.

In Figure 2.2 the throughput of the femtocell tier is presented as a function of the MAP (ρ_f) for the main diversity schemes analysed, and with different values of the wall partition loss W_f. It can be seen that there is an optimum value ($\rho_f^\star$) that maximizes the throughput, and this varies depending upon the interference experienced. With a fixed density of femtocells deployed in the area, a higher value of W_f translates

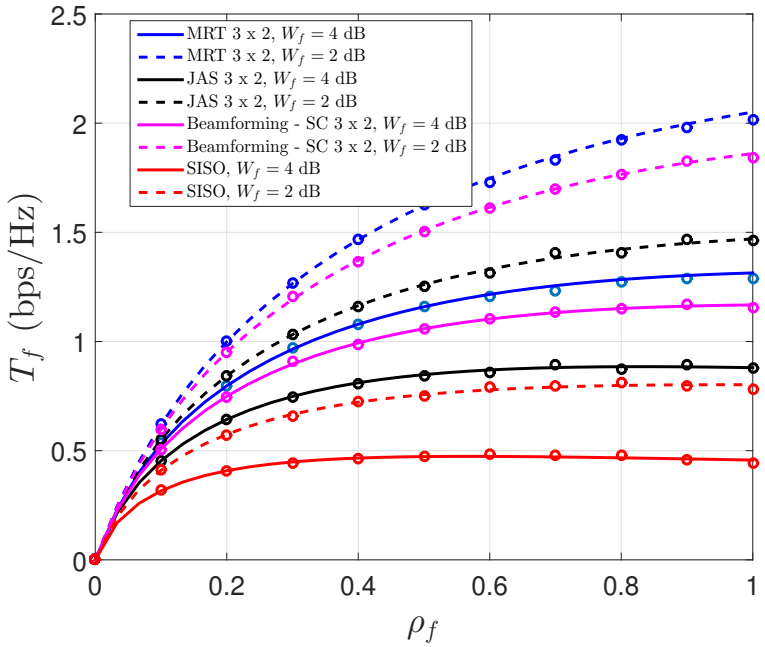

Figure 2.2: Femtocell throuhgput for the diversity schemes as a function of MAP (ρ_f). Circles represent Monte Carlo simulations and lines represent analytical results.

into a smaller interference experienced in the desired link, and so, the optimum MAP $\rho_f^\star$ has a higher value. On the other hand, a small value for W_f represents a higher interference, and so $\rho_f^\star$ is smaller.

In Figure 2.3 the total throughput of the network (numerator of (2.2)) is presented normalized over the area size for comparison purposes, i.e. the results are given as bps/Hz/m^2 which is also known as the area spectral efficiency. In order to clarify the comparison, we kept the same diversity scheme and antenna configuration in the macro-cell tier, i.e. MRT with $M_m^t = 4, M_m^r = 2$. On the other hand, in the femtocell tier we show a contrast between different diversity schemes and antenna configurations and considering the optimum MAP ($\rho^\star$). As expected, a MRT scheme in both tiers represents the maximum gains in throughput. Additionally, the throughput in the network increases with the number of antennas used. These results also serve as comparison

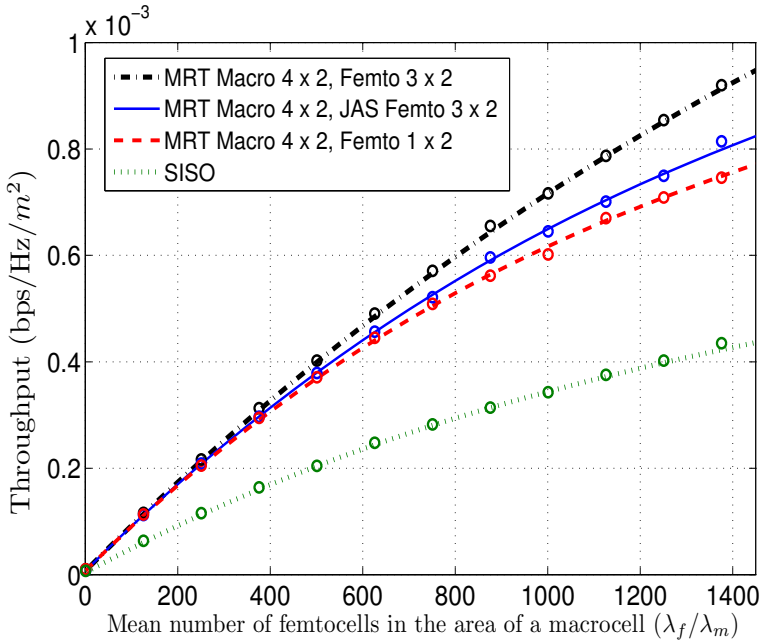

Figure 2.3: Throughput of the network as a function of the density of femtocells deployed in the area. Circles represent Monte Carlo simulations and lines represent analytical results.

point with the EE when the power is also taken into account. This will be illustrated in Fig. 2.4.

In Figure 2.4, we present a comparison between the achievable EE when different diversity schemes are used in the femtocell tier. These results in combination with the ones presented in Fig. 2.3 help us to gain some insight into the inherent tradeoff of throughput and EE. For example, while using MRT at the femtocell tier would result in the highest achievable throughput for femtocell users, a scheme with JAS outperforms MRT in terms of EE for the same number of antennas ($M_f^t = 3, M_f^r = 2$ in this case). Given that in a JAS scheme there will only be one RF chain left turned on at the transmitter and receiver whereas in MRT all the RF chains remain on, the results show that selectively keeping just a few chains for transmission generates higher gains on the overall EE. Therefore, a tradeoff between the throughput and the power of the system

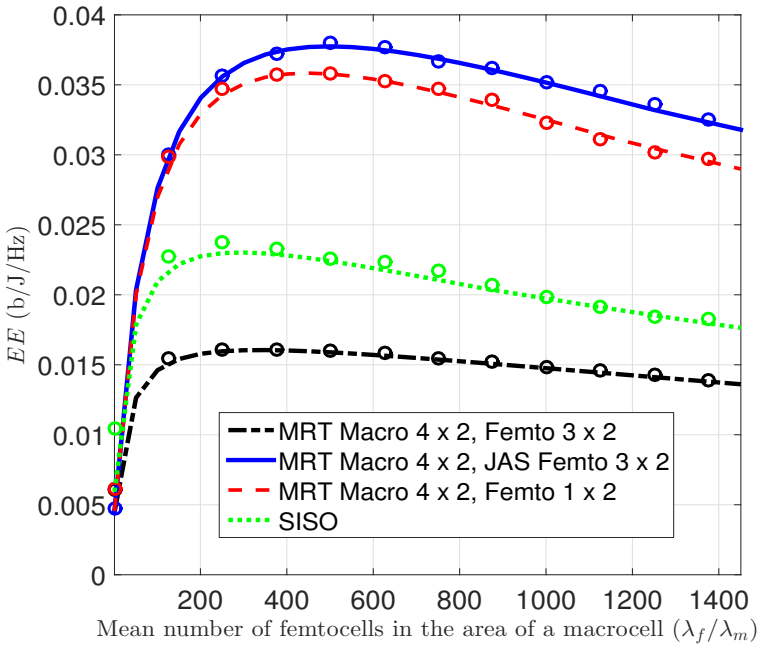

Figure 2.4: Comparisons of diversity schemes and antenna configurations for the EE (see EE in (2.2)) versus average number of femtocells in the area of a macro-cell $\left(\frac{\lambda_f}{\lambda_m}\right)$ with $b_f \neq b_m \neq 0$ in (2.24) and (2.25) (i.e., both transmit power and other sources included). Circles represent Monte Carlo simulations and lines represent analytical results.

is evident. These results further corroborate our proposed model that maximizes the energy efficiency while pushing the throughput constraints to a minimum acceptable QoS. Moreover, we also observe that the EE achieved with a MRT scheme with $M_f^t = 3, M_f^r = 2$ in the femtocell tier is actually inferior to the SISO case. Additionally, we note that a simple MRC in the femtocell tier (MRT with $M_f^t = 1$) can actually outperform a MRT with multiple antennas at the FAP (MRT with $M_f^t > 1$). This result not only reinforces the previous statement about the gains in EE due to savings in energy resulting from the use of less RF chains, but it also shows that not all MIMO schemes achieve gains over a SISO case and the antenna configuration needs to be carefully selected for different combinations of diversity schemes.

In Figure 2.5 the EE of the system is presented when only the power related to transmission is considered at the transmitter (i.e., $b_f = b_m = 0$ in (2.24) and (2.25)). This scenario is important when the main concern in the system is the amount of transmit power radiated at the transmission side. The plots presented correspond to some of the schemes yielding the best performance (given all the possible schemes from table 2.2) and the SISO case is included for comparison purposes. It can be seen that increasing the number of available antennas at the transmitter side (for both macro- and femtocells) has the direct effect of increasing the EE in most of the configurations. So regardless of the number of femtocells deployed, the use of more antennas is usually desirable at the transmitter side. Additionally, the diversity schemes that provide the better results are the ones that use a higher number of the available antennas (from all those available), e.g. MRT (in which all RF chains are used), BF-SC (where all RF chains at the transmitter are used, while at the receiver only one RF remains turned on) and their combinations. In contrast, diversity schemes involving JAS (in which only one RF chain remains on at transmitter and receiver side) do not achieve the best performance in these scenarios. This can be understood intuitively, given the fact that by fixing the same amount of transmitted power for all configurations, the gains in throughput also account for higher gains in EE.

In Figure 2.6 the EE of the system is obtained when we consider the total power (i.e., transmit power plus all other power components) at the transmitter side. The configurations with the highest achieved EE, along with results for a SISO system, are all presented. It can be seen that the increase in the number of femtocells increases the EE of the system up to a certain threshold, after which the energy consumed by the femtocells outweighs the gain in throughput, thus reducing the overall EE. We observe that, when the mean number of femtocells deployed in the area of a macro-

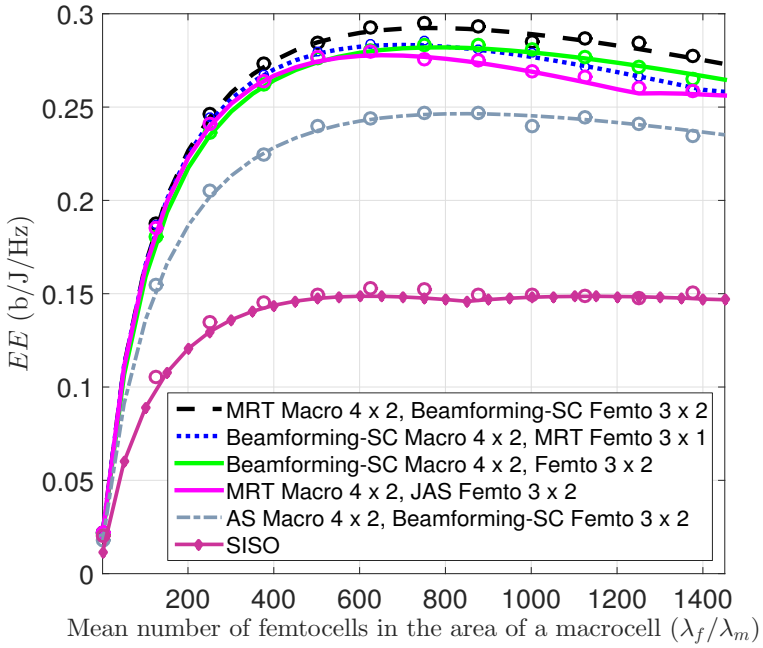

Figure 2.5: Energy efficiency (see EE in (2.2)) versus average number of femtocells in the area of a macro-cell $\left(\frac{\lambda_f}{\lambda_m}\right)$ with $b_f = b_m = 0$ in (2.24) and (2.25) (i.e., only transmit power considered). Circles represent Monte Carlo simulations and lines represent analytical results. (Note that table 2.2 shows all the possibilities that we have examined but only schemes with the most significant results are presented in the graphs - similar for the rest of figures).

cell is approximately below 390, the best performance in EE is provided by a system with AS-MRC at both the macro-cell and femtocell tier with $M_m^t = 4$, $M_m^r = 2$ and $M_f^t = 3$, $M_f^r = 2$. However, when the mean number of femtocells exceeds this value, a system with MRT at the macro-cell tier ($M_m^t = 4$, $M_m^r = 2$) and JAS at the femtocell tier ($M_f^t = 3$, $M_f^r = 2$) shows better results. These results show that the savings in power by not using all the RF chains is more beneficial to the EE than the gains in throughput obtained when all chains remain on. This is in contrast to the case when only the power used for transmission was considered. Moreover, for each antenna configuration there is a mean number of femtocells which maximizes the EE of that configuration. From the results we also observe that in the femtocell tier, the

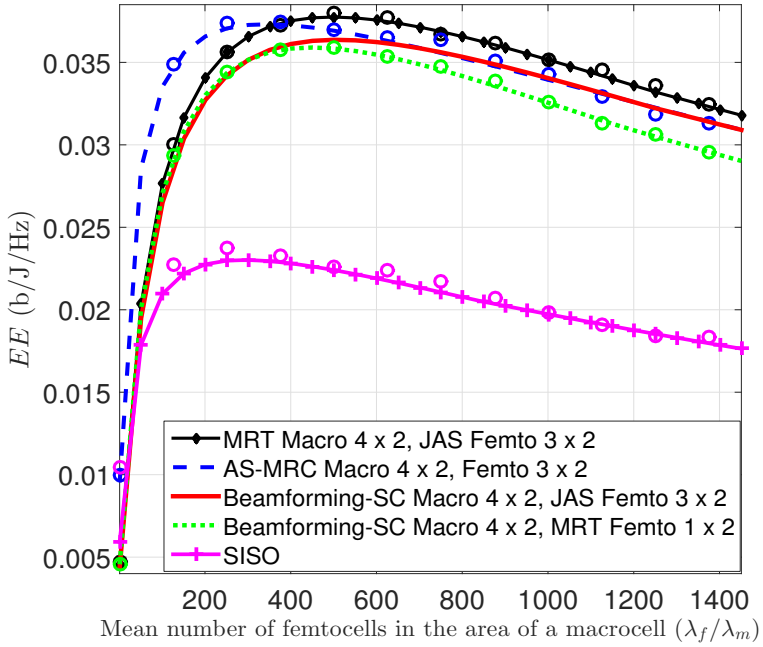

Figure 2.6: Energy efficiency (see EE in (2.2)) versus average number of femtocells in the area of a macro-cell $\left(\frac{\lambda_f}{\lambda_m}\right)$ with $b_f \neq b_m \neq 0$ in (2.24) and (2.25) (i.e., both transmit power and other sources included). Circles represent Monte Carlo simulations and lines represent analytical results.

power consumed in the RF chains has a greater effect on the total EE compared to the increased gains in throughput resulting from using all the RF chains. That is, the gains in throughput obtained have much lesser impact on the EE than the total power used when a higher number of antennas (and their respective RF chains) are employed.

In Figure 2.7 the improvements in the EE of the network can be observed when the femtocells are equipped with sleep mode capabilities (using (2.26)). The schemes which provided the highest gains in EE at high femtocell density are presented. It can be seen that the results can be divided into three regions. In the first region, the number of femtocells deployed is small enough so that the interference in this tier is low and deploying more femtocells is directly reflected in an increase in the EE of the system, up to a maximum value where the interference dominates the gains in throughput. In

the second region, the increase in the number of femtocells creates high interference in the tier, and so, the power consumed by the FAPs starts outweighing the increase in throughput, and the overall EE starts to decrease. Finally, there is a third region, in which the interference is still high and so there is not a lot of gain in the throughput, but the number of femtocells which start to go into sleep mode is higher, and the power savings associated with this boosts the overall EE of the system. It is interesting to see that the results can provide insight into two main behavioural parts: the diversity scheme (and antenna configuration) dominating part, and the sleep mode dominating part. It can be concluded that for relatively small interference in the femtocell tier, the highest gains in EE of the system come from the particular diversity scheme selected and the number of antennas used. Alternatively, for high interference, the savings in power consumption by using sleep mode have a bigger impact on the EE of the system than the achievable gains of the diversity schemes.

2.8 Conclusions

In this chapter, the achievable EE was obtained for different MIMO diversity schemes in a two-tier network consisting of macro-cells and femtocells. The optimal diversity schemes and antenna configurations were obtained for realistic parameters found in practice, and as we vary these parameters, (e.g., propagation exponent, wall partition loss and MBS density) the optimal configurations vary as well. The results illustrate the tradeoff between the energy consumption and the performance expected in terms of overall throughput. We observe that in general, for the macro-cell tier a higher number of antennas is normally desirable, regardless of the diversity scheme used. Additionally, the best performance in EE comes for a combination of different diversity

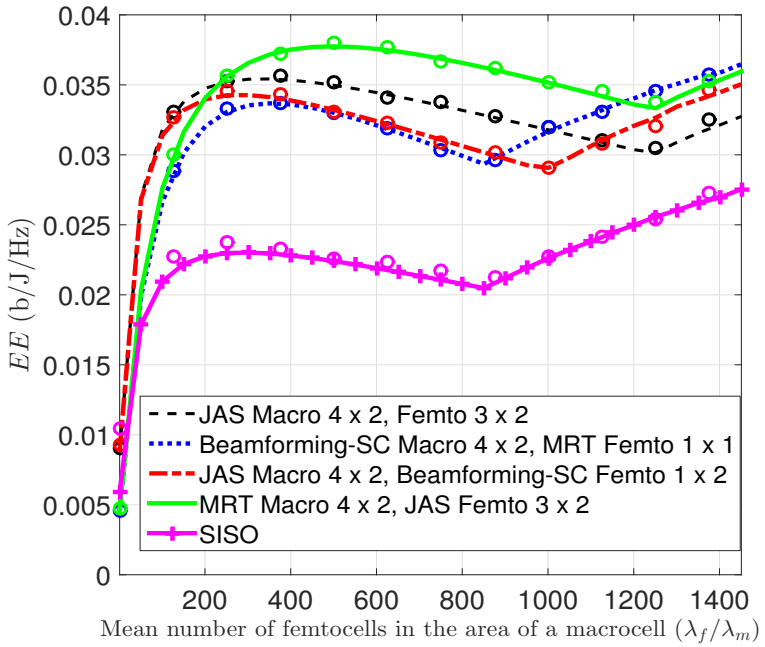

Figure 2.7: Effect of incorporating sleep mode on the EE (using (2.26)) versus average number of femtocells in the area of a macro-cell. Circles represent Monte Carlo simulations and lines represent analytical results.

schemes in the macro- and femtocell tier, along with their respective optimum antenna configurations.

Results also show that when only the RF transmission power is considered for the EE, the use of a larger number of antennas (on both femtocell and macro-cell downlink) increases the EE of the network (assuming the same transmitted power in all antenna configurations). Moreover, in this scenario diversity schemes using more RF chains such as combinations of MRT and BF-SC have the best performance. Alternatively, when other contributions to the overall network power consumption are also considered, a direct increase in the number of antennas can reflect gains in the EE, but the antenna configuration must be carefully selected in order to obtain gains in EE with respect to a SISO system. Furthermore, the optimal diversity schemes are normally the ones in which not all the antennas (and their respective RF chains) are used, such as

combinations of BF-SC and JAS. Further improvements in the EE of the system were observed by equipping femtocells with sleeping mode capabilities directly related to the medium access probability. We noted that there exists a threshold for the number of femtocells which can be deployed in the network. Below this threshold, the best performance in EE comes by having all the femtocells transmitting and the diversity schemes are the dominating factor. Alternatively, above this threshold some femtocells can be shut down, effectively increasing the EE and the sleep mode then becomes the dominating factor for the overall EE of the system. This latter case applies to scenarios with high traffic loads.

3 Antenna tilt angle design for EE improvements

IN THIS CHAPTER:

The antenna tilt optimization problem is addressed for a two-tier cellular network consisting of macrocells and femtocells, where both tiers share the same spectrum and their positions are modelled via two independent PPPs. First, we derive the coverage probability for a traditional cellular network consisting only of macrocells and obtain the optimum tilt angle that maximises the overall EE. Gains of up to 400% in EE were found for a scenario (approximately) equivalent to a hexagonal cell deployment with cell radius of 200 m when the optimum tilt was selected. We then proceed to model the HetNet scenario where femtocells are also deployed in the network's area. We observe that the macro users performance is highly sensitive to the interference emanating from the femtocell tier. In order to circumvent this issue, interference coordination by employing a guard zone for the macrocell user is proposed. Subsequently, we formulate a joint optimization problem where we derive both, the radius of a guard zone protecting the macro user and the tilt angle that maximize the EE of the network.

3.1 Introduction

In chapters 1 and 2 we elaborated on the importance that the EE of telecommunication systems has as a major aspect for future network deployments due to both, economi-

cal and ecological repercussions. Therefore, new techniques and algorithms are being deployed in order to address these aspects. Additionally, we pointed out that the deployment of HetNets has the potential benefit of increasing the overall system coverage and throughput by placing tiers of several smaller cells. This is supported by the fact that smaller cells can provide service to specific areas with the advantage of having a smaller path loss given that the transmitting base stations are placed closer to the users [8]. However, a large scale and unplanned deployment of these smaller cells can incur a significant power penalty if the EE is not considered in the design of the HetNet.

On the other hand, in order to cope to the ever changing demands and configurations of a network, Self Optimizing Networks (SONs) are being studied for future network deployments [57]. In principle, a SON pursues the goal of adapting to the changes in the conditions of the network to provide good performance in a fast and flexible manner. The response to the environmental changes in a SON should be made in an acute manner (agility), in an acceptable period of time (stability), and regardless of the increase in the size or scale of the system (scalability). Among the solutions considered in the context of SONs, the antenna tilt angle has been proposed as a way of self optimizing a network. The antenna tilt, defined as the angle of the main beam of the antenna below the horizontal plane [58], has the potential to achieve gains in the performance of the network by focusing most of the power radiated into a desired location. Additionally, with the use of a remote electrical tilt (RET), a network can reconfigure itself. That way, the performance of the network can be greatly enhanced without the need to physically change the position of the antennas in the BSs. Moreover, the antenna tilting design has been recognized by industry as a powerful technique for future SONs due to its impact on both the interference, and the coverage as

pointed out by JDS Uniphase Corporation in its white paper [59]. Furthermore, there have been extensive simulations in the past that have examined which antenna tilt angle provides the best gains for the network in terms of coverage and/or data rates. However, while considering a SON scenario, an open issue still remains as fast convergent algorithms are needed in order to cope with the rapid changes in network parameters. Moreover, it still remains unclear how the tilt angle should be adjusted in a HetNet to cope with the existence of other tiers of interferers in the network, while still achieving an acceptable performance.

Now, the use of stochastic geometry to model the behaviour of infrastructure-less networks such as ad-hoc and femtocell networks has been increasing over the past years and it has recently been expanded to the case of HetNets, [15,17,20,26,60]. This is due to the fact that it provides a means by which the behaviour of a network (where the nodes are randomly positioned) can be evaluated analytically and in a tractable manner. Hence, with the use of stochastic geometry, a network-wide characterization of the performance can be achieved. Therefore, in this chapter we address the issue of determining the tilt angle that maximizes the EE of a two-tier network consisting of macrocells and femtocells when constraints on the minimum Quality of Service (QoS) in each tier are considered. Employing well established tools from stochastic geometry, we model the positions of both, the macro base stations (MBSs) and the femtocell access points (FAPs) as independent Poisson Point Processes (PPPs). The use of PPPs to characterize the macrocell tier provides a lower bound on the actual performance of this tier with a tractable analytical framework [14,61,62]. This is in contrast with the typical hexagonal grid model, which provides an upper bound at the cost of tedious and time consuming simulations and/or numerical integrations. The proposed methodology takes into account the vertical pattern, while making use of the thinning property

of a PPP to characterize the behaviour on the horizontal plane. Thus, the developed model provides a realistic, yet accurate 3-D representation of a system, considering the antenna pattern. With the proposed PPPs we can provide an analytical framework from which the overall performance of the network can be evaluated without the need to run time and resource consuming simulations. We first address the issue of tilt optimization for a traditional cellular network (only macrocells deployed). We show the existence of an optimum tilt angle that maximizes both the coverage probability and the EE. Then, we analyse the case of a two-tier HetNet where both macro- and femtocell tiers share the same spectrum. It turns out that the interference created by the femtocells has a great effect on the macrocell users' performance. In order to cope with this issue, we propose an interference coordination scheme in which a guard zone protecting the macrocell user is utilized. Accordingly, we formulate an optimization problem over a guard zone radius (protecting the macrocell users from femto interference) and the tilt angle that would maximize the EE of the network with constraints on the minimum coverage probability of each tier.

3.1.1 Related Work

There have been a number of papers considering the issue of the antenna tilt optimization for cellular networks. However, in order to characterize the performance of the network, most of them make use of time consuming simulations and have only studied the case of a traditional cellular network consisting of macrocells only. In [58], a comparison in terms of coverage is carried out between systems with mechanical tilt, electrical tilt and a combination of both. The network is modelled with a hexagonal grid and through simulations, the optimum tilt angle is found for scenarios with different inter-site distance. In [63], an optimization problem is proposed for a network with

the presence of hotspots where a high number of users is identified. A hexagonal grid with cells having 3 sectors is assumed. The complexity of the original problem consisting of obtaining the tilt angle that maximizes the throughput of all users is first reduced by considering an optimization of the tilt over a center of gravity where a hot spot is located. Then, the system wide problem is decomposed into a local sub-problem which considers the triplet of adjacent (most interfering) sectors in order to find a decentralized solution. The same approach is followed in [64] but in the context of a network with macrocells and relays which are placed at random positions. At most one relay is placed in each base station sector to provide service where there is a coverage hole or where the concentration of users around that location forms a hotspot.

Now, in the case of HetNets, there are only a few works which consider the effect of the antenna tilt in the presence of other tiers of interferers. In [65] the issue of antenna tilt is addressed for both, a traditional network consisting of macro base stations and a HetNet considering the inclusion of femtocells to provide service to hotspots. The parameters used follow LTE specifications and the results are found via simulations. The emphasis of the chapter is to obtain a better performance in EE and throughput fairness (ratio of the cell edge users throughput to the cell mean user throughput). A reinforced machine learning algorithm is proposed, in which each base station individually can change its antenna tilt angle and the learning comes from observing the effects of the actions taken. In [66], direct and indirect (learning theory and game theory) biomimetrics approaches are studied in a scenario where macrocells are sectorized and each sector has at most one outdoor femtocell which acts as a fixed relay. In the direct approach, the original problem of optimizing the tilt angles (so that the aggregate throughput in all femtocells achieves a maximum), is decomposed into a local subproblem consisting of finding the optimum angle when a triplet of closest

interferers is considered in each case.

In contrast with the normal approach used when modelling wireless networks via PPP, recent works have moved one step forward towards more realistic models by including the antenna radiation pattern in the calculations. In [67], the authors developed a model to characterize the performance of a HetNet with directional antennas having a 2D radiation pattern. A methodology to characterize the performance of the network in terms of the coverage probability is proposed for a model in which a user is associated with the BS and sector which provides the highest long term (fading being averaged) received power. Moreover, authors analysed the performance of two different antenna patterns and compared the results with the omnidirectional case. In [68], the effect of the beamwidth and orientation error on the coverage and throughput were investigated for a system with directional antennas where transmitters rotate the foresight of their antennas towards the direction of the intended receivers. With the use of stochastic geometry a model was proposed for a network in which transmitters and receivers are located at a fixed distance. A simplification of the directional antenna pattern was made, in which the gains in the main and back lobes are considered to be constant. An extension of directional antennas to millimeter wave cellular networks has been considered in [69], where a line of sight (LOS) probability model was developed as a function of the distance between transmitter and receiver. Coverage and rate expressions are provided for a system where the impact of blockages is taken into account. The simplified model provided considers a fixed gain for the main and back lobes of the antennas, and an approximation of the LOS region as a ball with fixed size. A similar model has been used in [70] where a fixed value for both, the main and back lobes is considered in a millimeter wave system. A new model is proposed by taking into account the channel and blockage empirical models recently reported. Additionally, a

“two ball" approximation is proposed to model the state of the links. The model also accounts for beamforming pointing errors. Expressions for the expected coverage and data rates are provided for two cell association policies, namely, smallest path loss and the highest received power. The impact of the horizontal antenna pattern and blockages in a dense urban cellular network is presented in [71]. The authors quantized the accuracy of the point process model by comparing it with experimental data from an actual deployment of base stations. Additionally, the authors proposed models of both blockages and antenna pattern which result in a tractable analytical framework. Results showed that the point process is suitable for the modelling of future dense urban networks, when the models for blockages and antenna patterns are accurate.

3.1.2 CONTRIBUTIONS

In contrast to previous works on antenna tilt optimization, we follow a stochastic geometry approach to model the location of the base stations on the network for both, traditional cellular macro network and a HetNet consisting of macro- and femtocells. Employing the well established framework of point processes from stochastic geometry, we can obtain tractable expressions. These expressions can be employed to evaluate the overall performance of the network, without the need to run time consuming simulations, effectively providing a theoretical framework from which the performance of a traditional cellular macro network, and a HetNet can be analysed. Additionally, we address the case of an ultra dense user deployment in which the number of femtocells in the area can vary according to the number of users who purchase them, or through sleep mode scheduling, etc. Therefore, the density of femtocells changes according to the users’ needs and it is not a controlled variable, in contrast with scenarios where the tilt is modified in order to serve a particular hotspot. Thus, we can obtain pseudo

closed-form expressions with which the scalability of the network can be addressed. It is worthwhile noticing that the results cannot be used in a SON manner, as there is a need to solve the optimization problems formulated. However, these results provide an overall optimum performance in the entire network which could easily be used as a starting point for a SON algorithm or as a tool to adapt to a slowly varying network. The main contributions of this chapter are as follows.

- *Stochastic approach with full antenna pattern*: Most of the works where stochastic geometry has been used to model the network do not consider an antenna pattern and resort to an omnidirectional antenna assumption. On the other hand, works where an antenna pattern is considered (with the use of stochastic geometry) have traditionally focused on a 2-D horizontal antenna pattern [67–69, 71], and make use of a fixed main and back lobe gain. In this chapter we attempt to create a bridge between these two approaches by proposing a simplistic (yet realistic) model of the 3-D antenna pattern to go along with a stochastic approach for the positioning of the base stations. This is done by taking as baseline the antenna pattern model recommended by 3GPP [72] with some simplifications in the horizontal plane thanks to stochastic geometry properties. On the vertical plane, we make use of the exact antenna patter proposed in [72] which provides an exact characterization. Thus, the analysis is simplified while maintaining a realistic model.

- *Optimum tilt angle for a traditional network*: In contrast to previous works which deal with the horizontal antenna pattern properties, we focus on the impact of the vertical antenna pattern on the system performance. We derive coverage and EE formulas for the case of a traditional network. In this scenario, the opti-

mum tilt is the one that provides the best performance in terms of the coverage probability and EE. With the resulting expressions, the dependency of the optimum tilt angle on the density of the macrocells is investigated without the need to run time consuming scenario-specific simulations.

- *Optimum tilt angle for a two-tier network when both macro- and femtocells share the same resources*: In this scenario, as it was obtained from simulations, the interference from the femtocell tier to the macrocell users is really high, and so the performance in the macrocell tier is significantly deteriorated. Therefore, we propose the use of a guard zone to protect the macrocell user from the femto-tier interference. Then, we formulate an optimization problem to jointly select the optimum antenna tilt angle and guard zone that provide the highest EE of the network (when minimum constraints on Quality of Service (QoS) are considered for each tier).

3.1.3 Chapter Organization

The outline of this chapter is the following. The proposed system model is described in section 3.2 for both the macro and femto tiers. In section 3.3, we obtain the coverage probability expressions for both macrocells and femtocells. Section 3.4 describes the EE metric used and the optimization problems proposed. In section 3.5 we present the numerical results of this chapter. Finally, in section 3.6, concluding remarks are presented.

3.2 System Model

Consider the downlink of a two-tier cellular OFDMA system (such as LTE) consisting of macro- and femtocells, where both share the same resources for transmission, which are assigned as a time-frequency pair. Then in each time slot a user can be served on an available subchannel. We model the base stations in both tiers as independent Poisson Point Processes (PPPs) Φ_i, $i \in \{m, f\}$, where m and f stand respectively, for macro- and femtocell. The number of base stations N_i, follows a Poisson random variable with parameter λ_i, i.e. $N_i \sim \text{Pois}(\lambda_i \mathcal{S})$, $i \in \{m, f\}$, where $\mathcal{S}$ is the deployment area of the network. The base stations are randomly (uniformly) distributed across $\mathcal{S}$. The assumption of femtocells modelled as a PPP follow the lines of other works [31, 33, 73, 74] where it is assumed that users acquire their FAPs and place them inside their houses, offices, etc., where an increase in coverage and/or data rates is required. The propagation model is a composite of Rayleigh fading (with $h_{j,i} \sim \mathcal{CN}(0, 1)$ representing the channel between j-th transmitter and i-th receiver) and path loss $l(R) = R^{-\alpha_i}$, dependent on the distance R from transmitter to receiver and the path loss exponent α_i, $i \in \{m, f\}$. Each MBS is assumed to be sectorized with N_s sectors. We assume an ultra dense user scenario where all base stations always have a user to serve and also assume that a symbol $s_{j,k}$, is sent in each time slot, where $\mathbb{E}\left[|s_{j,k}|^2\right] = 1$. We also assume that all N_s sectors operate in a different subchannel. In the macrocell tier, each user connects to the base station which provides the highest long term expected received power. In other words, the users will be assigned to the closest base station. Under this scheme, the network cells form a Voronoi tessellation [14]. This means that the size (and shape) of the macrocells are variable, in contrast with the typical regular grid shapes commonly used (e.g., the hexagonal grid). In order to provide a realistic

scenario for the sizes of the macrocells, we match the mean area of a Voronoi cell with the area of a hexagonal grid cell, e.g., in a PPP with density value of $\lambda = 1.54$ x 10^{-6} the (mean) Voronoi cell area corresponds to that of a hexagonal shape cell with radius 500 m, approximately. In the case of femtocells, we assume that each FAP has a user to serve and which is located indoors and uniformly distributed in the femtocell coverage area with radius R_f. The FAP radiation pattern is assumed to be omnidirectional in accordance with 3GGP specifications [44]. Also according to LTE specifications, for the MBSs we model the antenna vertical radiation pattern G, which expressed in [75] as

$$G_{dB}(\phi_{tilt}) = -\min\left(12\left(\frac{\phi + \phi_{tilt}}{\phi_{3dB}}\right)^2, A_{dB}\right) \tag{3.1}$$

where $\phi < 0$ is the angle between the base station antenna and the receiver, $\phi_{tilt} > 0$ is the tilt angle, ϕ_{3dB} represents the 3 dB beamwidth with value 10, and A_{dB} is the minimum power which is leaked to the sectors other than the desired one, and which has a typical value of 20 dB. As for the horizontal plane, we make use of the thinning property of a PPP, and so we thin the PPP by a factor equal to the number of sectors, i.e., we consider an omnidirectional pattern in the horizontal plane, but the effective density of interferers is expressed as $\frac{\lambda}{N_s}$. This assumption is justified given that in the downlink, the radiation pattern of the antennas is symmetric in the horizontal plane, i.e., modifying the pattern of all antennas in the network similarly (as a result of sectorization) does not modify significantly the SIR perceived by the desired user. In addition, as each sector is assumed to operate in a different subchannel, the interference is reduced by a factor of N_s. In section 3.5 the accuracy of this assumption is verified. The angle (ϕ) between the base station antenna and the desired user's antenna can be expressed as a function of the effective height H_{eff} (difference in heights between

transmitter and receiver antenna), and the distance R between the transmitting base station and a receiver, as

$$\phi = -\tan^{-1}\left(\frac{H_{eff}}{R}\right) \tag{3.2}$$

where $H_{eff} = H_a - H_{ue}$ represents the effective height that results from substracting the user equipment's height H_{ue} from the base station's antenna height H_a. Applying this definition to (3.1), and converting to linear scale, we obtain

$$G(R,\phi_{tilt}) = 10^{-\min\left(12\left(\frac{-\tan^{-1}\left(\frac{H_{eff}}{R}\right)+\phi_{tilt}}{\phi_{3dB}}\right)^2, A_{dB}\right)/10}. \tag{3.3}$$

The antenna vertical pattern as well as the tilt angle are depicted in Figure 3.1. Now, from the definition of (3.3) we observe that $G(R,\phi_{tilt})$ can be divided into 2 or 3 parts (depending upon the tilt angle), because of the limiting value of A_{dB}. So, for small values of ϕ_{tilt}, there is only a value of $R = r_{th1}$ at which $G(R,\phi_{tilt})_{dB}$ reaches $-A_{dB}$. However, when ϕ_{tilt} is large enough, there are two values of R (r_{th1} and r_{th2}) at which the function reaches its limit. And so, solving for the threshold distances r_{th1} and r_{th2}, we obtain

$$r_{th1} = \frac{H_{eff}}{\tan\left(\sqrt{A_{\text{dB}}/12}\ \phi_{3dB} + \phi_{tilt}\right)} \tag{3.4}$$

$$r_{th2} = \frac{H_{eff}}{\tan\left(-\sqrt{A_{\text{dB}}/12}\ \phi_{3dB} + \phi_{tilt}\right)}. \tag{3.5}$$

Note from Eq. (3.5) that r_{th2} only takes positive values when the condition $\phi_{tilt} \geq$

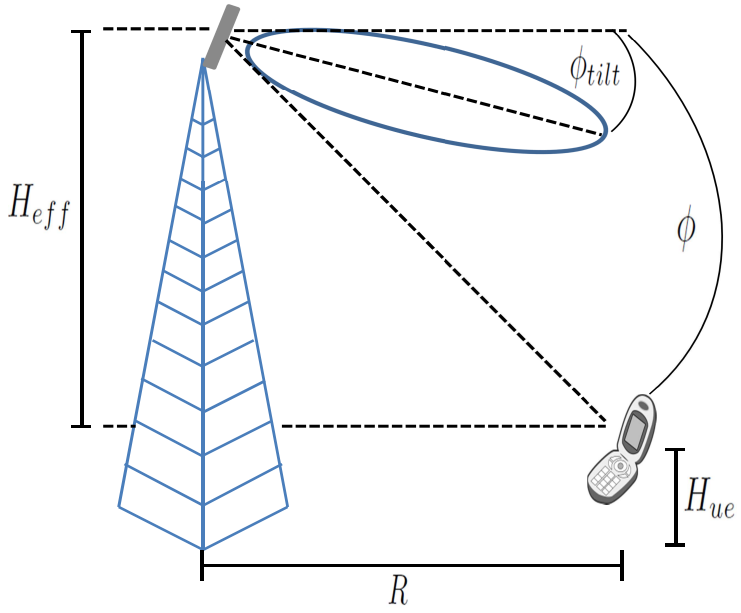

Figure 3.1: Vertical antenna pattern and tilt angle.

$\sqrt{A_{\text{dB}}/12}\ \phi_{3dB}$ is fulfilled, and so, Eq. (3.3) can be expressed as follows

$$G(R,\phi_{tilt}) = \begin{cases} A, & \text{if } R < r_{th1} \\ 10^{-1.2\left(\frac{-\tan^{-1}\left(\frac{H_{eff}}{R}\right)+\phi_{tilt}}{\phi_{3dB}}\right)^2}, & \text{if } R \geq r_{th1} \end{cases} \tag{3.6}$$

for $\phi_{tilt} < \sqrt{A_{dB}/12}\ \phi_{3dB}$, and

$$G(R,\phi_{tilt}) = \begin{cases} A, & \text{if } R < r_{th1} \\ 10^{-1.2\left(\frac{-\tan^{-1}\left(\frac{H_{eff}}{R}\right)+\phi_{tilt}}{\phi_{3dB}}\right)^2}, & \text{if } r_{th1} \leq R < r_{th2} \\ A, & \text{if } R \geq r_{th2} \end{cases} \tag{3.7}$$

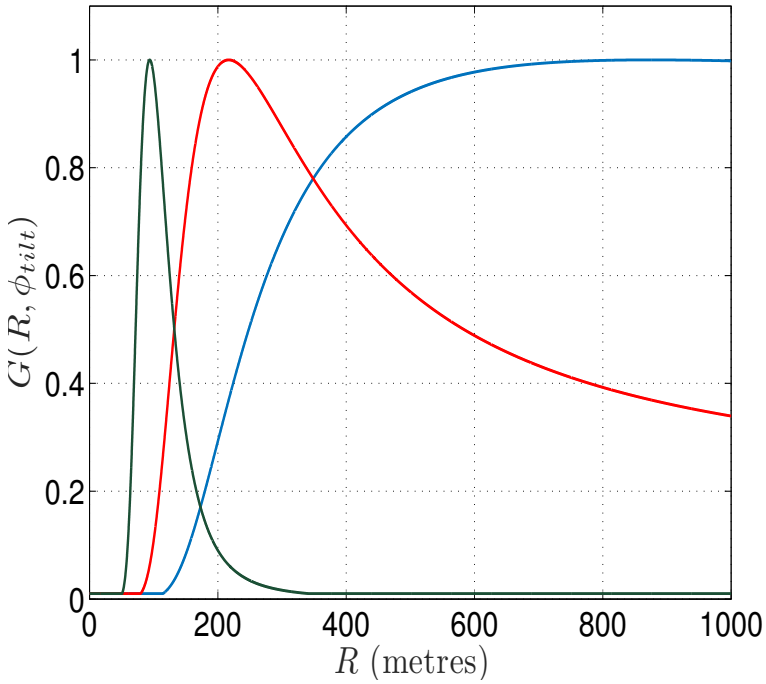

Figure 3.2: Vertical antenna pattern (3.3), as a function of the distance R from base station to the user for antenna tilt values $\phi_{tilt} = 2°, 8°$ and $18°$. Note that depending on the tilt angle, the shape of the lines change and the function can be further defined by parts as in (3.6) or (3.7).

for $\phi_{tilt} \geq \sqrt{A_{dB}/12}\ \phi_{3dB}$, where A is the value of $-A_{dB}$ in linear scale. The vertical antenna pattern, re-defined in terms of the distance from the MBS to the user, is presented in Figure 3.2 for values of antenna tilt $\phi_{tilt} = 2°, 8°$ and $18°$. Note that the maximum angle between the user and the MBS is $0°$, when $R \to \infty$, and so the horizontal axis sets a limit on the values that the function $G(R, \phi_{tilt})$ can take. Therefore, it can be seen that when the antenna tilt is small ($\phi_{tilt} < \sqrt{A_{dB}/12}\ \phi_{3dB}$) the function is defined by 2 parts as in (3.6) because the function $G(R, \phi_{tilt})$ never reaches the value A as R increases. However, as the tilt angle becomes large enough ($\phi_{tilt} \geq \sqrt{A_{dB}/12}\ \phi_{3dB}$), the function is now defined by 3 parts as in (3.7) due to the fact that for a given value of R the function does attain value A.

3.3 Coverage

In this section, we obtain the coverage probability expressions first for a traditional network (macrocells only) and then for a HetNet consisting of femtocells overlaid with the macrocell tier. We consider an interference limited scenario, and so the effect of noise will be neglected. However, it could be easily included into the calculations in a straightforward manner.

3.3.1 Traditional Macrocell Network

For a macrocell traditional network, there is one PPP Φ_m used to model the positions of the MBSs. Considering that the user connects to the closest MBS, the received signal at the user in a given time slot is expressed as

$$y = \sqrt{P_m^{tx}\, l\left(r_{0,0}\right) G(r_{0,0}, \phi_{tilt})}\; h_{0,0}\, s_{0,0} + \sum_{j \in \Phi_m \setminus \{0\}} \sqrt{P_m^{tx}\; l\left(r_{j,0}\right) G(r_{j,0}, \phi_{tilt})}\; h_{j,0}\, s_{j,j} \tag{3.8}$$

where P_m^{tx} is the MBS transmit power, $r_{j,k}$, $h_{j,k}$ and $s_{j,k}$ are respectively, the distance, channel gain and symbol sent from the j-th base station to the k-th user. Note that $r_{0,0}$ represents the distance from the closest base station to the desired user. For ease of representation we drop the subscripts in the desired link. Using Slivnyak's theorem [16], placing a typical point at the origin does not change the statistics of the PPP, and so we locate the typical user at the origin and obtain its statistics. The signal to interference ratio (SIR) is given by

$$SIR = \frac{|h|^2\, r^{-\alpha}\, G(r, \phi_{tilt})}{\sum\limits_{j \in \Phi_m \setminus \{0\}} |h_{j,0}|^2\, r_{j,0}^{-\alpha}\, G(r_{j,0}, \phi_{tilt})}$$

$$= \frac{|h|^2 \, r^{-\alpha} \, G(r, \phi_{tilt})}{I_{\Phi_m}} \tag{3.9}$$

where I_{Φ_m} is the effective interference from the base stations and $|h_{j,k}|^2 \sim \text{Exp}(1)$. The coverage probability $\mathcal{P}^c$ is defined as the probability that the received SIR in the entire service area is above a certain threshold β, which depends on the network's Quality of Service (QoS). From (3.9), we have

$$\begin{aligned}
\mathcal{P}^c(\beta, \phi_{tilt}) &= \mathbb{P}(SIR > \beta) \\
&= \mathbb{E}_{r, I_{\Phi_m}} \left[\exp\left(-s \, I_{\Phi_m}\right) \right] \big|_{s = \beta r^{\alpha} \, G(r, \phi_{tilt})} \\
&= \mathbb{E}_r \left[\mathbb{E}_{I_{\Phi_m}} \left[\exp\left(-s \, I_{\Phi_m}\right) \right] \right] \\
&= \mathbb{E}_r \left[\mathcal{L}_{I_{\Phi_m}}(s) \right]
\end{aligned} \tag{3.10}$$

where $\mathcal{L}_{I_{\Phi_m}}(s)$ is the Laplace transform of the interference I_{Φ_m}, and the expectation with respect to r is obtained using the fact that the distance to the closest base station for a PPP is Rayleigh distributed [14], i.e. $f(r) = 2\pi\lambda r \, e^{-\lambda \pi r^2}$. The value of the Laplace transform is expressed as

$$\begin{aligned}
\mathcal{L}_{I_{\Phi_m}}(s) &= \mathbb{E}_{\Phi_m, |h_{j,0}|^2} \left[e^{-s \sum\limits_{j \in \Phi_m} |h_{j,0}|^2 \, r_{j,0}^{-\alpha} \, G(r_{j,0}, \phi_{tilt})} \right] \\
&= \mathbb{E}_{\Phi_m} \left[\prod_{j \in \Phi_m} \mathbb{E}_{|h_{j,0}|^2} \left[e^{-s \, |h_{j,0}|^2 \, r_{j,0}^{-\alpha} \, G(r_{j,0}, \phi_{tilt})} \right] \right].
\end{aligned} \tag{3.11}$$

Given the fact that $|h_{j,0}|^2$ is independent for all $j \in \Phi_m$ and $|h_{j,0}|^2 \sim \text{Exp}(1)$, by taking the inner expectation in (3.11), we obtain

$$\mathcal{L}_{I_{\Phi_m}}(s) = \mathbb{E}_{\Phi_m} \left[\prod_{j \in \Phi_m} \left(1 + s \, r_{j,0}^{-\alpha} \, G(r_{j,0}, \phi_{tilt}) \right)^{-1} \right]. \tag{3.12}$$

Using the definition of the generating functional of a PPP [16] we obtain

$$\mathcal{L}_{I_{\Phi_m}}(s) = \exp\left(-\frac{2\pi\lambda_m}{Ns}\int_r^\infty \frac{y\ \mathrm{d}y}{1+s^{-1}\,y^{\alpha_m}\,G^{-1}(y,\phi_{tilt})}\right)$$
$$= \exp\left(-\frac{2\pi\lambda_m}{Ns}\int_r^\infty \frac{y\ \mathrm{d}y}{1+\left(\frac{y}{r}\right)^{\alpha_m}\frac{G^{-1}(y,\phi_{tilt})}{\beta\,G^{-1}(r,\phi_{tilt})}}\right). \tag{3.13}$$

Substituting (3.13) into (3.10), and using the definitions in (3.6) and (3.7) the following theorem describing the coverage probability is obtained.

Theorem 3.1. *In a macrocell-only network with full antenna pattern, the coverage probability can be expressed as in (3.15), where* $\zeta(a,b) = {}_2F_1\left(1,1-\frac{2}{a};2-\frac{2}{a};-b\right)$ *is the Gauss hypergeometric function,* $\rho(a,b,c) = \int_a^b \frac{y\,dy}{1+\left(\frac{y}{r}\right)^{\alpha_m}c}$, *and we made use of the following function definition*

$$F(a,\phi_{tilt}) = 10^{-1.2\left(\frac{-\tan^{-1}\left(\frac{H_{eff}}{a}\right)+\phi_{tilt}}{\phi_{3dB}}\right)^2}. \tag{3.14}$$

Proof. The derivation of (3.15) is found in appendix C. □

3.3.2 Heterogeneous network

We now consider the case of a HetNet consisting of macro- and femtocells deployed in the coverage area. The femtocells are assumed to operate in CSG, meaning that they only serve their subscribed users which are assumed to be located indoors. As mentioned in section 3.2, the antennas of the FAPs are all assumed to have an omnidirectional pattern [44]. The FAPs are also assumed to operate on the same frequencies

$$\mathcal{P}^c(\beta,\phi_{tilt}) = \begin{cases} \int_0^{r_{th1}} 2\lambda_m\pi r \;\; e^{-\lambda_m\pi\left(r^2+\frac{2}{Ns}\left[\frac{\beta r^{\alpha_m}}{\alpha_m-2}\left(r^{-\alpha_m-2}\,\zeta_1-r_{th1}^{-\alpha_m+2}\,\zeta_2\right)+\rho_1\right]\right)}\, dr \\ + \int_{r_{th1}}^{\infty} 2\lambda_m\pi r \;\; e^{-\lambda_m\pi\left(r^2+\frac{2}{Ns}\rho_2\right)}\, dr \\ \text{if } \phi_{tilt} < \sqrt{\frac{A_{dB}}{12}}\;\; \phi_{3dB} \\ \int_0^{r_{th1}} 2\lambda_m\pi r \;\; e^{-\lambda_m\pi\left(r^2+\frac{2}{Ns}\left[\frac{\beta r_m^{\alpha}}{\alpha_m-2}\left(r^{-\alpha_m+2}\,\zeta_1-r_{th1}^{-\alpha_m+2}\,\zeta_2\right)+r_{th2}^{-\alpha_m+2}\zeta_3+\rho_3\right]\right)}\, dr \\ + \int_{r_{th1}}^{r_{th2}} 2\lambda_m\pi r \;\; e^{-\lambda_m\pi\left(r^2+\frac{2}{Ns}\left[\rho_4+\frac{\beta AF^{-1}(r,\phi_{tilt})\, r^{\alpha_m} r_{th2}^{-\alpha_m+2}}{(\alpha_m-2)}\,\zeta_4\right]\right)}\, dr \\ + \frac{\exp\left(-\lambda_m\pi r_{th2}^2\left(1+\frac{2}{Ns}\left[\frac{\beta}{\alpha_m-2}\,\zeta_1\right]\right)\right)}{1+\frac{2}{Ns}\left(\frac{\beta}{\alpha_m-2}\zeta_1\right)} \\ \text{if } \phi_{tilt} \geq \sqrt{\frac{A_{dB}}{12}}\;\; \phi_{3dB} \end{cases} \tag{3.15}$$

with $\zeta_1 = \zeta\left(\alpha_m,\beta\right), \zeta_2 = \zeta\left(\alpha_m, \left(\frac{r_{th1}}{r}\right)^{-\alpha_m}\beta\right), \zeta_3 = \zeta\left(\alpha_m, \left(\frac{r_{th2}}{r}\right)^{-\alpha_m}\beta\right), \zeta_4 = \zeta\left(\alpha_m, \left(\frac{r_{th2}}{r}\right)^{-\alpha_m}\beta AF^{-1}(r,\phi_{tilt})\right)$,
$\rho_1 = \rho\left(r_{th1},\infty,\frac{AF^{-1}(y,\phi_{tilt})}{\beta}\right), \rho_2 = \rho\left(r,\infty,\frac{F^{-1}(y,\phi_{tilt})}{\beta\, F^{-1}(r,\phi_{tilt})}\right), \rho_3 = \rho\left(r_{th1},r_{th2},\frac{AF^{-1}(y,\phi_{tilt})}{\beta}\right), \rho_4 = \rho\left(r,r_{th2},\frac{F^{-1}(y,\phi_{tilt})}{\beta\, F^{-1}(r,\phi_{tilt})}\right)$.

as the macrocells. Therefore, there is inter-tier interference from macro- to femtocells and vice-versa. As previously stated, the femtocell users are uniformly distributed in the coverage area of their serving FAP, which corresponds to a circular area of radius R_f. A wall partition loss W_f, defined as the amount of power which is lost when the signal goes through a wall, is also considered.

Now, as the macrocell users are seriously affected by the femtocell tier interference, we propose the use of a guard zone with radius R_c protecting the macrocell users from the nearby FAPs interference. In this scenario, a cooperation is assumed between

femto and macro tiers, where if femtocells detect a macrocell user within a distance R_c, they will restrain themselves from transmitting. This assumption is supported by considering that both macro and femtocells are deployed by the same network operator, which can have an estimate on the location of their macrocell users. This information in turn, can be made available to femtocells by means of a macro to femto interface, such as the X2 interface. This model is then equivalent to having a macrocell user with a guard zone preventing any femtocell transmissions within a distance R_c. The potential use of a guard zone has been reported previously to protect a given user from interference [60, 76]. So, with this model we analyse the effect of the guard zone and the tilt angle when changes in the density of femtocells are perceived. Once again, we place the typical users at the origin and then, the received signals by a macrocell user (y_m) and femtocell user (y_f) are given by

$$y_m = \sqrt{P_m^{tx}\, l\,(r_{0,0})\, G(r_{0,0}, \phi_{tilt})}\;\; h_{0,0}\, s_{0,0} + \sum_{j \in \Phi_m \setminus \{0\}} \sqrt{P_m^{tx}\;\, l\,(r_{j,0})\, G(r_{j,0}, \phi_{tilt})}\;\; h_{j,0}\, s_{j,j} + \sum_{k \in \Phi_f} \sqrt{P_f^{tx}\;\, l\,(d_{k,0})\, W_f}\;\; g_{k,0}\, z_{k,k} \tag{3.16}$$

$$y_f = \sqrt{P_f^{tx}\, l\,(d_{0,0})}\;\; g_{0,0}\, z_{0,0} + \sum_{j \in \Phi_m} \sqrt{P_m^{tx}\;\, l\,(r_{j,0})\, G(r_{j,0}, \phi_{tilt}) W_f}\;\; h_{j,0}\, s_{j,j} + \sum_{k \in \Phi_f' \setminus \{0\}} \sqrt{P_f^{tx}\;\, l\,(d_{k,0})\, W_f^2}\;\; g_{k,0}\, z_{k,k} \tag{3.17}$$

where $\mathcal{B}(x, b)$ represents the 2-dimensional ball with radius b centered at x, P_m^{tx} (P_f^{tx}) is the transmission power of a MBS(FAP), $r_{j,k}$ ($d_{j,k}$) is the distance from the j-th MBS (FAP) to the k-th user, $h_{j,k}$ ($g_{j,k}$) is the Rayleigh fading channel between the j-th MBS (FAP) and the k-th user and $s_{j,k}$ ($z_{j,k}$) is the transmitted symbol from the j-th MBS

(FAP) to the k-th user, with $|s_{j,k}|^2 = 1$ ($|z_{j,k}|^2 = 1$). Additionally, Φ'_f represents the femtocell resulting point process after all FAPs that fall within the guard zone of a macrocell user have been removed in each macrocell. Note that in the femtocell tier, we use W_f^2 given the assumption that femtocell users are located indoors, and so the interfering signal has to get through two walls. For ease of representation, from now on we drop the subscript in the desired links. The SIRs are given as

$$SIR_m = \frac{|h|^2 \, r^{-\alpha_m} \, G(r, \phi_{tilt})}{I^m_{\Phi_m} + I^m_{\Phi'_f}} \tag{3.18}$$

$$SIR_f = \frac{|g|^2 \, d^{-\alpha_f}}{I^f_{\Phi_m} + I^f_{\Phi'_f}} \tag{3.19}$$

where $I^m_{\Phi_m} = \sum\limits_{j \in \Phi_m \setminus \{0\}} |h_{j,0}|^2 \, r_{j,0}^{-\alpha_m} \, G(r_{j,0}, \phi_{tilt})$ and $I^m_{\Phi'_f} = \sum\limits_{k \in \Phi'_f} |g_{j,0}|^2 \eta \; d_{k,0}^{-\alpha_f} W_f$, represent, respectively, the interference from the macrocell and femtocell tier observed by the macrocell user. Additionally, $I^f_{\Phi_m} = \sum\limits_{j \in \Phi_m} |h_{j,0}|^2 \, r_{j,0}^{-\alpha_m} \, G(r_{j,0}, \phi_{tilt})$ and $I^f_{\Phi'_f} = \sum\limits_{k \in \Phi'_f \setminus \{0\}} |g_{k,0}|^2 \, d_{k,0}^{-\alpha} W_f^2$ represent, respectively, the interference from the macrocell and femtocell tier perceived by the femtocell user. Following the same approach as for the traditional network, the coverage probability in the macrocell tier is given as

$$\begin{aligned}
\mathcal{P}^c_m(\beta_m, \phi_{tilt}) &= \mathbb{P}(SIR_m > \beta_m) \\
&= \mathbb{E}_{r, I^m_{\Phi_m}, I^m_{\Phi'_f}} \left[\exp\left(-s \, I^m_{\Phi_m}\right) \exp\left(-\eta W_f s \, I^m_{\Phi'_f}\right) \right] \\
&= \mathbb{E}_r \left[\mathbb{E}_{I^m_{\Phi_m}} \left[\exp\left(-s \, I^m_{\Phi_m}\right) \right] \mathbb{E}_{I^m_{\Phi'_f}} \left[\exp\left(-\eta W_f s \, I^m_{\Phi'_f}\right) \right] \right] \\
&= \mathbb{E}_r \left[\mathcal{L}_{I^m_{\Phi_m}}(s) \, \mathcal{L}_{I^m_{\Phi'_f}}(\eta W_f s) \right]
\end{aligned} \tag{3.20}$$

where $s = \beta_m r_m^{\alpha} \, G^{-1}(r, \phi_{tilt})$ and $\eta = \frac{P^{tx}_f}{P^{tx}_m}$. The Laplace transform of the macrocell

tier can be expressed as

$$\mathcal{L}_{I^m_{\Phi_m}}(s) = \exp\left(-\frac{2\pi\lambda_m}{Ns}\int_r^\infty \frac{y\ \mathrm{d}y}{1+\left(\frac{y}{r}\right)^{\alpha_m}\ \frac{F^{-1}(y,\phi_{tilt})}{\beta_m\ F^{-1}(r,\phi_{tilt})}}\right). \tag{3.21}$$

where the definition of the generating functional of a PPP was again used. It is worthwhile to notice that we have approximated (3.3) by (3.14) in this case. This approximation was not used in section 3.3.1, because a macrocell only network, not providing a minimum radiated power (A_{dB}), results in not considering the minimum amount of interference leaked, which in turn is reflected in the optimum tilt angle always taking the maximum allowable value. In the case of the HetNet, this assumption is possible, since the femtocell tier provides the baseline interference. Note also that the Laplace transform for the macrocell interference I_{Φ_m} can be neglected in some scenarios where a large number of femtocells are deployed in the area. This depends on the values of the wall partition loss and path loss exponent. This assumption can greatly simplify the analysis (and speed up the result of the proposed optimization).

On the other hand, the Laplace transform of the interference from femtocells to macrocells ($L^m_{\Phi'_f}$) forms a hole point process for which an approximation (lower bound) can be expressed by considering the interference outside R_c and using the formula for Rayleigh fading in [77]. The Laplace transform is then given by

$$\mathcal{L}_{I^m_{\Phi'_f}}(\eta W_f s) = e^{-\lambda_f\pi\left((\eta W_f s)^{\delta_f}\mathbb{E}_h\left[h^{\delta_f}\gamma\left(1-\delta_f,\eta W_f s h R_c^{-\alpha_f}\right)\right]-\frac{R_c^2\eta s}{\eta W_f s+R_c^{\alpha_f}}\right)} \tag{3.22}$$

where $h \sim \mathrm{Exp}(1)$. We further extend (3.22) and express $\mathcal{L}_{I^m_{\Phi'_f}}$ as

$$\mathcal{L}_{I^m_{\Phi'_f}}(\eta W_f s) = e^{\lambda_f\pi R_c^2} \times e^{-\lambda_f\pi R_c^2\ {}_2F_1\left(1,-\delta_f;1-\delta_f;-\beta_m r^{\alpha_m} F^{-1}(r)\eta W_f R_c^{-\alpha_f}\right)}. \tag{3.23}$$

The derivation of (3.23) is given in appendix C. The following theorem describes the coverage probability for the macrocell tier.

Theorem 3.2. *In a two-tier heterogeneous network with full antenna pattern, the coverage probability in the macrocell tier is expresed as in (3.28), where* $C\left(\alpha_m, \phi_{tilt}, r\right) = \int_r^\infty \frac{y \ \mathrm{d}y}{1+\left(\frac{y}{r}\right)^{\alpha_m} \frac{F^{-1}(y,\phi_{tilt})}{\beta_m \ F^{-1}(r,\phi_{tilt})}}$.

Proof. The macrocell tier coverage probability in (3.28) is found using the expressions for the Laplace transforms found in (3.21) and (3.23). □

In the case of the femtocell tier, the number of femtocells which are interfering with each other is reduced due to the fact that all the femtocells, which fall within the circular area formed by a radius R_c surrounding a macrocell user, will not transmit. Therefore, we use the thinning property of a PPP [16], in which case the effective density of interfering femtocells is given by $p\lambda_f$, where p is the thinning probability. Consider $\mathcal{V} = \bigcup_{j\in\Phi_m} \mathcal{V}_j$ as the set of all Voronoi cells formed from the PPP Φ_m, where $\mathcal{V}_j$ represents the Voronoi cell having point $x_j \in \Phi_m$ as seed. The thinning probability represents the probability that a femtocell placed at a point $x_k \in \Phi_f$ is located inside a Voronoi cell $\mathcal{V}_j$ and outside the area with radius R_c surrounding a macrocell user located at a point x_u uniformly distributed inside V_j. This applies to all the Voronoi cells in the network as we consider that all cells have a user to serve in each time slot.

Thus, the thinning probability can be expressed as

$$\begin{aligned} p &= \mathbb{P}(x_k \notin \mathcal{B}(x_u, R_c) \mid x_k \in \mathcal{V}_j),\ \forall j \in \Phi_m \\ &= 1 - \mathbb{P}(x_k \in \mathcal{B}(x_u, R_c) \mid x_k \in \mathcal{V}_j) \\ &\overset{(a)}{\approx} 1 - \frac{\pi R_c^2}{A_{cell}} \\ &= 1 - \lambda_m \pi R_c^2 \end{aligned} \tag{3.24}$$

where A_{cell} is the typical (mean) area of a Voronoi cell, which is by definition $A_{cell} = \frac{1}{\lambda_m}$. Note that the approximation in step (a) is obtained by using the ratio of the circular area covered by a radius R_c and the area of the Voronoi cell. Note also from (3.24), that the maximum radius permissible is $R_c^{max} = \frac{1}{\sqrt{\lambda_m \pi}}$. With this value the area covered by the guard zone equals the mean value of the Voronoi cells. Now, because a femtocell will only transmit if it is outside a radius R_c from a macrocell user, there can be two types of outage: the first is the one that occurs when a femtocell does not transmit (with probability $1 - p$) and second is one that takes place when the femtocell does transmit (with probability p) but the perceived SIR_f at the femtocell user is below β_f. Taking this into account, we obtain the mean coverage probability for the femtocell tier as

$$\begin{aligned} \mathcal{P}_f^c(\beta_f, \phi_{tilt}) &= p\, \mathbb{P}(SIR_f > \beta_f) \\ &= (1 - \lambda_m \pi R_c^2) \times \\ &\quad \mathbb{E}_d \left[\mathbb{E}_{I^f_{\Phi_m}} \left[\exp\left(-s' \eta^{-1} d^{\alpha_0}\, I^f_{\Phi_m} \right) \right] \mathbb{E}_{I^f_{\Phi'_f}} \left[\exp\left(-s' W_f d^{\alpha_0}\, I^f_{\Phi_f} \right) \right] \right] \\ &= (1 - \lambda_m \pi R_c^2)\, \mathbb{E}_d \left[\mathcal{L}_{I^f_{\Phi_m}} (s' \eta^{-1} d^{\alpha_0})\, \mathcal{L}_{I^f_{\Phi'_f}} (s' W_f d^{\alpha_0}) \right] \end{aligned} \tag{3.25}$$

where $s' = \beta_f W_f$. In order to simplify the analysis, and thanks to the small expected

distances between femtocells users and their serving FAPs, we use Jensen's inequality in (3.25), in which case the femtocell coverage probability is approximated by

$$\mathcal{P}_f^c(\beta_f, \phi_{tilt}) \approx (1 - \lambda_m \pi R_c^2)\, \mathcal{L}_{I^f_{\Phi_m}}(s'\eta^{-1}\bar{R_f}^{\alpha_0})\, \mathcal{L}_{I^f_{\Phi'_f}}(s'W_f\bar{R_f}^{\alpha_0}) \tag{3.26}$$

where $\bar{R_f} = \frac{2R_f}{3}$, is the expected value of the distance from femtocell users to their designated FAP. This expected value was found using the fact that the pdf of the distance D to the origin of a user uniformly distributed in a circular area of radius R_f is $f_D(d) = \frac{2d}{R_f^2}$ [31]. The results of simulations presented in section 3.5 show that this approximation is indeed very accurate. Using the definition of the generating functional of a PPP like in the macrocell only case, the Laplace transform of the macrocell interference can be expressed as

$$\mathcal{L}_{I^f_{\Phi_m}}(s'\eta^{-1}\bar{R_f}^{\alpha_0}) = e^{-\frac{2\pi\lambda_m}{N_s}\int_0^\infty \frac{x\,dx}{1+\beta_f^{-1}\bar{R_f}^{-\alpha_0}F^{-1}(x,\phi_{tilt})x^{\alpha_m}}}. \tag{3.27}$$

On the other hand, the Laplace transform $\mathcal{L}_{I^f_{\Phi'_f}}(s'W_f\bar{R_f}^{\alpha_0})$ in (3.25) can be obtained directly from [46], considering the reduction of the interfering femtocells by a factor p. The following theorem states the coverage probability in the femtocell tier for the two-tier network addressed.

Theorem 3.3. *For a two-tier heterogeneous network with full antenna pattern, the coverage probability in the femtocell tier is given in (3.29).*

Proof. Using the values for the Laplace transforms previously described, the femtocell tier coverage probability in (3.29) is obtained. □

$$\mathcal{P}_m^c(\beta_m, \phi_{tilt}) = e^{\lambda_f \pi R_c^2} \int_0^\infty 2\lambda_m \pi r \times e^{-\lambda_m \pi r^2 \left(1+\frac{2C(\alpha_m,\phi_{tilt},r)}{r^2 N_s}\right) - \lambda_f \pi R_c^2 \, {}_2F_1\left(1,-\frac{2}{\alpha_f};1-\frac{2}{\alpha_f};\frac{-\beta_m r^{\alpha_m}\eta W_f}{F(r,\phi_{tilt})R_c^{\alpha_f}}\right)} dr \tag{3.28}$$

$$\mathcal{P}_f^c(\beta_f, \phi_{tilt}) = \left(1 - \lambda_m \pi R_c^2\right) \times e^{-\lambda_f\left(1-\lambda_m \pi R_c^2\right)\left(\bar{R_f}^{\alpha_0}\beta_f W_f^2\right)^{\delta_f} \frac{\pi^2 \delta_f}{\sin\left(\pi\delta_f\right)} - \frac{2\pi\lambda_m}{N_s}\int_0^\infty \frac{x\,dx}{1+\frac{\beta_f^{-1}\bar{R_f}^{-\alpha_0}}{F(x,\phi_{tilt})}x^{\alpha_m}}} \tag{3.29}$$

Same as in the macrocell coverage probability, for a highly dense scenario and depending on the wall partition loss the interference from the macrocell tier could be neglected, resulting in a closed form expression for the femtocell coverage probability for those particular scenarios.

3.4 Energy efficiency

We use the inverse of the Energy Consumption Rating (ECR) to characterize the EE of the network, which is given by

$$EE = \frac{T}{P} \quad \text{b/J/Hz} \tag{3.30}$$

where T is the achievable throughput in bps/Hz and P is the total power consumed in Watts. So, the EE for the traditional and heterogeneous networks is given by

$$EE = \frac{\sum\limits_{i\in\{m,f\}} \lambda_i P_i^c \log_2(1+\beta_i)}{\sum\limits_{i\in\{m,f\}} \lambda_i P_i} \tag{3.31}$$

where P_i is the total power consumed by a base station in the i-th tier. For P_i, we make use of the commonly used model [36,37,48], which for macro- and femtocells is given by

$$P_m = N_s \left(a_m P_m^{tx} + b_m \right) \tag{3.32}$$

$$P_f = a_f P_f^{tx} + b_f \tag{3.33}$$

where P_i^{tx} is the transmit power in the i-th tier, b_i is the constant power component related to the signal processing, cooling of the site as well as battery backup in the i-th tier and a_i is a factor related to the efficiency of the power amplifier in the i-th tier. The power related component values, along with the other network's parameters are presented in Table 3.1. We proceed to define the EE optimizations for both the traditional and two-tier networks.

3.4.1 Traditional Macrocell Network

For the case of an traditional network, the expression in (3.31) is simplified and the optimization problem proposed consists of finding the optimum antenna tilt (ϕ_{tilt}^*) that maximizes the EE of the network, i.e.

$$\phi_{tilt}^* = \arg\max_{\phi_{tilt}} \underbrace{\frac{\mathcal{P}^c(\beta_m, \phi_{tilt}) \log_2(1+\beta_m)}{N_s \left(a_m P_m^{tx} + b_m \right)}}_{EE}. \tag{3.34}$$

Due to the complexity of the expression for EE in (3.34), we cannot find a closed-form solution. However, as the tilt angle is limited (same as its sensitivity in practice), the solution can be found for a small number of steps using a greedy search over the

Table 3.1: SIMULATION PARAMETERS

Parameter	Value	Description
ϕ_{3dB}	10	Half beamwidth
H_a	32 m	Base station antenna height
H_{ue}	1.5 m	User equipment antenna height
R_f	30 m	Femtocell radius
α_m	3,4	Path loss exponent for the macrocell tier
α_0	2.5, 3	Path loss exponent for the femtocell tier in the desired link
α_f	3,4	Path loss exponent for the femtocell tier in an interference link
W_f	5, 10, 20 dB	Wall partition loss for the femtocell tier
N_s	3, 6	Number of antenna sectors for the macrocell tier
P_f^{tx}	100 mW	Femtocell transmission power
P_m^{tx}	20 W	Macrocell transmission power
a_f	4	Femtocell power component dependent of the transmission power
a_m	3.77	Macrocell power component dependent of the transmission power
b_f	9.6	Femtocell constant power component related to signal processing, site cooling, battery backup
b_m	68.73	Macrocell constant power component related to signal processing, site cooling, battery backup

possible tilt values. Therefore, the complexity of the algorithm is simply $n_{degrees}$, where $n_{degrees}$ is the number of possible antenna tilts that the RET can provide. The results obtained for the traditional network are found in section 3.5.

3.4.2 HETEROGENEOUS NETWORK

In the case of the two-tier network described in section 3.3, the guard zone R_c has the effect of enhancing the performance of the macrocell tier by reducing the received interference from femtocells located in the vicinity of a macrocell user, therefore a bigger value of R_c is desired in this case. However, the selection of the size of R_c has a

negative impact in the femtocell tier, given the fact that increasing its size would cause a higher number of femtocells to stop transmitting, and so, the coverage probability in this tier would be reduced. This leads to the conclusion that there must be a tradeoff in the selection of the guard zone size to balance the performance of macro- and femtocell tiers. On the other hand, as described in section 3.1, the selection of the tilt angle ϕ_{tilt} can significantly increase the performance of the macrocell tier, and with the inclusion of a tier of interfering femtocells its optimum value is different from the one found for a traditional network. Furthermore, we are interested in obtaining the values of R_c and ϕ_{tilt} that would yield a good performance in terms of the overall network energy efficiency. Taking into account the considerations just described, we propose an optimization problem to maximize the energy efficiency of the network with constraints on the QoS requirements of both tiers. We aim to find both the optimum antenna tilt angle ϕ^*_{tilt} and guard zone R^*_c that maximize the energy efficiency with the required constraints. Formally, the problem is described as follows

$$\phi^*_{tilt}, R^*_c = \arg\max_{\phi_{tilt}, R_c} \underbrace{\frac{\lambda_m \mathcal{P}^c_m(\beta_m, \phi_{tilt})\log_2(1+\beta_{\mathrm{m}}) + \lambda_f \mathcal{P}^c_f(\beta_f, \phi_{tilt})\log_2(1+\beta_{\mathrm{f}})}{\lambda_m N_s\,(a_m P^{tx}_m + b_m) + \lambda_f (a_f P^{tx}_f + b_f)}}_{EE} \tag{3.35}$$

$$\text{s.t.} \quad \mathcal{P}^c_m(\beta_m, \phi_{tilt}) \geq 1 - \epsilon_m,$$
$$\mathcal{P}^c_f(\beta_f, \phi_{tilt}) \geq 1 - \epsilon_f$$

where ϵ_m and ϵ_f are respectively, the maximum outage probabilities permitted for macro and femto tiers. We denote $EE^\star$ as the maximum energy efficiency that can be achieved by selecting the optimum values $\phi^\star_{tilt}$ and $R^\star_c$. Although the proposed optimization problem cannot adapt to the changes in the environment in an online

fashion, it can still provide an overall solution to the system without the need to run time consuming simulations. Therefore, when a change in the system parameters (such as the densities of macro- and/or femtocell) occurs, the network operators can obtain a centralized solution that will yield a good performance depending upon the changes in the system.

For the expressions in (3.35), we proceed to use a non-linear software package in Matlab, using an interior point method to solve the optimization problem. In particular, the non-linear programming solver *fmincon* found in the optimization toolbox. The numerical results are presented in section 3.5.

3.5 Results

The numerical results of this chapter are presented in figures 3.3 to 3.10, where the lines correspond to the analytical results while the circles represent the results of Monte Carlo simulations. The system parameters used in the simulations are presented in Table 3.1, where we have used typical values found in practice. For the simulations, we first generate a random number of MBSs in the area following a PPP. Then, we proceed to obtain the Voronoi tessellation with the MBSs deployed. The typical user is located at the origin and associated with the closest MBS, according to Slivnyak's theorem. Then, we obtain the interference from the other MBSs considering the distant-dependent vertical pattern, while at the same time, the number of interferers is reduced randomly by a factor equal to N_s (number of sectors). In the case of the simulations for the HetNet, the two independent tiers are generated and the same process previously described is used to create the Voronoi cells. Next, in all the Voronoi cells of the network, a randomly (uniformly) distributed user is generated within the area of each

Voronoi cell. Then, a circular area of radius R_c is considered around each user and all the FAPs that fall within its circular area are considered inactive. The performance of both macro- and femtocell users is obtained by considering only the femtocells which remain active. Additionally, the simulations for the femtocell tier are obtained by considering that the user is uniformly distributed in the coverage area of its serving FAP, while the analytical results are calculated by using the expected value of the distance from the user to its serving FAP, as presented in the theoretical analysis. As mentioned before, we focused on a RET system, where the downtilt of the antenna can be remotely configured. Typical ranges for the electrical antenna tilt found in practice are $0 - 15°$ [78, 79]. However, state of the art antennas have been reported to achieve $18°$ [80], and even $20°$ [81]. Therefore we select the latter as the maximum permissible tilt angle in our setup.

In Figure 3.3 we verify the validity of our proposed model in terms of coverage probability by matching its performance with simulations obtained when a full $3D$ model (vertical and horizontal patterns) is used, for different values of the density of BSs. It can be seen that the use of thinning to model the horizontal pattern does not have a strong effect on the performance of a full $3D$ antenna pattern. Moreover, the antenna tilt value that maximizes the coverage probability of the network is the same in both approaches. Therefore, the accuracy of our simplified model is endorsed.

The coverage probability and EE of a traditional network are presented in Figure 3.4 as a function of the tilt angle. Figures 3.4(a) and 3.4(b) show the coverage probabilities for antennas with $120°$ ($N_S = 3$) and $60°$ ($N_S = 6$) sectorization, respectively. It can be seen that there is an antenna tilt angle that maximizes the coverage probability (and therefore, the energy efficiency). The former can be explained as follows: for low values of ϕ_{tilt} the coverage probability is low, due to the fact that the direction of the

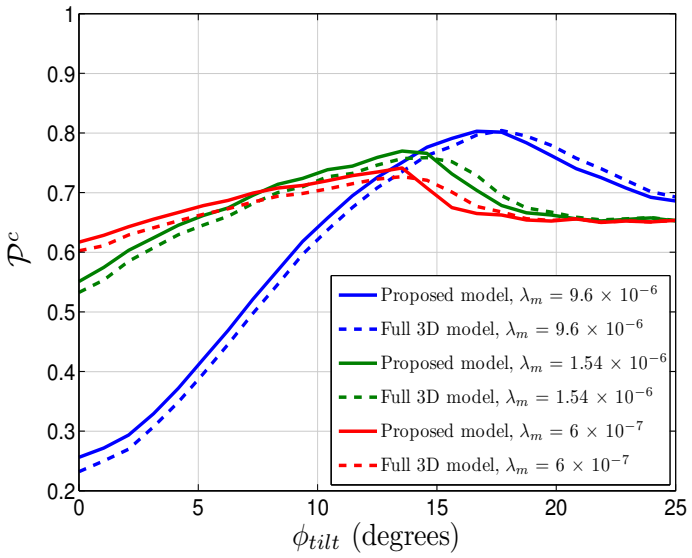

Figure 3.3: Macrocell-only coverage probability of the proposed model in comparison with a full $3D$ antenna pattern model as a function of tilt angle with $\beta = 3$. The straight lines represent the results obtained with our model, while the dashed lines represent the results of simulations with a $3D$ antenna pattern.

main lobe of the antenna does not point to the desired coverage area of each cell. As ϕ_{tilt} increases, most of the radiated power is pointed towards the area of the desired cell and less interference is created at the neighbouring cells, which is reflected in an increase in the coverage (and energy efficiency) of the network. Finally, the coverage reaches a maximum at the point where a significant portion of the radiated power is projected towards the desired cell while little interference is caused at the other cells. After that maximum, increasing ϕ_{tilt} cause very little interference but would also cover a very small portion of the desired cell, which would make the coverage probability drop. Additionally, it can be seen that (as expected) the optimum tilt angle is strongly coupled with the density of macro stations. This is due to the fact that with a higher density, the mean area of the cells is smaller and so a higher value of the antenna tilt is required to point to the smaller cell area. As is expected, the coverage probability

is further increased with the use of more antenna sectors, as the interference is further reduced. On the other hand, Figures 3.4(c) and 3.4(d) show the performance in terms of the EE. It can be seen that while the lines follow the same trends as in the case of coverage probability, the 120° sectorized antennas outperform the 60° sectorized antennas. This is due to the fact that the power consumed by using extra antenna sectors has more impact on the EE than the gains in throughput. Therefore, an inherent trade-off between the throughput and the EE of the system can be perceived.

In Figure 3.5 the coverage probability for the macrocell and femtocell tiers are shown as a function of the antenna tilt angle and guard zone, respectively. The results are presented for an average number of femtocells ($20, 50$ and 100 deployed per macrocell), and for different values of path loss exponents and wall partition loss. In 3.5(a), the coverage probability of the macrocell tier is displayed as a function of the antenna tilt angle when a guard zone of $R_c = 200$ m is used. It can be seen that the interference from the femtocell tier has the effect of decreasing the value of the optimum tilt angle in comparison with a traditional network. We observe that the tilt angle that maximizes the coverage probability is highly dependent on both, the path loss exponent and the wall partition loss. In general, a higher value of W_f results in a higher value of the optimum tilt angle. This is due to the fact that a higher wall partition loss prevents interference from the femtocell to seriously affect the macrocell user performance, and so, the results resemble one of a macrocell-only network. Additionally, in general the smaller the path loss exponent, the larger the value of tilt angle required to maximise the coverage probability. This also agrees with the behaviour previously described, in the sense that a smaller value of the path loss exponent results in an increase in the interference received from the femtocell tier. On the other hand, Figure 3.5(b) shows the coverage probability for the femtocell tier as a function of the macrocell's guard zone

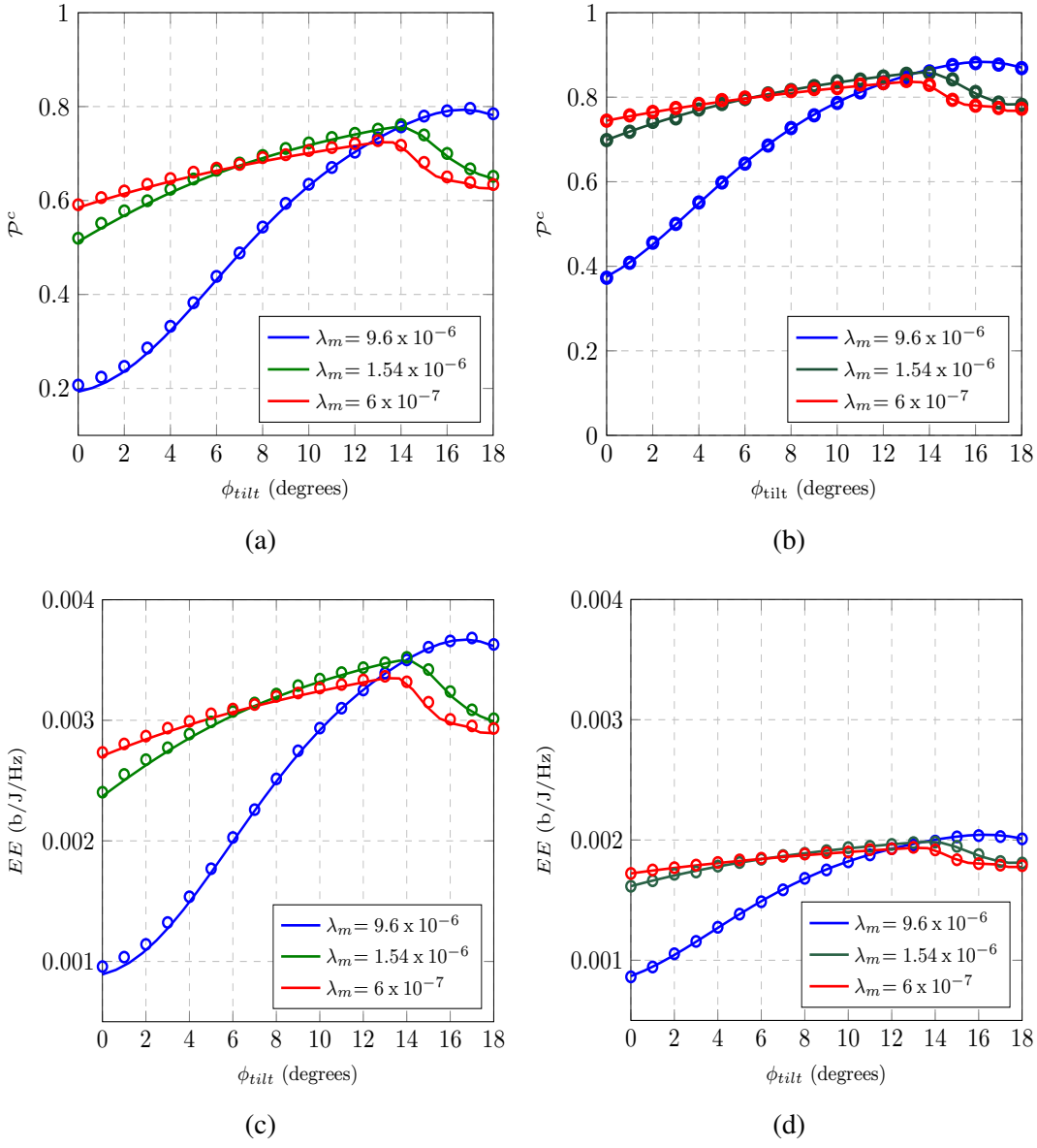

Figure 3.4: Coverage probabilities for (a) 3 sectors ($N_s = 3$) and (b) 6 sectors ($N_s = 6$), and energy efficiencies for (c) 3 sectors ($N_s = 3$) and (d) 6 sectors ($N_s = 6$) of a traditional network as a function of ϕ_{tilt},. In all figures, $\beta_m = 3$ and we present the results for $\lambda_m = 9.6 \times 10^{-6}$, 1.54×10^{-6} and 6×10^{-7} .

R_c. As an increase in the size of R_c would prevent a larger number of femtocells from transmitting in the proximity of a macrocell user, the overall coverage in the femto

tier is reduced. In this case, a smaller value of the path loss exponent results in an increase in the femtocell user performance. This is due to the small distances between a femtocell user and its serving FAP, for which a smaller path loss exponent results in a stronger signal received at the desired link, effectively increasing the performance. We also observe that the wall partition loss does not have such a strong effect on the femtocell tier as opposed to the case of the macrocell tier. This is due to the fact that the signal from an indoor FAP to another has to transverse through 2 walls. Moreover, the scenarios with wall partition loss of 10 dB and 20 dB present almost identical performances.

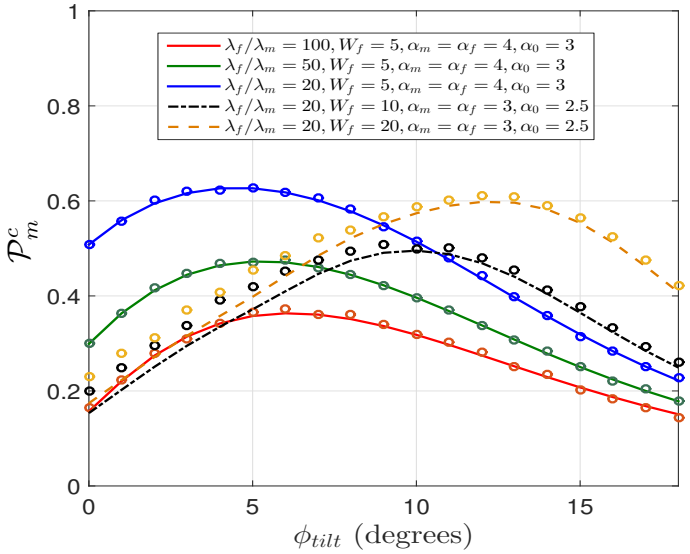

(a)

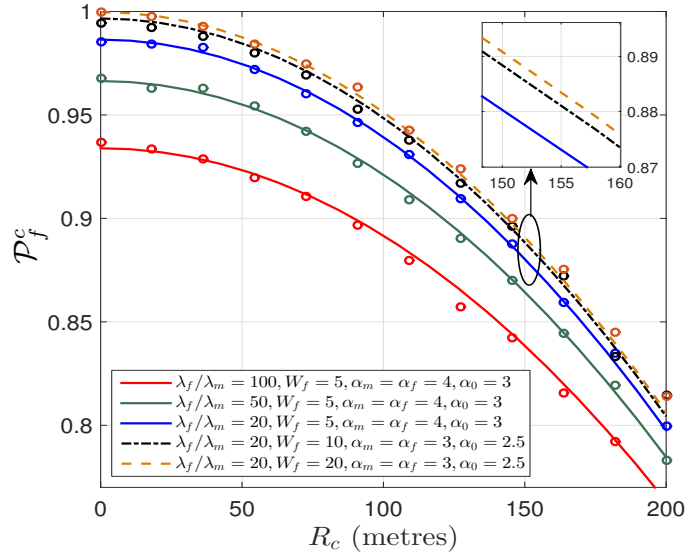

(b)

Figure 3.5: Coverage probability of a heterogeneous network, with $\beta_m = \beta_f = 3$, $W_f = 5$ dB, $\alpha_m = \alpha_f = 4$, $\alpha_0 = 3$, $\lambda_m = 1.54$ x 10^{-6} (typicall hexagonal cell radius of 500 m.), and $\lambda_f/\lambda_m = 20$, 50 and 100 for (a) macrocell as a function of ϕ_{tilt} (with fixed $R_c = 200$ m), and (b) femtocell tier as a function of R_c.

Figure 3.6 shows two views of the coverage probability of the macrocell tier as a function of both, ϕ_{tilt} and R_c. It is evident that a bigger guard zone is desirable in this

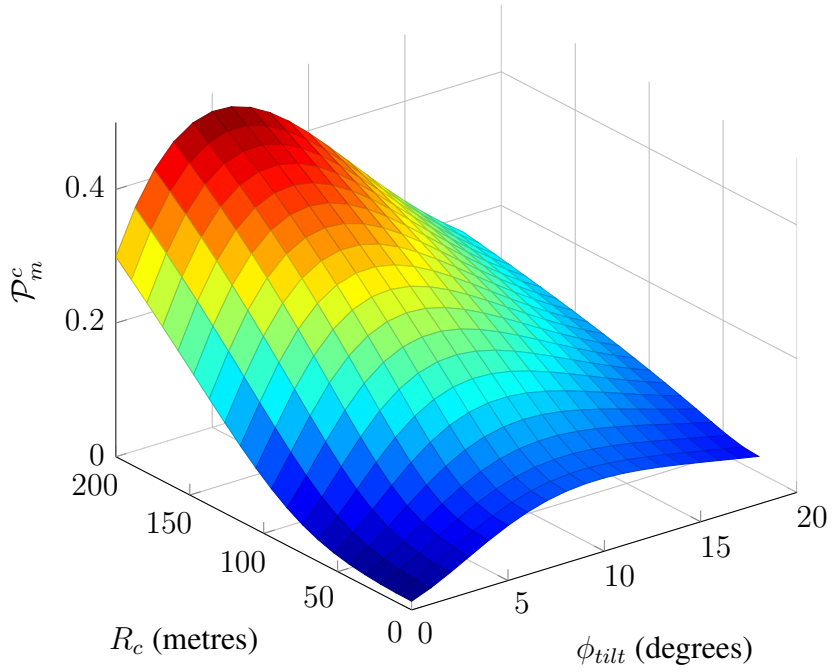

Figure 3.6: Macrocell coverage probability as a function of ϕ_{tilt} and R_c with $\beta_m = \beta_f = 3$, $W_f = 5$ dB, $\alpha_m = \alpha_f = 4$, $\lambda_m = 1.54 \text{ x } 10^{-6}$ (typical hexagonal cell radius of 500 m), and $\frac{\lambda_f}{\lambda_m} = 50$.

tier, as it would protect the macrocell users from a higher number of interferers. Also from Figure 3.6, it can be seen that the tilt angle ϕ_{tilt} that maximizes the coverage probability varies with R_c. In general, the values of ϕ_{tilt} in this scenario are smaller than the ones found for the traditional network, when the number of femtocells deployed is relatively small. On the other hand, increasing λ_f results in an increase of the tilt angle that maximizes the coverage in this tier.

Figure 3.7 shows the EE for a two-tier network as a function of R_c and ϕ_{tilt}. It can be seen that there is an antenna tilt angle that maximizes the EE for each value of R_c. Also, the smaller the value of R_c, the higher is the EE of the network. This is entirely related to the femtocell tier, given the fact that the femtocells provide high gains in the total throughput of the network, and so, with a higher number of active femtocells

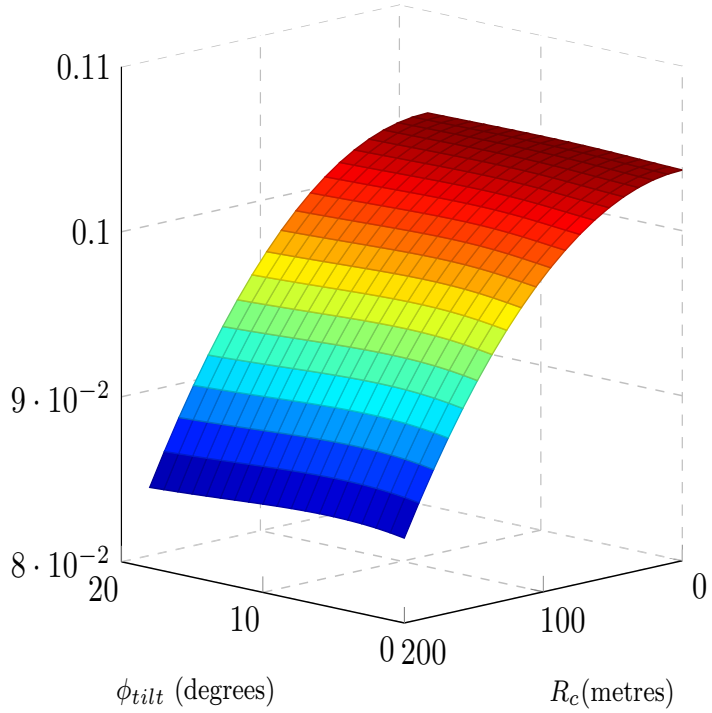

Figure 3.7: Energy efficiency of a two-tier network as a function of R_c and ϕ_{tilt} for a two-tier network with $\beta_m = \beta_f = 3$, $W_f = 5$ dB, $\alpha_m = \alpha_f = 4$, $\alpha_0 = 3$, $\lambda_m = 1.54 \text{ x } 10^{-6}$ (typical cell radius of 500 m), and $\frac{\lambda_f}{\lambda_m} = 50$.

(smaller value of R_c), there are more gains in the EE of the system. However, as can be seen from 3.6, the coverage in the macrocell tier is highly sensitive to the interference created by the femtocells. Therefore, optimizing only with respect to the EE of the network would result in an unfair treatment of the macrocell tier. Therein lies the importance of the constraints in (3.35) to guarantee a minimum QoS in this tier. In other words, there is a tradeoff between the coverage probability and the EE of the network, which is effectively captured by setting the constraints in the optimization problem.

The results from the optimization problem are presented in figures 3.8 to 3.10. Figure 3.8 shows $\phi^{\star}_{tilt}$ as a function of the density of femtocells deployed per macrocell.

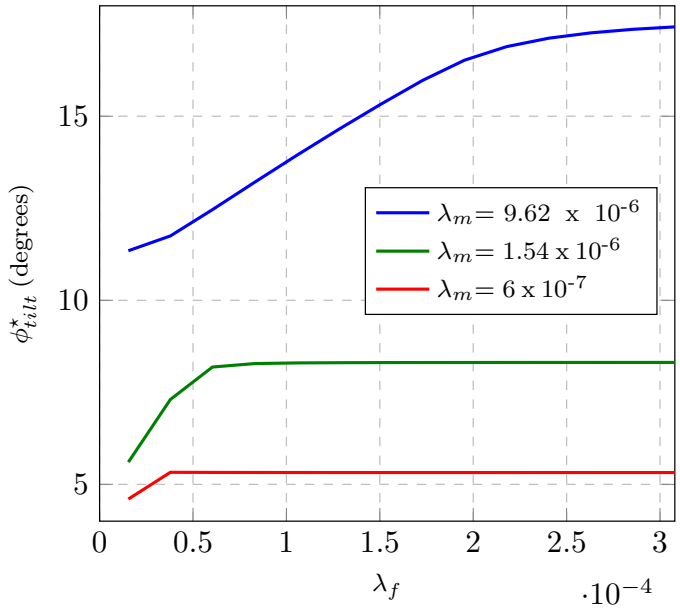

Figure 3.8: Optimum tilt of a two-tier network as a function of the density of femtocells for a two-tier network with $W_f = 5$, $\beta_m = \beta_f = 3$, $\lambda_m = 9.6$ x 10^{-6}, 1.54 x 10^{-6} and 6 x 10^{-7}, $\epsilon_m = 0.3$ and $\epsilon_f = 0.8$.

It can be seen that for a small number of femtocells, the optimum tilt angle is also small. However, as the interference from the femtocell tier increases, the tilt angle that maximizes the EE (and satisfies the constraints) increases until it settles at a fixed value when the number of femtocells deployed is high enough. Intuitively, as the number of femtocell increases, the edge users suffer the most damage to their received signal strength, and so a higher value for the tilt angle would steer the main lobe to an area closer to the edge of the cell to compensate for the interference from the femto tier.

Figure 3.9 shows $R_c^{\star}$ as a function of the density of femtocells deployed per macrocell. As expected, as the number of femtocells increases, a bigger guard zone is required in order to protect the macrocell users from the femtocell tier interference.

Figure 3.10 shows the optimum EE that complies with the constraints of the optimization problem when the density of femtocells per macrocell varies. It can be seen

that when the number of femtocells increases from a small value, the EE of the network is significantly increased. This is in accordance with the overall expected gains in throughput in the network that come from having more femtocells deployed. However, if the number of femtocells deployed is too high, the maximum achievable EE_{max} first reaches a limit and then it starts to decay. This occurs when the interference starts to have a major effect and the gains in throughput are not as high when compared with the total power consumed in the network. In other words, the power consumed starts to outweigh the gains in throughput obtained by deploying a higher number of femtocells in the network. It is worthwhile to notice that even in the highest number of femtocells analysed in this chapter (200), the overall EE of the network is still superior to the case of the traditional network when the same value of λ_m is used. However, the performance in the macrocell tier in terms of the coverage is significantly reduced. This motivates the selection of the optimization parameters by the network designer in order to cope with the trade-off between the EE of the network and the coverage in the macrocell tier.

3.6 Conclusion

In this chapter we provided a stochastic geometry framework to analise the performance of the network in terms of EE when the antenna tilt angle of macrocells is considered as an optimization parameter. In the case of a traditional network, we observe that our results can be easily scaled with regards to the density of macrocells deployed in the network. As expected, the higher the density of macrocells, the bigger is the antenna tilt angle that optimizes the overall coverage and EE. In the case of a heterogeneous network consisting of macro- and femtocells we observe that even for

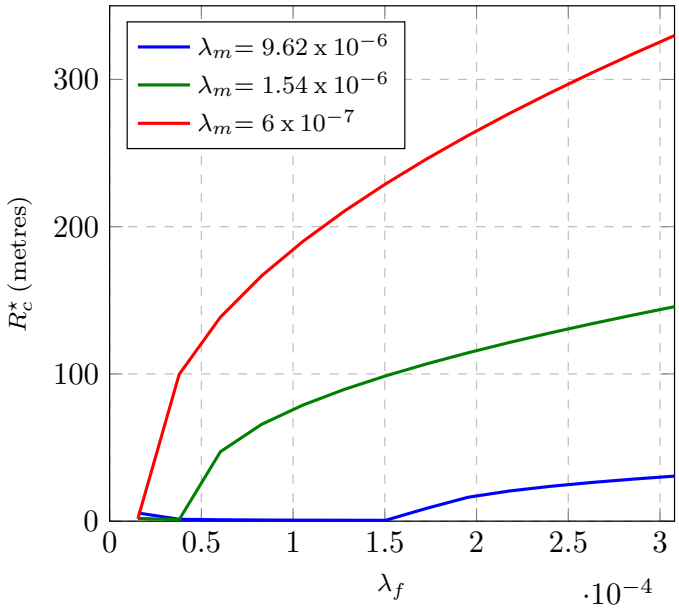

Figure 3.9: Optimum R_c (i.e., R_c^*) of a two-tier network as a function of the density of femtocells for a two-tier network with $W_f = 5$, $\beta_m = \beta_f = 3$, $\lambda_m = 9.6$ x 10^{-6}, 1.54 x 10^{-6} and 6 x 10^{-7} m.), $\epsilon_m = 0.3$ and $\epsilon_f = 0.8$.

a small number of femtocells deployed in the network, the performance of the macrocell user significantly decreases. Therefore, the use of a guard zone along with the tilt angle was proposed. From the results, it was verified that the EE of the network can be greatly increased by the inclusion of femtocells in comparison with a traditional network. However, the inclusion of femtocells using the same channel as a macrocell significantly deteriorates the performance of macrocell users. Therefore there is a trade-off between the minimum QoS requirements in terms of coverage or throughput and the EE in the macrocell tier. In general, the optimum tilt angle that maximizes the EE of the network is smaller for a heterogeneous network compared with that obtained in a traditional network with the same macro base station density. Additionally, as the number of femtocells in the network increases, the optimum tilt angle decreases to compensate for the performance loss in the edge users. Our suggested model can be

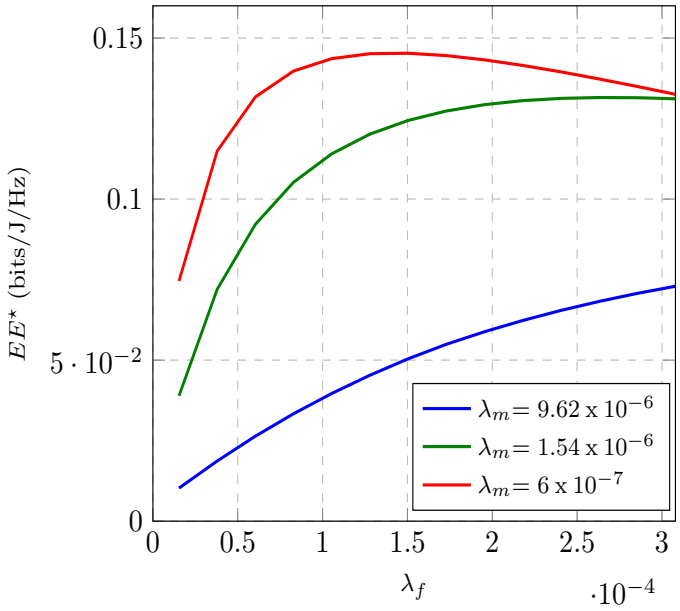

Figure 3.10: Optimum energy efficiency of a two-tier network as a function of the density of femtocells for a two-tier network with $W_f = 5$, $\beta_m = \beta_f = 3$, $\lambda_m = 9.6 \text{ x } 10^{-6}$, $1.54 \text{ x } 10^{-6}$ and $6 \text{ x } 10^{-7}$, $\epsilon_m = 0.3$ and $\epsilon_f = 0.8$.

used as a starting point in the context of a Self Organising Network, where the number of femtocells can be greatly increased, and with this information, the system can effectively adapt the tilt angle to obtain the best average performance in terms of the EE.

4 EE femtocell deployment

IN THIS CHAPTER:

A non uniform deployment of femtocells overlaying the macrocell tier is studied. While stochastic geometric models based on PPP provide a tractable approach for the analysis of uniform two-tier network deployments, the performance evaluation of a non-uniform deployment still remains an open issue which we address in this paper. This is due to the fact that smaller cells can be more efficiently deployed in areas where the QoS of traditional macro base stations is poor. Therefore, in this paper we introduce Stienen's model which allows us to analyse such non-uniform deployment. In contrast to traditional PPP based analysis, performance characterization under Stienen Model are more challenging due to location and density dependencies. However, we demonstrate that the performance can be approximated in a tractable manner. the developed statistical framework is employed to characterize the gains in terms of EE for non-uniform deployments. Results show that the edge user performance in terms of coverage, throughput and EE is significantly increased by the addition of femtocells, while the performance in the macrocell tier is just slightly reduced, depending upon the density of users in the area. Additionally, the EE gains of the proposed model are highlighted. These gain are complemented with the fact that the OPEX and CAPEX are reduced due to a lesser number of FAPs deployed.

4.1 Introduction

4.1.1 MOTIVATION

In chapter 1 we discussed the deployment of HetNets as a promising solution for NGNs to cope with the demands for better coverage and higher data rates. We also addressed the potential of of HetNets has to provide both the required coverage and increase the data rates of the users. However, realising such a potential may incur a significant energy penalty if the EE is not used as a metric to design the HetNet. This can be attributed to the fact that dense network deployment with aggressive frequency reuse does not come without increased co-channel interference. Thus network resources/available degrees-of-freedom should be engineered with the aim of maximizing EE without sacrificing the desired quality of service (QoS). Additionally, the densification of the network as a result of dealing with traffic growth creates challenges for the efficient management of the available spectrum. Therefore, new algorithms, topologies and technologies are being studied with the goal of efficiently making use of the available resources and network architectures to improve the EE.

Originally envisioned as user deployed devices, the trend in the study of femtocell deployments has shifted to an operator deployed perspective over the past years. This is due to the potential gains that are foreseen when network operators place femtocells in areas where the required QoS cannot be provided otherwise. While the typical assumption in the modelling of HetNets via PPPs has been to consider a uniform deployment of several tiers of BSs across the area of service, this assumption lacks the notion of smart and efficient deployment. This is because areas close to a MBS are expected to have higher performance in comparison with areas close to the edge of macrocells. Moreover, it is well established that traditionally the bottleneck of the

cellular system resides in the edge user performance.

Characterizing the performance of non-uniform two-tier networks deployment is a non-trivial task. This can be attributed to the fact that within stochastic geometric analysis [1] the edge of a typical Voronoi cell does not have a fixed shape. The exact geometry depends on the number of neighbors which is a random variable with unknown distribution. Additionally, due to the polygonal nature of the cell edge, the distances across different edges may vary. Thus, analysing cell edge type deployments becomes challenging. Consequently, there is a need for a tractable model where non-uniform deployments (which are parametrized by the cell-size and cell-edge deployment densities) can be investigated. In this chapter, we introduce Stienen's model which can address the above mentioned challenges. Stienen's model was originally proposed in [82] for material science related application.

STIENEN'S MODEL OVERVIEW

Stienen's model can be constructed from a Poisson-Voronoi Tessellation. Assume a cellular network where each mobile user is associated to the closest macro BS. The complement of the coverage areas of all MBS then form a Voronoi Tessellation. For a typical MBS, a Stienen cell can be formed by constructing a disc whose radius is equal to half of the distance between the MBS and its nearest neighbour (see Figure 4.1). Note that the Voronoi cell of the typical MBS is larger than its Stienen cell. In other words, each Voronoi cell can be decomposed into two regions, namely, the Stienen cell and its complementary area. Such decomposition of a typical Voronoi cell allows to model different deployment densities in these two areas. Moreover, as compared to traditional hardcore models such as Matern processes, the exclusion disc via Stienen's

[1] which is often employed to characterize the performance of large scale cellular network

model intrinsically captures the impact of the cell size. Since the coverage area of each MBS is not isotropic (and polygonal in nature), it would make less sense to have a fixed size disc centered at each MBS and then deploy FAPs outside such a disc. This is because some cell edges are far more closer to MBS than others. Stienen's Model also intrinsically captures this irregularity in distances to different cell edges.

In this chapter, we present an analytical framework to model non-uniform two-tier HetNet deployments via Stienen's Model. We show that improvements in coverage, throughput and EE are possible for a non-uniform deployment which will also reduce the OPEX and CAPEX due to the smaller number of smaller cells deployed.

4.1.2 Related Work

The gains in coverage, throughput and EE of HetNets have been analysed in several works, where the improvements have been reported for different techniques and algorithms. The EE of a two-tier network consisting of both macro- and picocells was analysed in [39] where both tiers were modelled with independent PPPs. Analytical results on the coverage probability, data rates and EE (in bps/m^{-2}/J) were obtained as a function of the base station densities. Also, by considering independent PPPs, [40] evaluated the EE in a scenario consisting of microcells and picocells. An optimization problem was formulated to obtain the density of picocells that maximized the EE of the network with constraints on the outage probabilities of both tiers. The study of EE with the use of PPPs was extended to the multi-antenna case in [83] and [33]. An analysis of the EE of different MIMO diversity schemes was carried out in [83] for a two-tier network consisting of macro and femtocells. The optimum antenna configuration and diversity schemes that yielded the maximum EE (while keeping some QoS constraints) were presented for different system parameters. Alternatively, in [33] a scenario con-

sisting of a single macrocell overlaid with a tier of femtocells modelled with a PPP was analysed. The authors examined the throughput and the EE of a MIMO system with an opportunistic interference alignment scheme in order to mitigate interference. While the results of this works show the potential improvements in the performance of the network in terms of coverage, data rates and energy efficiency by deploying HetNets, the assumption that there is not an inter-tier dependency on the locations of different tiers is simply not realistic. This is due to the fact that the base stations in different tiers are expected to be deployed only in areas where the expected QoS perceived by a user is not sufficient, e.g. hotspots, malls, or areas with poor received signal strength from a MBS.

Lately, the need to consider a non-uniform deployment of base stations among different tiers in a HetNet has been reported as this allows a more realistic modelling of the behaviour of an actual network, where the positions of the base stations in different tiers are not independent across tiers. In [84], a non-uniform deployment of a heterogeneous network is proposed where 4 tiers (each one modeled by a PPP) are deployed in the area. While an independence is assumed in tiers 1 and 4, tiers 2 and 3 depend on the positions of all the nodes of tier 1. In this model, in the fist stage a Voronoi tesselation is created with the points generated by the PPP of tier 1. Then, all the points of tiers 2 and 3 are restricted to the edges and vertices (respectively) of the Voronoi cells of tier 1. By varying the parameters and intensities of the respective PPPs, different cases of interest are highlighted and the cell sizes, as well as the effective received power in the area, are illustrated through a series of simulations. However, an analytical framework is not provided. In [85] the coverage and throughput are analysed for two-tier networks consisting of macro- and femtocells. Both, MBSs and FAPs are uniformly deployed across the area. However, only femtocells which are located outside a circular area

surrounding each MBS are activated. The paper [85] assumes a fixed size exclusion radius surrounding each MBS and a highest instantaneous received power association scheme. Users which fall within the circular area surrounding each MBs are assumed to always receive service from that macro base station, while users located outside these circular areas could receive service from a MBS or a FAP depending upon the instantaneous power received from each. In [86] a two-tier HetNet consisting of macro and pico cells is considered. The MBS tier follows a PPP, while the picocell tier follows a Poisson hole process (PHP). Therefore, the picocells are only deployed in the locations outside a circular area surrounding a MBS with a fixed radius of exclusion. By assuming a fixed position from a typical macrocell user to its designed MBS and a typical femtocell user to its tagged pico BS, bounds on the coverage probabilities for both users are obtained. Additionally, a fitted Poisson cluster process is used to approximate the Poisson hole process obtained when the exclusion regions surrounding each MBS are considered.

4.1.3 CONTRIBUTIONS

The need to plan in a more efficient manner the deployment of smaller cells creates a challenge in the analysis of the deployment of non-uniform tiers. Therefore in this chapter, we propose a tractable model for the non uniform deployment of a two-tier network consisting of macro- and femtocells. While the macrocells are uniformly distributed across the service area, the FAPs are only deployed outside a given disc of radius R_s (Stienen radius) centered at each MBS. Most of the works devoted to the study of non-uniform BSs assume a fixed exclusion region, which lacks a sense of realistic planning from a network operator perspective, as the size of the cell determines the areas where the potential placement of smaller cells can improve the performance.

Moreover, the interrelation between a cell edge user and the topology of the cell is lost. This is due to the fact that classifying a user as cell edge user depends on the location of the user with respect to its serving MBS. This cannot be captured by using a fixed radius as the size and shape vary from macrocell to macrocell. In contrast with those works, we propose the use of Stienen's model [82] to design the size of R_s. The resulting exclusion region is a function of the size of each Voronoi cell. The model then accounts for a more realistic model where the areas of possible femtocell locations depend on the size of the macrocell, while preserving the correlation of cell edge users with the topology of the cell. Additionally, the proposed model represents a tractable approach which can be easily scaled for a high number of femtocells deployed. The main contributions of this chapter are stated as follows.

- *Introducing Stienen's model*: We propose the use of Stienen's model [82] to characterize in a realistic manner a non-uniform deployment of femtocells overlaid to a macrocell network. In this model, the Stienen radius surrounding each MBS is designed as a function of the distance to its closest (interfering) MBS. On the other hand, the femtocell tier is deployed only in the areas outside the discs of Stienen radii. Users located in the areas enclosed by the Stienen radii will be served by the macrocell tier while the users located outside these areas (edge users) will be offloaded to the femtocell tier.

- *Improved edge user performance*: It is universally accepted that the bottleneck of cellular networks is the edge user, which experiences the worst performance due to the high path loss perceived at a distant user and also because the distances between the serving and interfering BSs to the user have the same order of magnitude. As shown in the results, with the proposed model, the edge user

performance can be greatly increased with the deployment of femtocells, while the macrocell user performance is not significantly reduced. This in turn helps to achieve a more balanced network throughout the entire service area.

- *Characterization of coverage, throughput and energy efficiency of users in both tiers*: With the use of tools from stochastic geometry, we provide a tractable approach to characterize the performance of users in both tiers. Namely, we find expressions for the coverage probability, average user throughput and overall EE of the network.

- *Improved coverage, throughput and energy efficiency*: By letting users located outside the discs of Stienen's radii to be served only by femtocells, the performance in terms of coverage, throughput and EE is improved in both tiers in comparison with a typical deployment. On one hand, due to the fact that the users served by the macrocell tier will be closer to their serving MBS in comparison with a normal deployment, they will experience a better QoS. On the other hand, given that the femtocells will only be deployed in areas where the average perceived power from a MBS is not very high, the use of resources is carried out in a more efficient manner, which is reflected in the enhanced performance.

4.1.4 Chapter Organization

The rest of the chapter is organized as follows. Section 4.2 introduces the system model. The coverage probability for the proposed model is obtained in 4.3. The expected throughput in each tier is derived in section 4.4. Section 4.5 describes the analysis of the energy efficiency for the proposed model. The numerical results are presented in section 4.6. Finally, conclusions are given in section 4.7.

4.2 System model

Consider a two-tier network consisting of MBSs and FAPs deployed in a given area. In contrast with chapters 2 and 3, we will assume an OSG scenario where users are allowed to freely associate to a nearby FAP. The MBSs are deployed across the entire area following a PPP Φ_m on $\mathbb{R}^2$, with density λ_m. The FAPs are only deployed outside the discs of radii R_s^j centered at each MBS located at $x_j \in \Phi_m$, where the superscript stands for the j-th MBS ($j \in \Phi_m$). The femtocell tier is then modelled via a PHP with effective intensity $\lambda_f p$, where λ_f is the original intensity of femtocells, while p is the probability that a FAP will be located outside the discs R_s^j, $\forall j \in \Phi_m$. In this model, the users that fall within the area covered by the discs will be served by the corresponding MBS. On the other hand, the users located outside the discs will be served by the femtocell tier. The advantages of this model are two-fold: deploying only femtocells in areas where the coverage is expected to be low (near the edge of the macro cells), and improving the macrocell expected performance, since the users served by the macrocell tier will be close to their serving MBS. Users are modelled by another PPP Φ_u of density λ_u and so, they are uniformly placed across the service area. We assume that each user is associated with the closest MBS. This is equivalent to a user associating with the MBS which provides the highest long term expected power. In the femtocell tier, we also assume that the users are associated with the nearest FAP. Under these assumptions, the resulting association scheme is formed by two Voronoi tessellations [14], i.e. one corresponding to the macrocell tier and the other one for the femtocell tier. The Voronoi cells formed represent the coverage regions for each BS in the network.

In contrast with previous works, in this chapter we propose the use of Stienen's

model to characterize the size of the macrocell coverage area, matching it with the area enclosed in the Stienen cells. Originally proposed for applications in material science, Stienen's model [82] is described as follows. Consider the homogeneous PPP Φ_m modelling the positions of the MBSs. The points generated by Φ_m are taken as seeds to construct a Voronoi tesellation. Now, around each point x_j, $j \in \Phi_m$ (each Voronoi cell seed), a disc of radius R_s^j equal to half of the distance to the closest neighbour of x_j is placed. We can extend the model to a more general case, in which the radius R_s^j is assumed to be the product of the closest neighbour and a scalar τ. When $\tau < 1/2$, the cell is located completely inside its Voronoi cell. On the other hand, for $\tau > 1/2$ the cell extends to other macrocells[2]. Note that due to the independence property of the PPP, the set of Stienen radii $\{R_s^j\}, j \in \Phi_m$ are all i.i.d. Therefore, we will refer to the Stienen radius only as R_s in the remaining of the chapter.

To model the location dependent femtocells, the FAPs with density λ_f are placed uniformly only in areas outside the Stienen cells. By definition, Stienen's model considers that the radius R_s surrounding each MBS is a function of the distance to the closest neighbour r_1. It is well-known that the distance of the typical user to its closest neighbour r_1 in a PPP follows a Rayleigh distribution, i.e. $f_{r1}(r_1) = 2\pi\lambda r_1 e^{-\pi\lambda r_1^2}$ [87]. Given that in this chapter it is assumed that $R_s = \tau r_1$, we can obtain the distribution

[2]Note that in the original Stienen model $\tau = 1/2$, in which case, the Stienen radius represents the maximum inscribing radius of its corresponding Voronoi cell.

of the radius of the Stienen cell as

$$\begin{aligned} f_{R_s}(R_s) &= \left.\frac{f_{r_1}(r_1)}{\left|\frac{dR_s}{dr_1}\right|}\right|_{r_1=\frac{R_s}{\tau}} \\ &= \left.\frac{2\pi\lambda_m r_1 e^{-\pi\lambda_m r_1^2}}{\tau}\right|_{r_1=\frac{R_s}{\tau}} \\ &= 2\pi\lambda_m R_s \tau^{-2}\, e^{-\pi\lambda_m\left(\frac{R_s}{\tau}\right)^2}. \end{aligned} \tag{4.1}$$

The following lemma defines the effective intensity of the femtocell tier, for the non-uniform deployment previously described.

Lemma 4.1. *Under Stienen's model for cellular systems, the effective density of femtocells is $\lambda_f p$, where*

$$p = \left(1+\tau^2\right)^{-1}. \tag{4.2}$$

Proof. In a PHP with fixed value of an exclusion region R_s, for each point $x_j \in \Phi_m$, all points of $\Phi_f \bigcap \mathcal{B}(x_j, R_s)$ are removed. In this case the effective intensity of the femtocell tier is given as $\lambda_f p$, where $p = e^{-\lambda_m \pi R_s^2}$, [19]. Now, as R_s is a random variable in the proposed model, then we must re-write p as, $p = \mathbb{E}_{R_s}\left[e^{-\lambda_m \pi R_s^2}\right]$. By taking the expectation using the pdf found in (4.1), the expression in (4.2) is obtained. □

The propagation model considered is assumed to be a composite of Rayleigh flat-fading channel and path loss. For the flat fading component, we define $h_{j,k}$ as the channel between the j-th transmitter and the k-th receiver, with $h_{j,k} \sim \mathcal{CN}(0,1)$. The

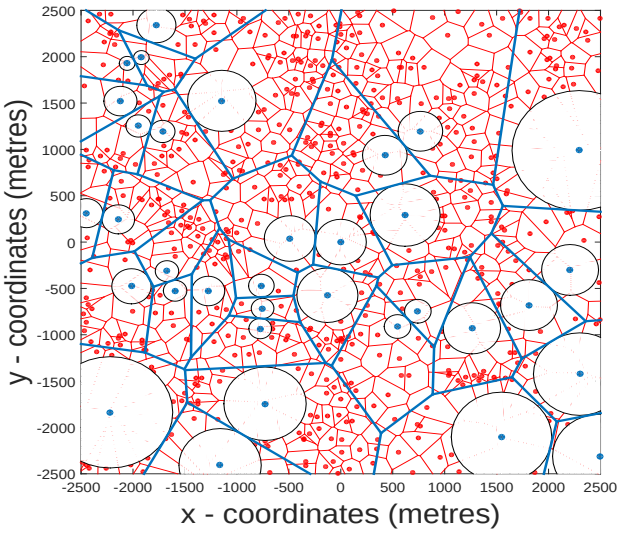

(a)

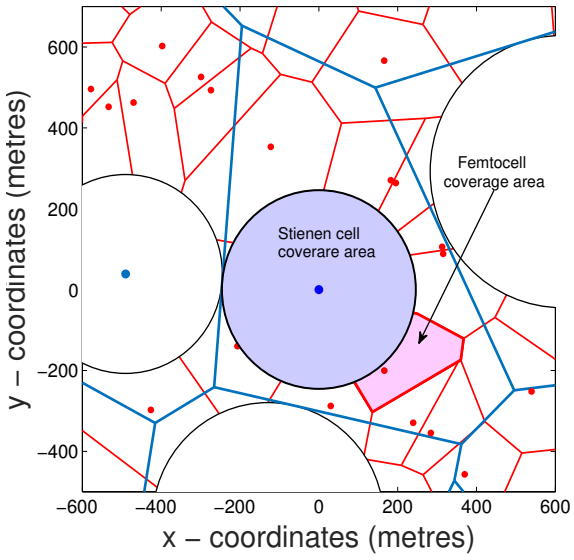

(b)

Figure 4.1: (a) Stienen's two tier network model. The blue dots represent the MBS, while the red dots represent the FAPs. The blue and red lines represent respectively, the boundaries of the macrocells and femtocells coverage regions. The discs surrounding the MBSs represent the Stienen cells. (b) Coverage regions of a Stienen cell (blue shaded disc) and a femtocell (red shaded polygon) in the typical Voronoi cell (area enclosed within the polygon determined by the blue lines).

path loss on the other hand is modelled as $l(r_{j,k}) = (r_{j,k})^{-\alpha_i}$, where $r_{j,k}$ is the distance from the j-th transmitter to the k-th receiver and α_i is the path loss exponent in tier i. We assume that the femtocells will be deployed outdoors by the network operator, and therefore the path loss exponents in both tiers are the same ($\alpha_m = \alpha_f = \alpha$). The mean total transmitted power of a base station in tier $i \in \{f, m\}$ is denoted as P_i^{tx}. It is assumed that when a complex symbol ($s_{j,k}$) is sent from the j-th transmitter to the k-th receiver, we have that $\mathbb{E}\left[|s_{j,k}|^2\right] = 1$.

In the model considered, due to the OSG assumption, the density of users in the area takes on an important role to characterize the number of users that will be served by each BS. Additionally, depending upon the density of users λ_u, some BSs in the network could be left off without any users within their coverage area. These BSs are considered to be inactive, as they do not have any users to serve. We will denote as (respectively) p_{ia} and $p_{in} = 1 - p_{ia}, i \in \{m, f\}$, the probabilities that a BS in the i-th tier is active or inactive. The following lemma defines the distribution of the number of users in the macrocell tier, from which p_{ma} and p_{mn} are derived.

Lemma 4.2. *The probability mass function (pmf) $f_{n_{um}}(n_{um})$ describing the number of users inside a macrocell coverage region following Stienen's model is given as*

$$f_{n_{um}}(n_{um}) = \frac{\lambda_m \tau^{-2}}{\lambda_m \tau^{-2} + \lambda_u} \left(\frac{\lambda_u}{\lambda_u + \lambda_m \tau^{-2}} \right)^{n_{um}}. \tag{4.3}$$

From (4.3) it is straightforward to obtain the probability of a macrocell being active (p_{ma}) and inactive (p_{mn}) as

$$p_{ma} = \frac{\lambda_u}{\lambda_m \tau^{-2} + \lambda_u} \quad \text{and} \quad p_{mn} = \frac{\lambda_m \tau^{-2}}{\lambda_m \tau^{-2} + \lambda_u}. \tag{4.4}$$

Proof. The pmf $f_{n_{um}}(n_{um})$ of the number of users inside Stienen's cell can be directly obtained as

$$\begin{aligned} f_{n_{um}}(n_{um}) &= \mathbb{E}_{R_s}\left[f_{n_{um}|R_s}(n_{um}|R_s) \right] \\ &= \int_0^\infty \left(\frac{(\lambda_u \pi R_s^2)^{n_{um}} e^{-\lambda_u \pi R_s^2}}{n_{um}!} \right) f_{R_s}(R_s)\, dR_s \\ &= \frac{(\lambda_u \pi)^{n_{um}} 2\pi \lambda_m \tau^{-2}}{n_{um}!} \int_0^\infty R_s^{2n_{um}+1} e^{-\lambda_m \pi \tau^{-2} R_s^2 \left(1 + \frac{\lambda_u}{\lambda_m \tau^{-2}}\right)}\, dR_s \\ &\overset{(a)}{=} \frac{(\lambda_u \pi)^{n_{um}} 2\pi \lambda_m \tau^{-2}}{n_{um}!} \times \frac{1}{2} \left(\lambda_m \pi \tau^{-2} \left(1 + \frac{\lambda_u}{\lambda_m \tau^{-2}} \right) \right)^{-1-n_{um}} \end{aligned} \tag{4.5}$$

where we used the property $\int_0^\infty x^a e^{-bx}\, dx = b^{-1-a}\, \Gamma(a+1)$ in step (a). After some algebra, we obtain the final result in (4.3). □

Lemma 4.3. *The pmf $f_{n_{uf}}(n_{uf})$ describing the number of users inside a femtocell coverage region following Stienen's model is given as*

$$f_{n_{uf}}(n_{uf}) = \frac{\left(1+\frac{\lambda_u}{3.5\lambda_f}\right)^{-3.5}\Gamma(3.5+n_{uf})}{n_{uf}!\,\Gamma(3.5)}\left(\frac{\lambda_u}{\lambda_u+3.5\lambda_f}\right)^{n_{uf}}. \tag{4.6}$$

From (4.6) it is straightforward to obtain the probability of a femtocell being active (p_{fa}) and inactive (p_{fn}) as

$$p_{fa} = 1-\left(\frac{3.5\lambda_f}{3.5\lambda_f+\lambda_u}\right)^{3.5} \text{ and } p_{fn} = \left(\frac{3.5\lambda_f}{3.5\lambda_f+\lambda_u}\right)^{3.5}. \tag{4.7}$$

Proof. The expression of $f_{n_{uf}}(n_{uf})$ in (4.6) can be obtained by following the same approach as in lemma 4.2, using the distribution $f_v(v)$ of the area v of a Voronoi cell. A very accurate approximation for this pdf was found in [88] as

$$f_v(v) = \frac{3.5^{3.5}}{\Gamma(3.5)}\lambda_f^{3.5}v^{3.5}e^{-3.5\lambda_f v} \tag{4.8}$$

With the use of (4.8), the final results in (4.6) and (4.7) are found. □

4.3 Coverage

In this section we analyse the coverage achieved in each tier. Formally, the coverage probability $\mathcal{P}_i^c(\beta_i)$ ($i \in \{m,f\}$) is defined as the probability that the signal to interference plus noise ratio ($SINR$) is above a certain threshold (β_i) in the entire service area, i.e., $\mathcal{P}_i^c(\beta_i) = \mathbb{P}(SINR_i > \beta), i \in \{m,f\}$. Considering that both tiers share the

same spectrum, the $SINR$ is expressed as

$$\begin{aligned} SINR_i &= \frac{P_i^{tx}|h|^2\, l\left(r_i\right)}{\sum\limits_{j\in\Phi_m} P_m^{tx}|h_{j,0}|^2\, l\left(r_{j,0}\right) + \sum\limits_{k\in\Phi_f} P_f^{tx}|h_{k,0}|^2\, l\left(r_{k,0}\right) + \sigma^2} \\ &= \frac{P_i^{tx}|h|^2\, r_i^{-\alpha}}{I_{\Phi_m} + I_{\Phi_f} + \sigma^2},\ \ i \in \{f, m\} \end{aligned} \tag{4.9}$$

where r_i represents the distance from the typical user to its closest BS in tier i, I_{Φ_m} and I_{Φ_f} represent, respectively, the received interference from the macro- and femtocell tiers and σ^2 represents the noise power. For ease of notation, from now on, we drop the "0" superscript for the interfering links to the typical user, i.e. $h_j = h_{j,0}$, $h_k = h_{k,0}$, $r_j = r_{j,0}$ and $r_k = r_{k,0}$. Using the fact that $|h|^2 \sim \mathrm{Exp}(1)$, the coverage probability is expressed as

$$\begin{aligned} \mathcal{P}_i^c(\beta_i) &= \mathbb{P}(SINR_i > \beta) \\ &= \mathbb{P}\left(\frac{P_i^{tx}|h|^2\, r_i^{-\alpha}}{I_{\Phi_m} + I_{\Phi_f} + \sigma^2} > \beta_i\right) \\ &= \mathbb{E}_{r_i, R_s, I_{\Phi_m}, I_{\Phi_f}}\left[\exp\left(-\frac{r_i^{\alpha}\beta_i}{P_i^{tx}}\left(I_{\Phi_m} + I_{\Phi_f} + \sigma^2\right)\right)\right] \\ &= \mathbb{E}_{r_i, R_s}\left[\exp\left(-\frac{r_i^{\alpha}\beta_i\sigma^2}{P_i^{tx}}\right)\mathcal{L}_{\Phi_m}\left(s\right)\mathcal{L}_{\Phi_f}\left(s\right)\right]\Big|_{s=\frac{r_i^{\alpha}\beta_i}{P_i^{tx}}} \end{aligned} \tag{4.10}$$

where $\mathcal{L}_{\Phi_i}\left(s\right)$ is the Laplace transform of the interference from the i-th tier, with $i \in \{m, f\}$.

Now, a very common assumption in HetNets is to consider an interference limited scenario, where the interference dominates the performance of the network and the effect of noise can be neglected, which is commonly the case for most modern cellular

networks [14][3]. Under this assumption, the coverage probability can be defined in terms of the SIR, in which case (4.10) becomes

$$\begin{aligned}\mathcal{P}_i^c(\beta_i) &\approx \mathbb{P}(SIR_i > \beta_i) \\ &= \mathbb{E}_{r_i,R_s}\left[\mathcal{L}_{\Phi_m}(s)\,\mathcal{L}_{\Phi_f}(s)\right]\Big|_{s=\frac{r_i^{\alpha}\beta_i}{P_i^{tx}}}. \end{aligned} \tag{4.11}$$

We proceed to obtain the statistics for the typical user in each tier. As required by Stienen's model, we place the center of the typical cell at the origin. As stated before, the distance from the typical user to the closest BS follows a Rayleigh distribution. Thus, we proceed to place the typical user at a distance r from the origin with $f_r(r) = 2\pi\lambda_m r\, e^{-\pi\lambda_m r^2}$, for $r > 0$. We assume that users inside Stienen's cells ($r < R_s$, where R_s is the radius of the Stienen cell) will be served by macro BSs, while those outside the cells ($r > R_s$) will be offloaded to the femtocells.

4.3.1 MACROCELL COVERAGE

The following theorem defines the coverage probability of the macrocell tier.

Theorem 4.1. *The coverage probability in the macrocell tier for Stienen's model is given in (4.12), where* $\zeta(a,b) = {}_2F_1(1, 1-2/a; 2-2/a; -b)$ *is the Gauss hypergeometric function.*

[3] As will be clear after the coverage probability analysis, we could easily include the noise factor in the coverage probability at the cost of an extra integration.

$$\mathcal{P}_m^c(\beta_m) \approx \int_0^1 \frac{\frac{2\tau^{-2}\psi(1+\tau^{-2})}{(\tau^{-2}+\psi^2)^2}\left(\frac{p_{ma}}{1+\beta_m\left(\frac{\psi}{(\tau^{-2}+\psi^2)^{1/2}}\right)^{\alpha}}+p_{mn}\right)\quad d\psi}{1+\frac{\beta_m\tau^2\psi^{\alpha}}{\alpha/2-1}\left[p_{ma}\left(\tau^{-1}-\psi\right)^{2-\alpha}\,\zeta\left(\alpha,-\beta_m\left(\frac{\psi}{(\tau^{-1}-\psi)}\right)^{\alpha}\right)+\frac{\lambda_f p p_{fa}\eta(1-\psi)^{2-\alpha}}{\lambda_m}\,\zeta\left(\alpha,-\beta_m\eta\left(\frac{\psi}{1-\psi}\right)^{\alpha}\right)\right]} \tag{4.12}$$

$$\mathcal{P}_f^c(\beta_f) \approx \int_0^{\infty} \frac{\left(2\lambda_m^2\lambda_f\, p\,\Delta\left(1+\tau^{-2}\right)\right)\frac{\lambda_m\left(2+\tau^{-2}+\frac{2\lambda_f\, p\,\Delta^2}{\lambda_m}\right)}{((\lambda_m+\lambda_f\, p\,\Delta^2)(\lambda_m(1+\tau^{-2})+\lambda_f\, p\,\Delta^2))^2}\left(\frac{p_{ma}}{1+\beta_f\eta^{-1}\Delta^{\alpha}}+p_{mn}\right)\quad d\Delta}{1+\frac{\beta_f}{(\alpha/2-1)}\left[p_{fa}\,\zeta\left(\alpha,-\beta_f\right)+\frac{\lambda_m p_{ma}\Delta^{\alpha-2}}{\lambda_f\, p\,\eta}\,\zeta\left(\alpha,-\frac{\beta_f}{\eta}\Delta^{\alpha}\right)\right]} \tag{4.13}$$

Proof. From (4.11), the coverage probability in the macrocell tier is expressed as

$$\mathcal{P}_m^c(\beta_m) = \mathbb{E}_{r_m}\left[\mathcal{L}_{\Phi_m}(s)\big|_{s=r_m^{\alpha}\beta_m}\,\mathcal{L}_{\Phi_f}(s)\Big|_{s=r_m^{\alpha}\beta_m\eta}\right] \tag{4.14}$$

where $\eta = \frac{P_f^{tx}}{P_m^{tx}}$ represents the ratio of the transmit powers employed by the tiers. Each Laplace transform corresponds exactly to the probability generating functional of a PPP [16], which is defined as $\mathbb{E}\left[\prod_{x_j\in\Phi} f(x_j)\right] = \exp(-\lambda\int_{\mathbb{R}^2}(1-f(x))dx)$, where $f(x_j)$ is any function on each point of the process. For the considered scenario, the exact computation of the Laplace transform is not feasible. However, we obtain an approximation by following the approach taken in [89] for a fixed user location, and extend it for a random position in the service area. In Figure 4.2 a sketch of the model used is presented. Under this scheme, the typical user which is located at a distance r from its serving MBS coincides with r_m, and so we have $f_{r_m}(r_m) = 2\pi\lambda_m r_m \exp(-\pi\lambda_m r_m^2)$. From Figure 4.2, it is clear that the closest a dominant interferer is always located at a distance D from the typical user, and at a distance $R_s\tau^{-1}$ from the serving MBS, with R_s being the Stienen radius of the typical macrocell. Therefore, the Laplace transform of the macrocell interference is decomposed

into two components, $\mathcal{L}_m = \mathcal{L}_m^D(s)\mathcal{L}'_m(s)$, where $\mathcal{L}_m^D$ denotes the Laplace transform of the dominant interfering MBS and $\mathcal{L}'_m$ denotes the Laplace transform of the rest of the interference from the other MBSs. Additionally, we define a variable $\psi = \frac{r_m}{R_s}$ which corresponds to the ratio between the distance from the typical user to its serving MBS and the Stienen radius of that MBS. Using the law of cosines we obtain

$$\begin{aligned} D =& \sqrt{(R_s\tau^{-1})^2 + r_m^2 - 2R_s\tau^{-1}r_m\cos(\phi)} \\ =& R_s\sqrt{\tau^{-2} + \psi^2 - 2\tau^{-1}\psi\cos(\phi)} \end{aligned} \tag{4.15}$$

where ϕ is the angle between triangle "sides" $R_s\tau^{-1}$ and r_m. Due to the fact that the typical user's position angle will be uniformly distributed, ϕ will also be uniformly distributed. In order to simplify the results, we approximate D as

$$D \approx R_s\sqrt{\tau^{-2} + \psi^2}. \tag{4.16}$$

This approximation was made by using the expected value of ϕ in 4.15. The expected value is obtained by taking into account that ϕ is uniformly distributed and it can take values in the $[0, \pi]$ range (or $[-\pi, 0]$, then the expected value of ϕ is $\mathbb{E}[\phi] = \frac{\pi}{2}$. The Laplace transform of the interference from the dominant interfering MBS can then be evaluated as

$$\begin{aligned} \mathcal{L}_{I_{\Phi_m}}^D(s) &= \mathbb{E}_{I_{\Phi_m}}\left[\exp(-s)|_{s=r_m^\alpha\beta_m}\right] \\ &= \mathbb{E}_{|h|^2}\left[\exp\left(-s|h|^2D^{-\alpha}\right)\right] \\ &\overset{(a)}{=} \mathbb{E}_{|h|^2}\left[\exp\left(-|h|^2\beta_m\left(\frac{\psi}{(\tau^{-2}+\psi^2)^{1/2}}\right)^\alpha\right)\right] \end{aligned}$$

$$= \frac{1}{1+\beta_m\left(\frac{\psi}{(\tau^{-2}+\psi^2)^{1/2}}\right)^{\alpha}} \tag{4.17}$$

where (a) was obtained using the substitution $r_m = \psi R_s$. Using the fact that the closest interfering MBS is active with probability p_{ma} and inactive with probability p_{mn}, the final expression is given as

$$\mathcal{L}^{D}_{I_{\Phi_m}} = \frac{p_{ma}}{1+\beta_m\left(\frac{\psi}{(\tau^{-2}+\psi^2)^{1/2}}\right)^{\alpha}} + p_{mn}. \tag{4.18}$$

As previously stated, the interference in the macrocell tier (other than the closest interferer) is not symmetric with respect to the typical user. In this case, an approximation is obtained by considering that the interference to the typical user comes from outside $\mathcal{B}\left(x_u, R_s(\tau^{-1}-\psi)\right)$, where x^u is the position of the user. The Laplace transform of the interference from other (not dominant) MBSs is then obtained as

$$\begin{aligned}
\mathcal{L}'_{I_{\Phi_m}}(s) &= \mathbb{E}_{I_{\Phi_m}}\left[\exp(-s)|_{s=r_m^{\alpha}\beta_m}\right] \\
&= \mathbb{E}_{\Phi_m,|h_j|^2}\left[\exp\left(-s\sum_{j\in\Phi_m}|h_j|^2\, r_j^{-\alpha}\right)\right] \\
&= \mathbb{E}_{\Phi_m,|h_j|^2}\left[\prod_{j\in\Phi_m}\exp\left(-|h_j|^2\beta_m\, r_m^{\alpha} r_j^{-\alpha}\right)\right] \\
&= \mathbb{E}_{\Phi_m}\left[\prod_{j\in\Phi_m}\frac{1}{1+\beta_m\left(\frac{r_j}{r_m}\right)^{-\alpha}}\right] \\
&\overset{(a)}{=} \exp\left(-2\pi\lambda_m p_{ma}\int_{R_s(\tau^{-1}-\psi)}^{\infty}\frac{v\,dv}{1+\left(\frac{v}{\beta_m^{1/\alpha}\psi R_s}\right)^{\alpha}}\right) \\
&\overset{(b)}{=} \exp\left(-\pi\lambda_m p_{ma}\beta_m^{2/\alpha}\psi^2 R_s^2\int_{\left(\frac{\tau^{-1}-\psi}{\beta_m^{1/\alpha}\psi}\right)^2}^{\infty}\frac{du}{1+u^{\alpha/2}}\right)
\end{aligned}$$

$$= e^{\frac{-\lambda_m \pi p_{ma} \beta_m \psi^\alpha \left(\tau^{-1}-\psi\right)^{2-\alpha} R_s^2}{\alpha/2-1} \, {}_2F_1\left(1,1-\frac{2}{\alpha};2-\frac{2}{\alpha};-\beta_m\left(\frac{\psi}{\tau^{-1}-\psi}\right)^\alpha\right)} \tag{4.19}$$

where (a) is obtained by using the probability generating functional of a PPP [16] and (b) is obtained by using the substitution $u = \left(\frac{r_j}{\beta^{1/\alpha}\psi R_s}\right)^2$. The Laplace transform for the interference from the femtocell tier is obtained by assuming a worst case scenario, in which the interference is assumed to come from outside $\mathcal{B}\left(x_u, R_s(1-\psi)\right)$, and so the typical user receives more interference than the one found in the scenario proposed. Considering this assumption, we then have

$$\begin{aligned}
\mathcal{L}_{I_{\Phi_f}}(s) &= \mathbb{E}_{I_{\Phi_f}}\left[\exp(-s)\big|_{s=r_m^\alpha \beta_m \eta}\right] \\
&= \mathbb{E}_{\Phi_f,|h_k|^2}\left[\exp\left(-s\sum_{k\in\Phi_m}|h_k|^2\, r_k^{-\alpha}\right)\right] \\
&= \mathbb{E}_{\Phi_f,|h_k|^2}\left[\prod_{k\in\Phi_f}\exp\left(-|h_k|^2 r_k^{-\alpha}\beta_m\eta\, r_m^\alpha\right)\right] \\
&= \mathbb{E}_{\Phi_f}\left[\prod_{k\in\Phi_f}\frac{1}{1+\beta_m\eta\left(\frac{r_k}{r_m}\right)^{-\alpha}}\right] \\
&= e^{\frac{-\lambda_f \pi p\, p_{fa} \beta_m\, \eta\, \psi^\alpha (1-\psi)^{2-\alpha} R_s^2}{\alpha/2-1} \, {}_2F_1\left(1,1-2/\alpha;2-2/\alpha;-\beta_m\eta\left(\frac{\psi}{1-\psi}\right)^\alpha\right)}
\end{aligned} \tag{4.20}$$

where the final expression is found by conducting a similar analysis as the one used for the macrocells. It is worth pointing out that in (4.11) the expression for the coverage probability requires averaging over r_m and R_s. With the substitution $r_m = \psi R_s$, the coverage probability can now be obtained by taking the average over R_s and ψ. We now proceed to find the pdfs of these parameters, i.e., $f_{R_s}(R_s)$ and $f_\psi(\psi)$.

The pdf of ψ is obtained by directly using the definition of the ratio distribution as

$$\begin{aligned} f_{\psi}(\psi) &= \int_{-\infty}^{\infty} |R_s| f_{R_s,r_m}(R_s, \psi R_s)\, dR_s \\ &= \int_{0}^{\infty} R_s \left(2\lambda_m \pi R_s \tau^{-2}\, e^{-\lambda_m \pi \left(\frac{R_s}{\tau}\right)^2}\right) \left(2\lambda_m \pi \psi R_s \tau^{-2}\, e^{-\lambda_m \pi (\psi R_s)^2}\right) dR_s \\ &= \frac{2\tau^{-2}\,\psi}{\left(\tau^{-2}+\psi^2\right)^2}. \end{aligned} \tag{4.21}$$

Finally, in order to effectively deal with the case when the user is served by the macrocell tier, we need to condition on the probability of the typical user being located inside the Stienen cell ($p_{um} = \mathbb{P}(x_u \in \mathcal{B}\,(0, R_s))$, which is equivalent to $\mathbb{P}(\psi < 1)$. From (4.21) it is straightforward to obtain this probability as $p_{um} = (1+\tau^{-2})^{-1}$. So the coverage probability in the macrocell tier is expressed as

$$\mathcal{P}_m^c(\beta) = \frac{1}{p_{um}} \int_0^1 \int_0^{\infty} \mathcal{L}^{D}_{I_{\Phi_m}} \mathcal{L}'_{I_{\Phi_m}} \mathcal{L}_{I_{\Phi_f}}\, f_{R_s}(R_s)\, f_{\psi}(\psi)\, dR_s\, d\psi. \tag{4.22}$$

Substituting the values found in (4.18), (4.19), (4.20), (4.1) and (4.21) into (4.22) and integrating with respect to R_s, the final expression in (4.12) is obtained. □

4.3.2 FEMTOCELL COVERAGE

The following theorem states the coverage probability in the femtocell tier.

Theorem 4.2. *The coverage probability in the femtocell tier for Stienen's model is given in (4.13).*

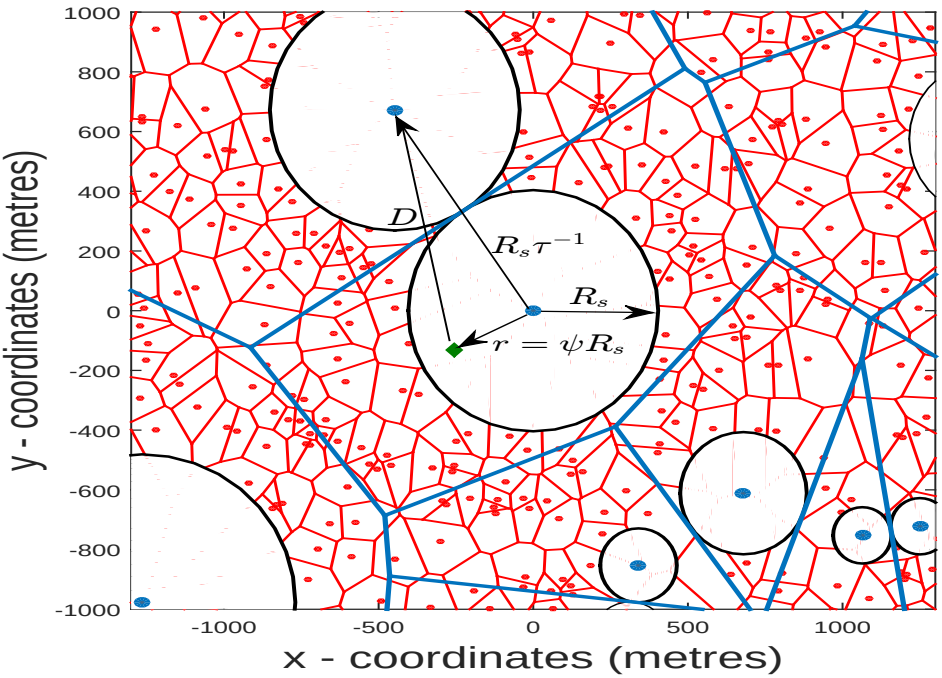

Figure 4.2: Model considered for the approximation. The green diamond represents the typical user located at a distance $r = \psi R_s$ from the serving MBS, where R_s is the Stienen radius for the typical cell. The typical macrocell closest interferer is located at a distance $R_s\tau^{-1}$ from the MBS located at the origin. The distance between the user and the closest interfering MBS is denoted as D.

Proof. From (4.11), the coverage probability in the femtocell tier is expressed as

$$\mathcal{P}_f^c(\beta_f) = \mathbb{E}_{r_f}\left[\mathcal{L}_{\Phi_m}(s)\big|_{s=r_f^\alpha \beta_f \eta^{-1}} \mathcal{L}_{\Phi_f}(s)\big|_{s=r_f^\alpha \beta_f}\right]. \tag{4.23}$$

The Laplace transform for the femtocell interference in this case is assumed to be the same as in a normal PPP Voronoi but also considering the thinning of the density of interferers by a factor p_{fa} accounting for the percentage of femtocells which are active (having at least one user in their coverage region). Therefore, the Laplace transform of

the femtocell tier is given as

$$\begin{aligned}
\mathcal{L}_{I_{\Phi_f}}(s) &= \mathbb{E}_{I_{\Phi_f}}\left[\exp(-s)|_{s=r_f^{\alpha}\beta_f}\right] \\
&= \mathbb{E}_{\Phi_f,|h_k|^2}\left[\exp\left(-s\sum_{k\in\Phi_m}|h_k|^2\, r_k^{-\alpha}\right)\right] \\
&= \mathbb{E}_{\Phi_f,|h_k|^2}\left[\prod_{k\in\Phi_f}\exp\left(-|h_k|^2\beta_f\, r_f^{\alpha}\right)\right] \\
&= \mathbb{E}_{\Phi_f}\left[\prod_{k\in\Phi_f}\frac{1}{1+\beta_f\left(\frac{r_k}{r_f}\right)^{-\alpha}}\right] \\
&= e^{\frac{-\lambda_f\pi\, p_{fa}\beta_f R_s^2}{\alpha/2-1}\,{}_2F_1\left(1,1-2/\alpha;2-2/\alpha;-\beta_f\right)}. \qquad (4.24)
\end{aligned}$$

For the macrocell tier interference, we note that the closest MBS (within the same Voronoi cell) now acts as an interferer, and it is always located at a distance r from the typical user, with the condition that $r > R_s$. Similar to the case of the macrocell tier, we define a variable $\Delta = \frac{r_f}{r}$ that will help to simplify the final expression for the coverage probability. With these considerations, we observe that the Laplace transform for the macrocell interference can once again be decomposed into two Laplace transforms, i.e. $\mathcal{L}_{I_{\Phi_m}} = \mathcal{L}^{r}_{I_{\Phi_m}}\mathcal{L}^{''}_{I_{\Phi_m}}$, where $\mathcal{L}^{r}_{I_{\Phi_m}}$ corresponds to the Laplace transform of the closest interferer (at a distance r, conditioned on $r > R_s$), and $\mathcal{L}^{''}_{I_{\Phi_m}}$ is the Laplace transform of the other (non-closest interferer) MBSs. The Laplace transform of the closest interferer is given as

$$\begin{aligned}
\mathcal{L}^{r}_{I_{\Phi_m}}(s) &= \mathbb{E}_{I_{\Phi_m}}\left[\exp(-s)|_{s=r_f^{\alpha}\beta_f\eta^{-1}}\right] \\
&= \mathbb{E}_{|h|^2}\left[\exp\left(-s|h|^2 r^{-\alpha}\right)\right] \\
&= \mathbb{E}_{|h|^2}\left[\exp\left(-|h|^2\beta_f\eta^{-1}\Delta^{\alpha}\right)\right]
\end{aligned}$$

$$= \frac{1}{1+\beta_f \eta^{-1} \Delta^{\alpha}}. \tag{4.25}$$

Considering that the closest MBS will be active with probability p_{ma} and inactive with probability p_{mn}, the final expression is given as

$$\mathcal{L}^{r}_{I_{\Phi_m}}(s) = \frac{p_{ma}}{1+\beta_f \eta^{-1} \Delta^{\alpha}} + p_{mn}. \tag{4.26}$$

For the Laplace transform of the other macrocell interference, we observe that the interference can be as close as $r = \frac{r_f}{\Delta}$ (with $r > R_s$). Therefore, we have

$$\begin{aligned}
\mathcal{L}^{''}_{I_{\Phi_m}}(s) &= \mathbb{E}_{I_{\Phi_m}}\left[\exp(-s)|_{s=r_f^{\alpha}\beta_f\eta^{-1}}\right] \\
&= \mathbb{E}_{\Phi_m,|h_j|^2}\left[\exp\left(-s\sum_{j\in\Phi_m}|h_j|^2\, r_j^{-\alpha}\right)\right] \\
&= \mathbb{E}_{\Phi_m,|h_j|^2}\left[\prod_{j\in\Phi_m}\exp\left(-|h_j|^2\, r_f^{\alpha}\, \beta_f\, \eta^{-1} r_j^{-\alpha}\right)\right] \\
&= \mathbb{E}_{\Phi_m}\left[\prod_{j\in\Phi_m}\frac{1}{1+\beta_f\eta^{-1}\left(\frac{r_j}{r_f}\right)^{-\alpha}}\right] \\
&\overset{(a)}{=} \exp\left(-2\pi\lambda_m p_{ma}\int_{\frac{r_f}{\Delta}}^{\infty}\frac{v\, dv}{1+\left(\frac{v}{\beta_f^{1/\alpha}\eta^{-1/\alpha}r_f}\right)^{\alpha}}\right) \\
&\overset{(b)}{=} e^{-\pi\lambda_m p_{ma}\left(\frac{\beta_f}{\eta}\right)^{2/\alpha} r_f^2 \int_{\left(\left(\frac{\beta_f}{\Delta}\right)^{1/\alpha}\Delta\right)^{-2}}^{\infty}\frac{du}{1+u^{\alpha/2}}} \\
&= e^{\frac{-\lambda_m \pi p_{ma}\beta_f\eta^{-1}\Delta^{\alpha-2}r_f^2}{\alpha/2-1}\,{}_2F_1\left(1,1-2/\alpha;2-2/\alpha;-\beta_f\eta^{-1}\Delta^{\alpha}\right)}
\end{aligned} \tag{4.27}$$

where (a) is obtained by using the PGF of a PPP, and $((b))$ is obtained by using the substitution $u = \left(\frac{r_j}{\beta_f^{1/\alpha}\eta^{-1/\alpha}r_f}\right)^2$.

Now, thanks to the use of the variable $\Delta = \frac{r_f}{r}$ previously defined, the final expression for the coverage probability needs to be averaged over the Δ and r_f. The pdf of r_f is directly obtained from the closest neighbour distribution of a PPP considering a thinning with probability p as

$$f_{r_f}(r_f) = 2\pi\lambda_f\, p\, r_f \exp\left(-\pi\lambda_f\, p\, r_f^2\right). \tag{4.28}$$

In order to obtain the pdf $f_\Delta(\Delta)$, we first need to obtain the pdf of the distance to the closest MBS conditioned on $r > R_s$. We will denote as R the random variable following the Rayleigh distribution for the closest neighbour with the condition that it can only take values above R_s. As R_s is a random variable itself, R follows a random truncated distribution. The pdf of R can then be found as

$$\begin{aligned} f_R(R) &= \int_0^R f\left(R|R_s\right) f(R_s) dR_s \\ &= \int_0^R 2\pi\lambda_m R\, e^{-\pi\lambda_m R^2} (2\pi\lambda_m \tau^{-2} R_s e^{-\pi\lambda_m \left(\frac{R_s}{\tau}\right)^2}) dR_s \\ &= 2\pi\lambda_m R\, e^{-\pi\lambda_m R^2} \left(1 - e^{-\pi\lambda_m \tau^{-2} R^2}\right). \end{aligned} \tag{4.29}$$

Once the distribution of R is found, the pdf of Δ can be obtained by means of the ratio distribution as

$$\begin{aligned} f_\Delta(\Delta) &= \int_{-\infty}^{\infty} |R|\, f_{R,r_f}(R, \Delta r_f)\, dR \\ &= \int_0^\infty R \left(2\pi\lambda_m R\, e^{-\lambda_m \pi R^2} \left(1 - e^{-\pi\lambda_m \tau - 2R^2}\right)\right) \left(2\pi\lambda_f\, p\, \Delta R\, e^{-\pi\lambda_f\, p \left(\Delta r_f\right)^2}\right) dR \\ &= 2\lambda_m^2 \lambda_f\, p\, \left(1 + \tau^{-2}\right) \Delta \left(\frac{\lambda_m \left(2 + \tau^{-2}\right) + 2\lambda_f\, p\, \Delta^2}{\left(\left(\lambda_m + \lambda_f\, p\Delta^2\right)\left(\lambda_m \left(1 + \tau^{-2}\right) + \lambda_f\, p\Delta^2\right)\right)^2}\right). \end{aligned} \tag{4.30}$$

With the expressions previously obtained and conditioning on the probability of the user being served by the femtocell tier $p_{uf} = 1 - p_{um}$, the femtocell coverage probability is given by

$$\mathcal{P}_f^c(\beta_f) = \frac{1}{p_{uf}} \int_0^\infty \int_0^\infty \mathcal{L}^r_{I_{\Phi_m}} \mathcal{L}''_{I_{\Phi_m}} \mathcal{L}_{I_{\Phi_f}} f_{r_f}(r_f) f_\Delta(\Delta) dr_f \, d_\Delta. \tag{4.31}$$

Substituting the values found in (4.24), (4.25), (4.27), (4.28) and (4.30) into (4.31) and integrating with respect to r_f, the final expression in (4.13) is found. □

4.4 Throughput

In this section, the throughput is defined for the BSs of each tier. The throughput in bps/Hz of each tier in the network is defined as a function of the coverage probability as

$$T_i = \log_2(1 + \beta_i)\mathcal{P}_i^c(\beta_i), \; i \in \{m, f\}. \tag{4.32}$$

Now, depending on the load, the effective throughput experienced by a typical user will vary. Thus, we now proceed to find the throughput achieved by the macro and femtocell typical users.

4.4.1 Macrocell user throughput

The macrocell typical user throughput is presented in the next theorem.

Theorem 4.3. *In Stienen's model the macrocell typical user throughput is expressed as*

$$T_{mu} = \int_0^1 \left(\frac{T_0}{p_{um}}\right)\left(\frac{p_{ma}}{1+\beta_m\left(\frac{\psi}{(\tau^{-2}+\psi^2)^{1/2}}\right)^{\alpha}}+p_{mn}\right)\times \left(\frac{\lambda_m\tau^{-2}}{\lambda_u}\right)\ln\left(\frac{1-\frac{\lambda_u}{\lambda_m\tau^{-2}(B+\tau^2)}}{1-\frac{\lambda_u}{\lambda_m\tau^{-2}B}}\right) f_{\psi}(\psi)d\psi \tag{4.33}$$

where $T_0 = \log_2(1+\beta_m)$ *and* $B = 1 + \frac{p_{ma}\beta_m\psi^{\alpha}\,\zeta\left(\alpha,-\beta_m\left(\frac{\psi}{(\tau^{-2}-\psi^2)^{1/2}}\right)^{\alpha}\right)}{\tau^{-2}(\tau^{-1}-\psi)^{\alpha-2}(\alpha/2-1)} + \frac{\lambda_f p p_{fa}\beta_m\eta\tau^2\psi^{\alpha}(1-\psi)^{2-\alpha}}{\lambda_m(\alpha/2-1)}\zeta\left(\alpha,-\beta_m\eta\left(\frac{\psi}{1-\psi}\right)^{\alpha}\right)+\frac{\lambda_u\tau^2}{\lambda_m}$.

Proof. In order to obtain the throughput in the macrocell tier, we need to take into account the fact that the pdf of a cell is modified when it is conditioned on the user being inside [85]. We proceed to find the pdf $f_{\hat{R}_s}(\hat{R}_s)$ of the typical Stienen's cell radius $\hat{R}_s$, by noting that it is a random truncated distribution which is conditioned on the event $r < R_s$ (typical user inside the Stienen cell). With this considerations the pdf of the typical Stienen cell conditioned on the typical user being inside it is given as

$$\begin{aligned} f_{\hat{R}_s}(\hat{R}_s) &= \frac{1}{p_{mu}}\int_0^{\hat{R}_s} f_{R_s|r}\left(\hat{R}_s|r\right) f(r)dr \\ &= \frac{1}{p_{mu}}\int_0^{\hat{R}_s} 2\pi\lambda_m\tau^{-2}\hat{R}_s\, e^{-\pi\lambda_m\tau^{-2}\hat{R}_s{}^2}\times\left(2\pi\lambda_m r e^{-\pi\lambda_m r^2}\right)dr \\ &= \frac{2\pi\lambda_m\tau^{-2}\hat{R}_s\, e^{-\pi\lambda_m tau^{-2}\hat{R}_s{}^2}\left(1-e^{-\pi\lambda_m\hat{R}_s{}^2}\right)}{p_{mu}}. \end{aligned} \tag{4.34}$$

Once $f_{\hat{R}_s}(\hat{R}_s)$ is found, the throughput for the typical user in the macrocell tier can

be obtained by taking into account the other users to be served in the typical Stienen cell. By taking the definition of the coverage probability of the macrocell tier in (4.22), but considering the conditioned pdf of the Stienen's radius ($\hat{R}_s$) recently found, the throughput of the macrocell typical user can be obtained as

$$T_{mu} = \mathbb{E}_{\psi,\hat{R}_s,n_{mu}}\left[T_0\left(\frac{\mathcal{L}^D_{I_{\Phi_m}}\mathcal{L}'_{I_{\Phi_m}}\mathcal{L}_{I_{\Phi_f}}}{1+n_{um}}\right)\right]$$
$$= \mathbb{E}_{\psi}\left[\frac{T_0}{p_{um}}\sum_{n_{um}=0}^{\infty}\int_0^{\infty}\left(\frac{\mathcal{L}^D_{I_{\Phi_m}}\mathcal{L}'_{I_{\Phi_m}}\mathcal{L}_{I_{\Phi_f}}}{1+n_{um}}\right)f_{n_{mu}}(n_{mu})f_{\hat{R}_s}(\hat{R}_s)\,d\hat{R}_s\right]. \quad (4.35)$$

Using the definitions of the Laplace transforms, $f_{n_{mu}}(n_{mu})$ and B, previously defined we have

$$T_{mu} = \mathbb{E}_{\psi}\left[\frac{T_0}{p_{um}}\left(\frac{p_{ma}}{1+\beta_m\left(\frac{\psi}{(\tau^{-2}+\psi^2)^{1/2}}\right)^{\alpha}}+p_{mn}\right)\times\right.$$
$$\left\{\sum_{n_{um}=0}^{\infty}\int_0^{\infty}\frac{2\pi\lambda_m\tau^{-2}\left(\lambda_u\pi\right)^{n_{mu}}\hat{R}_s^{\,2n_{mu}+1}}{1+n_{um}}\times\right.$$
$$\left.\left.\left(e^{-\pi\lambda_m\tau^{-2}\hat{R}_s{}^2B}-e^{-\pi\lambda_m\tau^{-2}\hat{R}_s{}^2(B+\tau^2)}\right)\,d\hat{R}_s\right\}\right]$$
$$= \mathbb{E}_{\psi}\left[\frac{T_0}{p_{um}}\left(\frac{p_{ma}}{1+\beta_m\left(\frac{\psi}{(\tau^{-2}+\psi^2)^{1/2}}\right)^{\alpha}}+p_{mn}\right)\times\right.$$
$$\left.\left\{\sum_{n_{um}=0}^{\infty}\frac{B^{-1}}{n_{mu}+1}\left(\frac{\lambda_u}{\lambda_m\tau^{-2}B}\right)^{n_{mu}}-\sum_{n_{um}=0}^{\infty}\frac{(B+\tau^2)^{-1}}{n_{mu}+1}\left(\frac{\lambda_u}{\lambda_m\tau^{-2}(B+\tau^2)}\right)^{n_{mu}}\right\}\right]$$
$$= \mathbb{E}_{\psi}\left[\frac{T_0}{p_{um}}\left(\frac{p_{ma}}{1+\beta_m\left(\frac{\psi}{(\tau^{-2}+\psi^2)^{1/2}}\right)^{\alpha}}+p_{mn}\right)\times\right.$$
$$\left.\left(\frac{\lambda_m\tau^{-2}}{\lambda_u}\right)\left\{-\ln\left(1-\frac{\lambda_u}{\lambda_m\tau^{-2}B}\right)+\ln\left(1-\frac{\lambda_u}{\lambda_m\tau^{-2}\left(B+\tau^{-2}\right)}\right)\right\}\right]$$

$$= \mathbb{E}_{\psi}\left[\frac{T_0}{p_{um}}\left(\frac{\lambda_m \tau^{-2}}{\lambda_u}\right)\left\{\ln\left(\frac{1-\frac{\lambda_u}{\lambda_m \tau^{-2}(B+\tau^2)}}{1-\frac{\lambda_u}{\lambda_m \tau^{-2} B}}\right)\right\}\right]. \tag{4.36}$$

Taking the expectation with respect to ψ in (4.36), we obtain the final expression in (4.33). □

4.4.2 FEMTOCELL USER THROUGHPUT

The femtocell user throughput is defined in the following theorem.

Theorem 4.4. *In Stienen's model the femtocell typical user throughput is expressed as*

$$T_{fu} = T_0\, \mathcal{P}_f^c(\beta_f)\left(\frac{\lambda_f}{\lambda_u}\left(1-\left[1+\frac{\lambda_u}{3.5\lambda_f}\right]^{-3.5}\right)\right) \tag{4.37}$$

where $\mathcal{P}_f^c(\beta_f)$ was previously defined in (4.13).

Proof. Similar to the analysis of the macrocell typical user throughput, we first proceed to obtain the pdf of the size of the Voronoi cell which contains the typical user. In this case we follow the approach proposed in [90] to derive the pdf ($f_{\hat{y}}(\hat{y})$) of the area ($\hat{y}$) of the Voronoi cell containing the typical user. In this approach, we consider that a user is more likely to be associated with a Voronoi cell of bigger size than with a smaller cell. Therefore, the distribution of the area of the Voronoi cell to which the typical user

belongs to is proportional to its area size:

$$\begin{aligned} f_{\hat{y}}(\hat{y}) &= c\hat{y} f_y(\hat{y}) \\ &= c\,\frac{3.5^{3.5}}{\Gamma\,(3.5)}\lambda_f^{3.5}\hat{y}^{3.5}e^{-3.5\lambda_f\hat{y}}. \end{aligned} \tag{4.38}$$

where $f_y(y)$ is the pdf of a typical Voronoi cell's area. In order to comply with the property stating that the integration of a pdf over its range should equal unity, we obtain the value of c as

$$c = \frac{1}{\int_0^\infty f_{\hat{y}}(\hat{y})\,d\hat{y}} = \frac{1}{\mathbb{E}[y]} = \lambda_f. \tag{4.39}$$

The pdf of $\hat{y}$ is then given as

$$f_{\hat{y}}(\hat{y}) = \frac{3.5^{3.5}}{\Gamma\,(3.5)}\lambda_f^{4.5}\hat{y}^{3.5}e^{-3.5\lambda_f\hat{y}}. \tag{4.40}$$

In this case it is difficult to find a relation between the size of the Voronoi $\hat{y}$ cell to which the typical user belongs and the distribution of SIR_f, so we assume an independence between them both. So, we proceed to find the pmf ($f_{\hat{n}_{uf}}$) of the number of users ($\hat{n}_{uf}$) inside the Voronoi cell containing the typical user as

$$\begin{aligned} f_{\hat{n}_{uf}}(\hat{n}_{uf}) &= \int_0^\infty f_{n_{uf}|y}\,(\hat{n}_{uf}|\hat{y}) f_{\hat{y}}(\hat{y})\,d\hat{y} \\ &= \int_0^\infty \frac{(\lambda_u\hat{y})^{\hat{n}_{uf}}\,e^{-\lambda_u\hat{y}}3.5^{3.5}}{\hat{n}_{uf}!\,\Gamma\,(3.5)}\lambda_f^{4.5}\hat{y}^{3.5}e^{-3.5\lambda_f\hat{y}}d\hat{y} \\ &\overset{(a)}{=} \frac{\lambda_u^{\hat{n}_{uf}}\lambda_f^{4.5}\,3.5^{3.5}\Gamma(\hat{n}_{uf}+4.5)}{\hat{n}_{uf}!\,\Gamma(3.5)}\;(\lambda_u+3.5\lambda_f)^{-\hat{n}_{uf}-4.5} \\ &= \left(\frac{\lambda_f}{\lambda_u+3.5\lambda_f}\right)^{4.5}\left(\frac{\lambda_u}{\lambda_u+3.5\lambda_f}\right)^{\hat{n}_{uf}} \times \frac{3.5^{3.5}\,\Gamma(\hat{n}_{uf}+4.5)}{\hat{n}_{uf}!\,\Gamma(3.5)}. \end{aligned} \tag{4.41}$$

where the step (a) was achieved by using the property $\int_0^\infty x^a e^{-bx} = b^{-1-a}\,\Gamma(a+1)$. Using the distribution of $\hat{n}_{uf}$ just found, and again assuming independence of SIR_f and $\hat{y}$ we obtain

$$\begin{aligned}
T_{fu} &= \mathbb{E}_{\hat{n}_{uf}}\left[\frac{\mathcal{P}_f^c(\beta_f)\log_2(1+\beta_f)}{1+\hat{n}_{uf}}\right] \\
&= \mathcal{P}_f^c(\beta_f)\,T_0 \sum_{\hat{n}_{uf}}^{\infty} \frac{f_{\hat{n}_{uf}}(\hat{n}_{uf})}{1+\hat{n}_{uf}} \\
&= \frac{\mathcal{P}_f^c(\beta_f)T_0\left(\frac{\lambda_f}{\lambda_u+3.5\lambda_f}\right)^{4.5} 3.5^{3.5}}{\Gamma(3.5)} \sum_{\hat{n}_{uf}}^{\infty} \frac{\left(\frac{\lambda_u}{\lambda_u+3.5\lambda_f}\right)^{\hat{n}_{uf}} \Gamma(\hat{n}_{uf}+4.5)}{(\hat{n}_{uf}+1)!} \\
&= \frac{\mathcal{P}_f^c(\beta_f)T_0\left(\frac{\lambda_f}{\lambda_u+3.5\lambda_f}\right)^{4.5} 3.5^{3.5}}{\Gamma(3.5)} \left[\frac{\Gamma(4.5)\left(1-\frac{\lambda_u}{\lambda_u+3.5\lambda_f}+\left(1-\frac{\lambda_u}{\lambda_u+3.5\lambda_f}\right)^{4.5}\right)}{\left(1-\frac{\lambda_u}{\lambda_u+3.5\lambda_f}\right)^{4.5}\left(\frac{\lambda_u}{\lambda_u+3.5\lambda_f}\right)(3.5)}\right] \\
&= \mathcal{P}_f^c(\beta_f)\,T_0\left(\frac{\lambda_f}{\lambda_u}\right)\left(1-\left(1+\frac{\lambda_u}{3.5\lambda_f}\right)^{-3.5}\right)
\end{aligned} \tag{4.42}$$

which concludes the proof. □

4.5 Energy Efficiency

In order to characterize the power consumed in the system, we make use of EARTH's model [91] given as

$$P_i = \frac{\frac{P_i^{tx}}{\eta_i^{PA}\left(1-\sigma_i^{feed}\right)} + P_i^{RF} + P_i^{BB}}{(1-\sigma_i^{DC})(1-\sigma_i^{MS})(1-\sigma_i^{COOL})} \tag{4.43}$$

where η_i^{PA} is the efficiency of the power amplifier, P_i^{RF} is the RF transceiver energy consumption, P_i^{BB} is the power consumption of the base band interface and σ_i^{feed} accounts for the feeder loses. Additionally, σ_i^{DC}, σ_i^{MS} and σ_i^{COOL} represent respectively the loss factor of the DC-DC power supply, main supply and cooling of the

sites. Moreover, the RF transceiver energy consumption (P_i^{RF}) is composed by the power used for transmission $P_i^{RF,tx}$ and the one used for reception $P_i^{RF,rx}$. On the other hand, the base band interface power consumption (P_i^{BB}) is formed by the reception/transmission radio power consumption $P_i^{BB,rx/tx}$, the LTE turbo encoding power consumption $P_i^{BB,LTE}$ and the power used in the processors $P_i^{BB,processors}$. Therefore, we have

$$P_i^{RF} = P_i^{RF,tx} + P_i^{RF,rx} \tag{4.44}$$

$$P_i^{BB} = P_i^{BB,rx/tx} + P_i^{BB,LTE} + P_i^{BB,processors} \tag{4.45}$$

A full list of each of the components of EARTH's model can be found in [91] while the typical values of the components used in this chapter are presented in Table 4.1. From (4.43) we see that the power consumption model agrees with the general model assumed in other works ([36, 52, 92]) which considers a component (a_i) dependent on the transmitted power and a component (b_i) independent of it. Note that in contrast with other chapters we have adopted EARTH's model due to the fact that its use has become more popular with time due to its detailed power consumption description. The power consumption can then be expressed as

$$P_i = a_i P_i^{tx} + b_i \tag{4.46}$$

where $a_i = \frac{1}{\eta_i^{PA}\left(1-\sigma_i^{feed}\right)(1-\sigma_i^{DC})(1-\sigma_i^{MS})(1-\sigma_i^{COOL})}$ and $b_i = \frac{P_i^{RF}+P_i^{BB}}{(1-\sigma_i^{DC})(1-\sigma_i^{MS})(1-\sigma_i^{COOL})}$.

The EE is defined in terms of the throughput and the power used to operate the cellular system. We use the definition provided in the Energy Consumption Rating

[47], as

$$EE = \frac{T}{P} \qquad \text{b/J} \tag{4.47}$$

where T is the throughput in bps, and P is the power used in the system in Watts. For the scenario analyzed in this chapter, the energy efficiency is given by

$$\begin{aligned} EE &= \frac{N_m p_{ma} T_m + N_f p p_{fa} T_f}{N_m P_m + N_f P_f} \\ &= \frac{\lambda_m p_{ma} T_m + \lambda_f p p_{fa} T_f}{\lambda_m \left(p_{ma} P_m + p_{mn} b_m\right) + \lambda_f \left(p_{fa} P_f + p_{fn} b_f\right)} \end{aligned} \tag{4.48}$$

where the EE is given in b/s/Hz and we used the substitution $N_i = \lambda_i A$, $i \in \{m, f\}$.

It is important to notice that one of the techniques for future deployment of HetNets which promises high savings in the overall EE of the systems is the sleep mode configuration in the different types of BSs. In order to quantize the extra savings in power consumption by equipping the BSs with sleep mode configuration, we assume that both MBSs and FAPs can turn off some of their components in a given time slot when they are not serving any users. In particular some of the power components of b_m and b_f in (4.48) are not needed when a BSs is not transmitting. Thanks to the breakdown of the power consumption in a BS provided in EARTH's project, a sleep mode power consumption can be quantized by assuming that some components of a BS can be shut down to save energy when the BS does not have any users to serve. In particular for a non-active BS, the transmitted power is $P_i^{tx} = 0$ Watts, and so there is no power consumed in the power amplifier. Also, we assume that in the baseband interface, only the processor remains on ($P_i^{BB,rx/tx} = P_i^{BB,LTE} = 0$ in (4.45)). Finally, in the small signal RF transceiver, we assume that the transmitter part can be shut down and only the power related to the receiver remains turned on for reception

($P_i^{RF,tx} = 0$ in (4.44)). With this assumptions, the total power consumption in a BS of the i-th tier operating in sleep mode is expressed as

$$P_i^{sleep} = \frac{P_i^{RF_{sleep}} + P_i^{BB_{sleep}}}{(1-\sigma_i^{DC})(1-\sigma_i^{MS})(1-\sigma_i^{COOL})}. \tag{4.49}$$

where $P_i^{RF_{sleep}} = P_i^{RF,rx}$ and $P_i^{BB_{sleep}} = P_i^{BB,processors}$. The values for the power consumption of the small signal transceiver $P_i^{RF_{sleep}}$ and the baseband interface $P_i^{BB_{sleep}}$ when a BS in the i-th tier is operating in sleep mode are obtained from [91], and presented in table 4.1. Under this scenario, (4.48) transforms into

$$EE_{sleep} = \frac{\lambda_m p_{ma} T_m + \lambda_f p p_{fa} T_f}{\lambda_m \left(p_{ma} P_m + p_{mn} P_m^{sleep}\right) + \lambda_f \left(p_{fa} P_f + p_{fn} P_f^{sleep}\right)} \tag{4.50}$$

where P_i^{sleep}, $i \in \{m, f\}$ is the power consumed when the BS in the i-th tier operates in sleep mode, as defined in (4.49).

With the expression for the throughput and the power consumption in each tier previously found, the overall system EE can be obtained. In the next section, the numerical results for the proposed model are presented.

Table 4.1: SIMULATION PARAMETERS

Parameter	Value	Description
$\lambda_m, \lambda_f, \lambda_u$	$1.54\text{x}10^{-6}$, $[0, 6.16 \text{ x } 10^{-4}]$, $\{1.54 \text{ x } 10^{-5}, 3.08 \text{ x } 10^{-5}, 4.62\text{x}10^{-5}\}$	Density of MBSs, FAPs and users respectively
$\alpha_m = \alpha_f = \alpha$	4	Path loss exponent
η_m^{PA}, η_m^{PA}	0.388, 0.052	Efficiency of the power amplifier in the macro- and femtocell respectively
P_m^{RF}, P_f^{RF}	10.9, 0.4	RF transceiver power in the macro- and femtocell respectively
P_m^{BB}, P_f^{BB}	14.8, 1.2	Baseband interface power in the macro- and femtocell respectively
$P_m^{RF_{sleep}}, P_f^{RF_{sleep}}$	5.1, 0.2	Sleep mode RF transceiver power in the macro- and femtocell respectively
$P_m^{BB_{sleep}}, P_f^{BB_{sleep}}$	5, 0.1	Sleep mode baseband interface power in the macro- and femtocell respectively
$\sigma_m^{DC}, \sigma_f^{DC}$	0.06, 0.08	Loss factor of the DC-DC power supply in the macro- and femtocell respectively
$\sigma_m^{COOL}, \sigma_f^{COOL}$	0.09, 0	Loss factor of the cooling of site in the macro- and femtocell respectively
$\sigma_m^{MS}, \sigma_f^{MS}$	0.07, 0.1	Loss factor of the main supply in the macro- and femtocell respectively
$\sigma_m^{feed}, \sigma_f^{feed}$	0, 0	Loss factor of the feeder in the macro- and femtocell respectively
τ	$\frac{1}{2}$	Stienen radius factor

4.6 Numerical results

In this section, we: (i) validate the already developed framework, and (ii) employ the developed analytical model in conjunction with Monte Carlo simulations to explore coverage, throughput and EE performances for the considered HetNet deployment. The results are presented in figures 4.3 to 4.8. It is worthwhile mentioning that in the simulations, for the case of the femtocell typical user ($r > R_s$) when we place a random user at a distance r from the typical MBS (located at the origin) following a Rayleigh distribution as detailed in section 4.3.2, if the value of r exceeds the size of the typical MBS, we suppress this point and generate another one, until it is located outside the Stienen radius ($r > R_s$) but inside the typical MBS. This approach is taken given that it is difficult to effectively model the distribution of a random variable describing the position of the user outside the Stienen radius but inside the typical MBS coverage region. This follows from the variation of a Voronoi cell and its asymmetry with respect to its seed. By placing the user in this manner, this will of course have and effect on the distribution of Δ in (4.30) and so the theory will differ from the simulations. However, as it will be seen in this section, the results are not greatly affected.

Figure 4.3 shows the coverage probability in the macrocell tier, when the number of femtocells is increased in the service area. We can see that for small values of β the proposed model highly resembles the results found through simulations. Moreover, for a value of $\beta = 20$ the variation between the results from simulations and the analytical results is around 3%. This deviation from the simulation results is due to the approximations used in order to keep a tractable mathematical model. Therefore, while more accurate results could be found, the resulting model would lack of the tractable frame-

work developed in this thesis. Moreover, we see that initially, increasing the number of femtocells deployed generates a decrease in the macrocell coverage probability due to the increase of interference. However, when the number of femtocells deployed is large enough, the macrocell coverage probability reaches a constant value. Intuitively, these results follow from the fact that for a small density of FAPs, the coverage region of each femtocell is big, and so they will serve more users. By increasing the density, the coverage region of each femtocell decreases, and more FAPs will be active (i.e., p_{fa} will be higher) in order to provide a service to the users located in the outermost areas of a macrocell. If the density of femtocells is high enough, the coverage region of each femtocell will be so small that it will only (approximately) serve one user. Therefore, the maximum density of active (interfering) FAPs λ_f^{max} will equal the density of users deployed in the femtocell tier coverage regions (i,e. $\lambda_f^{max} = \lambda_u p$). In other words, for a high number of femtocells, the maximum number of interferers is dictated by the density of users.

In Figure 4.4, we present the performance in terms of coverage probability for the femtocell tier, as a function of the femtocells deployed. We observe that increasing the number of femtocells in the area has a direct effect of increasing the coverage probability for a fixed value of λ_u and β. This is an expected behaviour given that increasing the density of femtocells derives into smaller coverage regions of each femtocells. This in turn is reflected into a smaller distance between a femtocell user and its designated FAP. Thus, from a coverage probability point of view, deploying a higher number of femtocells is always desirable in the femtocell tier. From the results of figures 4.3 and 4.4, we can conclude that placing the femtocell tier only in areas where the received signal from a MBS is expected to be low greatly improves the coverae probability of the femtocell tier, while the macrocell tier's coverage is not highly affected. Note that

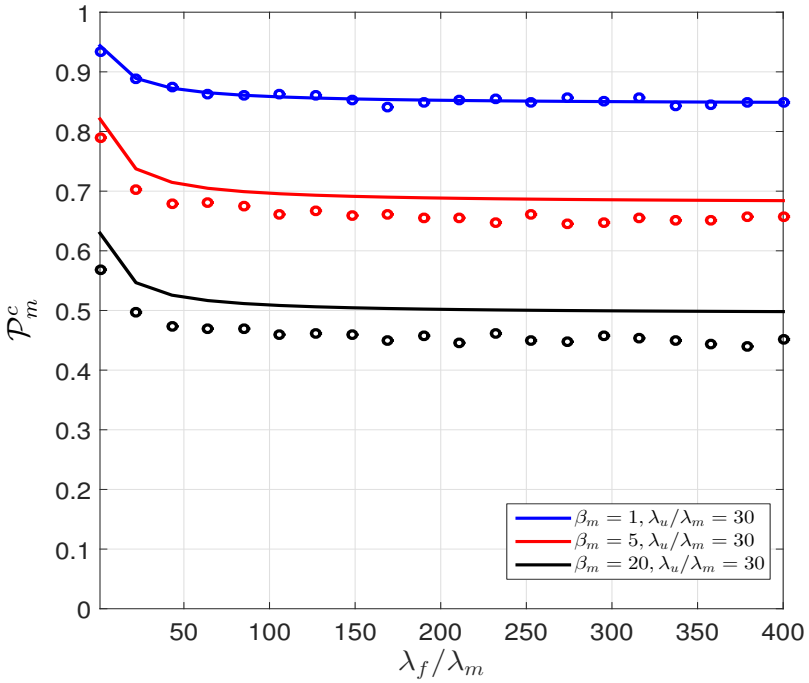

Figure 4.3: Macrocell coverage probability (4.12) as a function of the density of femtocells deployed in the area for different threshold values β_m, and $\frac{\lambda_u}{\lambda_m} = 30$. Circles represent the results from Monte Carlo simulations (with 5 x 10^4 runs for each point) while lines correspond to the analytical values.

by incorporating the strategic positioning of femtocells into the model, the coverage probability depends highly on the density of BSs. This is in contrast with results from other works which consider that all tiers are uniformly distributed in the area, in which case both the coverage and the data rates are independent of the density of BSs [14,15].

In Figure 4.5, the macrocell user throughput is presented as a function of the density of femtocells deployed in the area for the same threshold β and for different values of the density of users λ_u in the area. As expected, the increase in the density of users reduces the throughput achieved per user in the macrocell tier. Due to the behaviour of the coverage probability, the throughput per macrocell user follows the same trend.

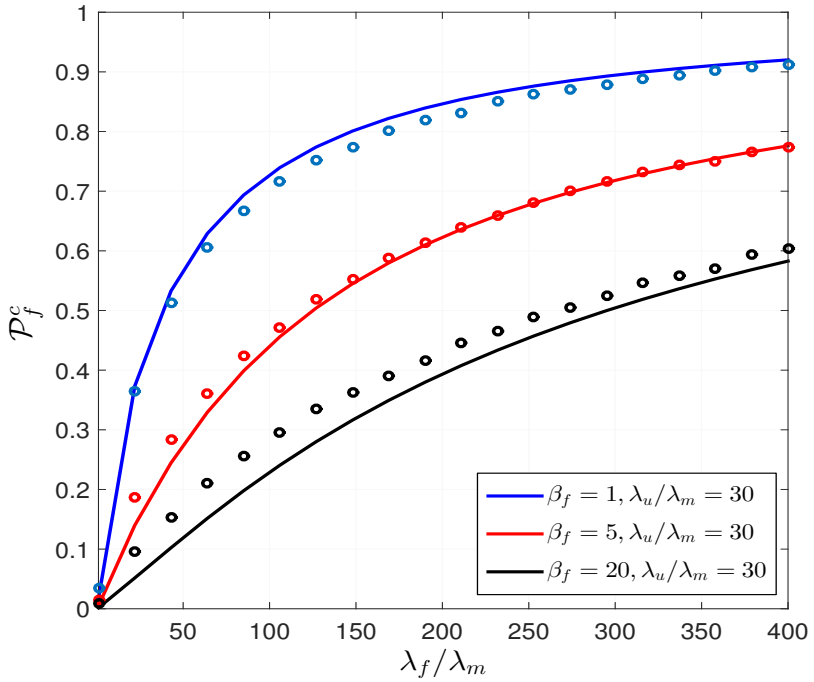

Figure 4.4: Femtocell coverage probability (4.13) as a function of the density of femtocells deployed in the area for different threshold values β_f, and $\frac{\lambda_u}{\lambda_m} = 30$. Circles represent the results from Monte Carlo simulations (with 5 x 10^4 runs for each point) while lines correspond to the analytical values.

Namely, by increasing the number of femtocells in the area, the throughput of the macrocell typical user is decreased until it reaches a minimum when the number of active interfering femtocells equals the number of users to be served by the femtocell tier.

The expected throughput per femtocell user is presented in Figure 4.6 as a function of the number of femtocells deployed by keeping the same value for the threshold β and having different values of the user density λ_u. In these case, an improvement in the perceived throughput per femtocell user is achieved by increasing the number of femtocells. These results provide the means by which network operators can plan the number of femtocells to be deployed in order to achieve a more balanced network in

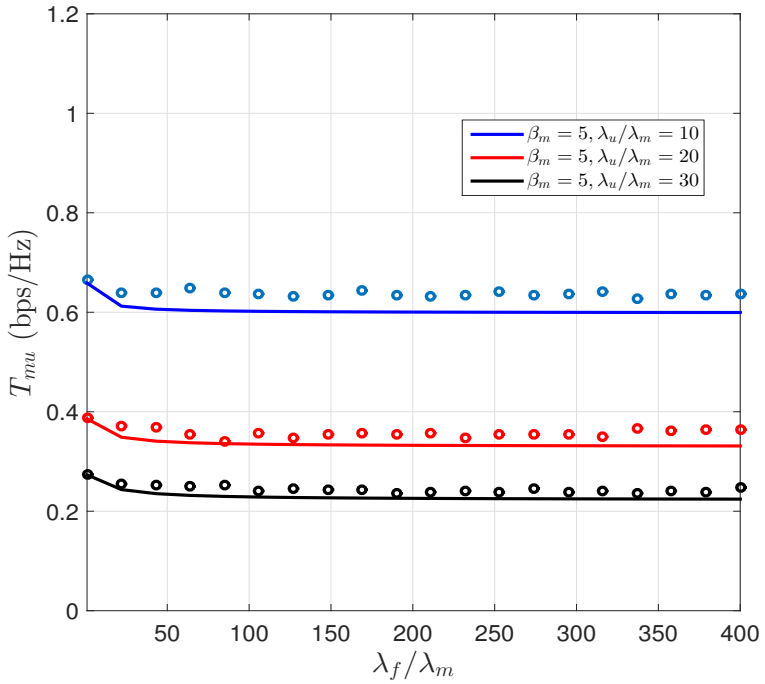

Figure 4.5: Macrocell typical user throughput (4.33) probability as a function of the density of femtocells deployed in the area for the same value of $\beta_m = 5$, and for different values of the density of users λ_u. Circles represent the results from Monte Carlo simulations (with 5 x 10^4 runs for each point) while lines correspond to the analytical values.

terms of the experienced user throughput. In other words, the operators can decide on the number of femtocells that would achieve the level of service required throughout the entire network, effectively eradicating the edge user bottleneck.

The EE of the network is presented in Figure 4.7 when the number of femtocells deployed is increased. We observe that the EE follows a quasi-concave shape, meaning that an increase in the number of femtocells is directly related to an increase in the energy efficiency of the network when the number of femtocells deployed is relatively small. However, as the number of femtocell increases beyond a given threshold (which varies with respect to β), the EE of the system starts to decrease. This behaviour agrees with previous works on EE, where a trade-off between the achievable through-

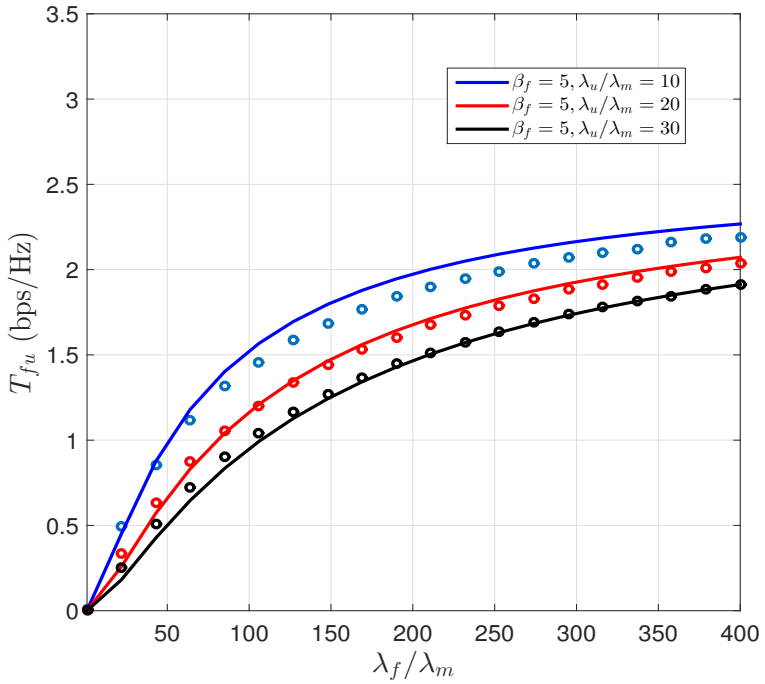

Figure 4.6: Femtocell typical user throughput (4.37) as a function of the density of femtocells deployed in the area for different threshold values β_f, and $\frac{\lambda_u}{\lambda_m} = 30$. Circles represent the results from Monte Carlo simulations (with 5 x 10^4 runs for each point) while lines correspond to the analytical values.

put (or spectral efficiency) and the EE has been observed. Intuitively, an increase in the number of femtocells deployed creates high gains in the expected throughput when this number is still relatively small. However, an increase in the number of FAPs deployed also generates an increase in the total power consumption of the network. As the achievable expected throughput is limited (given that the maximum value of $\mathcal{P}_f^c$ is 1), when the number of femtocells deployed is significantly increased, the power consumed in all FAPs overweighs the increase in throughput and so the EE starts decreasing. This is evident from figures 4.4 and 4.7, where we can see for example that for $\beta = 5$ and $\lambda_u = 30$, increasing the number of femtocells beyond $\frac{\lambda_f}{\lambda_m}$ would give an increase in the coverage probability, but it would also generate a decrease in the EE

of the network. However, it is worthwhile mentioning that even when the density of femtocells exceeds the value when the EE is still increased, the EE achieved by the proposed model can still be superior to a uniform deployment of base stations across the area.

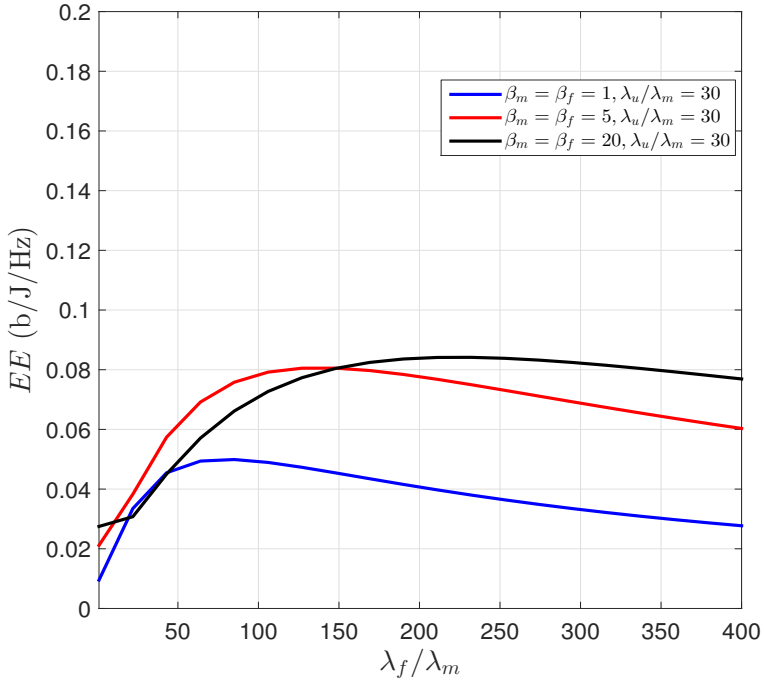

Figure 4.7: Energy efficiency (4.48) as a function of the density of femtocells deployed in the area for different threshold values $\beta_i, i \in \{m, f\}$, and $\frac{\lambda_u}{\lambda_m} = 30$. Circles represent the results from Monte Carlo simulations (with 5 x 10^4 runs for each point) while lines correspond to the analytical values.

In Figure 4.8, the EE of the network is plotted when both MBSs and FAPs have sleep mode capabilities. In this scenario, further improvements in the EE can be achieved by effectively turning off some components of the base stations in order to save power. We can see that even through the EE still follows a quasi-concave shape (as expected), the gradient with which the EE decays after reaching its maximum value is almost constant in comparison with the case without sleep mode. This gives the net-

work operator more room to further increase the expected throughput while still having an acceptable performance in terms of the overall EE. Moreover, from Figure 4.8 we observe an increase of about 87% in the maximum achievable EE with sleeping mode over the EE without sleeping mode for $\beta = 5$ and $\frac{\lambda_u}{\lambda_m} = 30$.

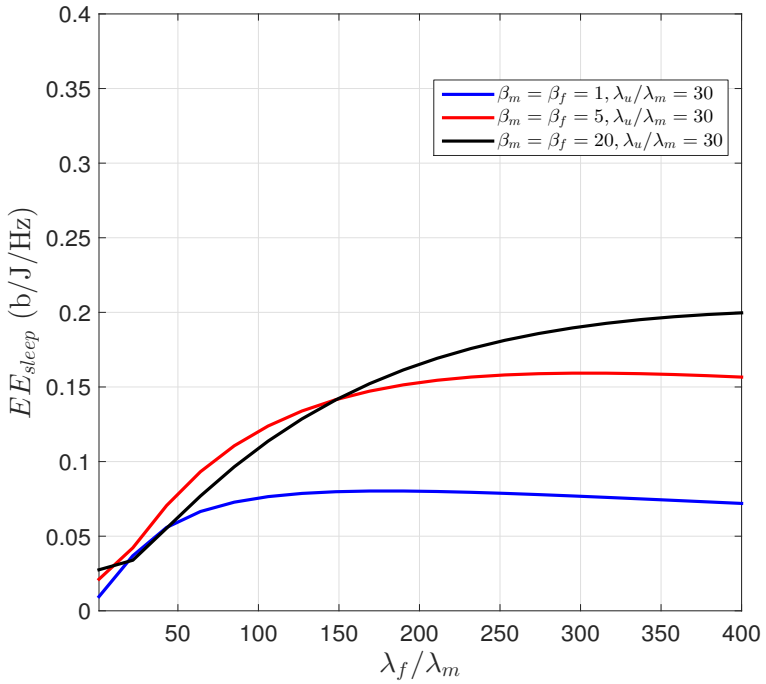

Figure 4.8: Energy efficiency with sleep mode capabilities (4.50) as a function of the density of femtocells deployed in the area for different threshold values β_i, $i \in \{m, f\}$, and $\frac{\lambda_u}{\lambda_m} = 30$. Circles represent the results from Monte Carlo simulations (with 5 x 10^4 runs for each point) while lines correspond to the analytical values.

The set of results presented in this section shows the increase in coverage probability, throughput and EE of the femtocell tier, while the performance of the macrocell tier is not greatly affected. Additionally, the coverage probability of the macrocell tier is increased in comparison with a typical macrocell deployment such as the one presented in [14]. It is worthwhile mentioning that while the values found do not represent the optimum topology in the femtocell tier, the results can be regarded as a worst case

scenario from which the network's design guidelines can be obtained. This is due to the fact that using a uniform distribution of femtocells across the area near the cell edge is not optimal as some of the FAPs could be either too close or too far from each other. In practice, depending upon the number of femtocells to be deployed, a uniform distance between neighbouring FAPs is to be expected. Nevertheless, the results of this chapter represent (as mentioned before), a worst case scenario, meaning that in practice we can expect a performance better than the one obtained analytically. Furthermore, having a set of femtocells very close to each other can be considered as a scenario with hotpots, where a higher number of FAPs are required in order to cope with the increase in traffic in particular areas.

4.7 Conclusions

In this chapter we introduced Stienen's model for the modeling of non-uniform network deployment. With this model, femtocells are only deployed outside the discs surrounding the macro base stations. Each of these radii depends on the distance to the closest MBS (and therefore depends also on each MBS size) which accounts for a realistic topology. Using stochastic geometry tools we found approximations for the coverage probability, expected user throughput and system energy efficiency of the network. Results confirm high gains in both throughput and the EE that can be achieved by cleverly placing femtocells in areas where the performance is expected to be low (near the edge of each MBS). Additionally, a more balanced network can be achieved, due to the fact that deploying higher number of femtocells in the area with this topology greatly increases the femtocell user performance (users closer to the MBS edge) while the macrocell user performance is not significantly decreased.

5 Conclusion & Future Work

IN THIS CHAPTER...

The concluding remarks following from the aforementioned work are now presented. Additionally, future directions as a result of this work, are identified as potential for future research.

5.1 Conclusions

Several conclusions have arisen from the study carried out in this thesis for the different deployment scenarios. First, the common denominator throughout the cases studied was the use of stochastic geometry tools to model the different tiers of the HetNets. As a result, a large scale characterization of different performance metrics of the network was attained. The use of stochastic geometry allowed us to explore the impact and quantize the particular effect of different design variables on the performance of the network while keeping an energy efficiency perspective. We have demonstrated that the often overlooked energy efficiency is a critical parameter that needs to be addressed for future HetNets, where the large number of base stations deployed means a large power consumption, which could outweigh the gains in throughput. Therefore, a trade-

off between the spectral efficiency (or throughput) and the energy efficiency takes an important part in several deployment scenarios studied for two tier networks. It is also important to notice that the use of stochastic geometry provides an accurate solution for the modelling of large scale networks. However, due to the highly non-linear behaviour of the performance metrics evaluated, in some cases the solution of the optimization problems cannot be found in a closed form expression. A workaround to this would be to try to approximate the resulting expressions with easier to handle functions that could improve either the speed of the iterative optimization process (like the interior point method used in chapter 3) or in some cases find a close form solution (like in the optimization addressed in 2). However, the accuracy of the final solutions found using these procedure would be reduced as a result of this approximation. Therefore, a compromise of the speed of the method and its accuracy would have to be addressed.

The energy efficiency of MIMO diversity schemes was studied in detail in chapter 2. We analysed the energy efficiency aspect of diversity schemes while keeping constraints on the expected user QoS. We demonstrated that the use of multiple antennas can improve both the throughput and the energy efficiency of the system. However, the number of antennas used needs to be judiciously selected to achieve those gains. A higher number of antennas is directly related to an increase in the throughput of the system but it is also related to a higher power consumption due to the power consumed in the RF chains. Additionally, as the interference becomes a paramount issue limiting the gains in throughput, we showed a direct relationship between the density of femtocells deployed and the number of antennas which effectively achieve gains in throughput in comparison with a SISO system. Moreover, we also demonstrated the existence of an optimum number of antennas for each diversity scheme which maximizes the energy efficiency. On the other hand, we also proved that the selection of an

optimum diversity scheme in terms of energy efficiency is also related to the amount of interference of the system. Therefore, for a given density of femtocells, there is a diversity scheme which maximizes the energy efficiency of the system. As a consequence of these findings we have concluded that there is an optimum diversity scheme and antenna configuration that yields the best performance in terms of energy efficiency when constraints on the QoS are imposed. From the results obtained we have also concluded that the diversity schemes which attain the best EE performance are the ones that strike a good balance between the achievable throughput and the power consumed, as both of them (i.e., throughput and power) increase with the number of antennas. These results show a trade-off between the spectral and energy efficiency in terms of the diversity schemes and antenna selection.

We have addressed the energy efficiency aspect of the antenna tilt in chapter 3, where we studied a co-channel deployment for macro- and femtocells. In the first stage a macrocell-only network was studied and with the aid of tools from stochastic geometry a simplified model was obtained from which the scalability of the network in terms of the density of MBSs can be quantized in the performance of the network. With the simplified model we have corroborated the findings of other works in which the existence of an optimum antenna tilt that maximizes the coverage probability of the network has been proven. We have shown that the aftermath of deploying a number of femtocells is a decrease of the optimum tilt angle that maximizes the coverage probability. Therefore, we can conclude that the increase of interference created by the femtocell tier, has a bigger impact on the cell edge user performance, and so the MBS main antenna beam should be pointed towards the edge of the macrocell coverage region in order to compensate for this. With this model, we have demonstrated that the optimum antenna tilt that maximizes both the coverage probability and the EE

of the network increases as the density of MBSs increases, and vice-versa. In the case of a two-tier network, in a first stage it was found that the macrocell user performance is considerably reduced in comparison with the femtocell user performance when a femtocell tier is deployed, and so a guard zone protecting macrocell users was proven to be a viable solution in this case. We have demonstrated that there is an optimum value of the antenna tilt that maximizes the coverage probability of the network which is dependent on system parameters such as the density of femtocells, the wall partition loss and the path loss exponent. Additionally, we have shown that this tilt angle does not correspond to the value that maximizes the energy efficiency, and so a compromise should be addressed while selecting the tilt angle. This can be done by imposing minimum QoS requirements, just as we have done in this thesis.

The topology of the network was shown to have great potential for improving the performance of the network in terms of coverage probability, network throughput and the energy efficiency. In chapter 4 a co-channel non-uniform deployment of femtocells overlaid the macrocell tier. We demonstrated that placing the femtocells towards the edge of the macrocell coverage region yields gains in the coverage probability, throughput and energy efficiency in the femtocell tier. We also proved that the macrocell user performance is not significantly compromised by the addition of femtocells and the additional interference that they convey due to the fact that macrocell users are located in areas where the power received from the MBS is high. Additionally, a limit on the number of interferers is imposed by the density of users as the density of femtocells which will remain active are the ones that have at least one user within their coverage region. And so, when the density of femtocells is high enough, each femtocell will serve a single user and the effective density of interfering FAPs will be equal to that of the users. On the other hand, we demonstrated that by appropriately

selecting the density of femtocells, the same performance in terms of coverage can be expected for both the typical users and the cell edge user. Therefore, with the strategic positioning of femtocells towards the edge of the macrocell service area a more balanced network can be achieved.

5.2 Future work

As a direct outcome of the study conducted in this thesis a series of future directions have been identified for the different scenarios and deployment strategies addressed.

A trade-off between the energy efficiency and the spectral efficiency for MIMO diversity schemes was identified in chapter 2. A highly dense scenario was addressed where it was assumed that both outdoor MBSs and FAPs always have a user to transmit. Under this consideration, a split spectrum was identified as a way to control the inter-tier interference. In future deployment scenarios, it is envisaged that there will be an ultra densification of the network in terms of serving BSs. In this case, the number of base stations can greatly exceed the density of users, in which case a split spectrum strategy would result in an underutilization of the available spectrum. Therefore, it would be interesting to compare the achievable energy efficiency of a co-channel deployment with that of a split spectrum strategy. Moreover, it would also be interesting to find the relationship between the density of users and BSs in which a split spectrum approach is preferred over a co-channel strategy, and vice-versa. Additionally, the study of the performance of multi-user MIMO in terms of the coverage and throughput has been addressed in recent works. However, the energy efficiency aspect has been overlooked. Therefore, an in-depth study of the interrelations and trade-offs between the spectral efficiency and the energy efficiency would be an interesting approach. Fi-

nally, a proposed solution for 5G requirements to cope with the higher demands for data rates is the use of large antenna arrays, which is commonly referred as massive MIMO. Among the different aspects that need to be considered for massive MIMO to become a reality, the characterization of the energy efficiency takes on an important role, as not only the transmission power would be incremented but also the power consumption related to the signal processing of such a high number of antennas. Thus, a proper modelling of the power consumption for massive MIMO is in place, as well as a characterization of the energy efficiency of massive MIMO HetNets.

The interrelationship between the antenna tilt angle and the energy efficiency of a two-tier HetNet was addressed in chapter 3. A straightforward path from the study carried out lies in the concept of vertical sectorization. While the traditional (horizontal) sectorization has been extensively studied in the past, recent works have considered the configuration of several beams in the vertical plane for further performance enhancements of the system. Therefore, an interesting direction for future study would be to develop an analytical approach for vertical sectorization with the use of stochastic geometry to asses the improvements in the energy efficiency. From the developed framework, an optimization of the antenna tilts would be the next step. Additionally, the millimetre band has been clearly identified as one of the possible enabling technologies for future 5G deployments. A common trend in these cases is to consider a directional beamforming. While recent works have developed initial models for millimetre wave technology, an in-depth analysis of the energy efficiency of HetNets in the millimetre band has not been explored yet. Moreover, a full 3D model that considers the antenna tilt in the vertical plane and directional beamforming in the horizontal plane is needed. Furthermore, the interdependence between the antenna tilt and the parameters of HetNets would need to be explored in order to optimize the tilt angle

accordingly.

The results obtained in chapter 4 showed that non-uniform deployments of HetNets have the potential to greatly increase the performance of the network and the energy efficiency. We consider typical values of the transmitted power in both, the macrocell and the femtocell tier. However, due to the difference in the size of the service areas by the BSs in both tiers, the use of different transmission power dependent on the extent of the regions to be covered can further increase the energy efficiency of the network. Additionally, transmitting with a reduced power can improve the throughput due to the interference reduction to neighbouring cells. Therefore, a direct step that follows is to consider a power control in the two tier network, with the aim to minimize the power consumption. On the other hand, for future deployments, where the intricacies associated with the positions of the users and the network conditions, the use of PPPs may not be appropriate to accurately model the expected performance. Recent works have introduced the Ginibre point process as a promising solution for repulsive networks, in which the points in the process appear to repel each other. Thus, the Ginibre point process can be suitable to create a bridge between the randomness of a network and its deterministic patterns. It would be interesting to address the trade-offs of such a modelling with regards to the potential energy efficiency gains.

Additionally, throughout the thesis the emphasis was to optimize the energy efficiency of the network while keeping constraints on the QoS of each tiers. This is along the lines of other works where the aim has been to either maximize the energy efficiency or minimize the power consumption subject to some constraints. A future direction however would be to consider multi-objective optimization scenario in which not only the energy efficiency but also the QoS in all the tiers are considered. Analysing and comparing these results with the ones obtained in this thesis would be

interesting. Finally, in this thesis the effect of the backhaul was not taken into account. So, a future direction would be to also include it in the analysis and evaluate the intricacies associated with a wired or wireless backhauling and its effect on the network's performance.

A Appendix of mathematical preliminaries

IN THIS APPENDIX:

The mathematical foundations that will help to fully understand the study carried out in this thesis are now presented.

A.1 Point process theory

As discussed in chapter 1, throughout this thesis we have made use of tools from stochastic geometry to study in-depth the performance of the network while having a mathematical framework to analyse the performance of a two-tier HetNet from an EE perspective.

In section 1.3 an informal introduction to point processes was presented. The point process theory is now formally addressed and its main mathematical properties are introduced. Among the different types of point processes available, the most widely used and studied is the Poisson point process (PPP) due to its many benevolent characteristics. This motivated the use of PPPs to model the different scenarios considered

in this thesis. Therefore, in the remainder of this appendix, the general characteristics which apply to all point processes are addressed while particularities of the PPP are elaborated when further specification is needed.

A.1.1 Overview

Formally, a point process Φ on $\mathbb{R}^d$, is defined as a measurable mapping from a probability space $[\Omega;\mathcal{A};P]$ to a measurable space $[\mathbb{N};\mathcal{N}]$, where Ω is the probability space, $\mathcal{A}$ is the set of all subsets of the probability space, P is the set of probabilities associated with each subset of $\mathcal{A}$, $\mathbb{N}$ is the family of all sequences of points of $\mathbb{R}^d$ and $\mathcal{N}$ is the algebra on $\mathbb{N}$. As explained in section 1.3 a less formal approach is to consider a point process as a random collection of points located in a given space $\mathbb{R}^d$. It can also be considered as random measures counting the number of points lying in a given spatial region. In this context, one can define a counting measure on the point process as

$$\Phi(B) = n \tag{A.1}$$

where $B \in \mathbb{R}^d$ is a given subset, and n is the number of points of the point process which are found in that subset.

The main characteristics of point processes are presented in the next sections. Throughout the study presented in this thesis these characteristics and parameters have been an intrinsic component of the analysis carried out.

A.1.2 Lebesgue measure

The concept of measure theory plays a particularly important role in the study of point processes. In common terms the measure serve as a way to quantize the characteristics

of sets. In this context, the Lebesgue measure arises as a generalization of the concept of volume into a d dimensional euclidean space. Also commonly referred as the d-dimensional volume, the Lebesgue measure $v_d(B)$ of a given bounded region $B \in \mathbb{R}^d$ corresponds to the volume for $d = 3$, the area for $d = 2$ and the length for $d = 1$ of that region. Formally, the Lebesgue measure on $[\mathbb{R}^d, \mathcal{B}^d]$ is defined as

$$v_d(Q) = (v_1 - u_1) \cdots (v_d - u_d) \tag{A.2}$$
$$\text{for} \quad Q = [v_1 - u_1] \times \cdots \times [v_d - u_d].$$

A.1.3 Intensity and intensity measure of a point process

The intensity $\lambda(\mathbf{x})$ of a point process is defined as the mean number of points per unit volume. In other words, the intensity of a point process determines the density of points found in a bounded region or set $B \in \mathbb{R}^d$. When the density of points is independent with respect to the coordinates, the point process is said to be homogeneous, in which case the intensity takes a constant value, i.e. $\lambda(\mathbf{x}) = \lambda$.

On the other hand, the intensity measure of a point process $\Lambda(B)$ corresponds to the expected number of points found in a given region $B \in \mathbb{R}^d$. It is expressed as

$$\Lambda(B) = \mathbb{E}(\Phi(B)) = \int_B \lambda(\mathbf{x}) d(\mathbf{x}). \tag{A.3}$$

For a homogeneous point process, A.3 transforms into

$$\Lambda(B) = \lambda \int_B d(\mathbf{x}) = \lambda v_d(B). \tag{A.4}$$

A.1.4 DISTRIBUTION OF A POINT PROCESS

An important and basic figure of merit in a point process is its distribution which corresponds to the probability of finding n points of the process in a given bounded region $B \in \mathbb{R}^d$. The distribution of a point process Φ can be expressed as

$$P(\Phi(B) = n). \tag{A.5}$$

Depending on the distribution of the number of points in (A.5), different point process can be defined. For the special case of PPP, the number of points follow a Poisson distribution. Therefore, for a PPP, the distribution is given as

$$P(\Phi(B) = n) = \frac{(\Lambda(B))^n \, e^{-\Lambda(B)}}{n!}. \tag{A.6}$$

A.1.5 VOID PROBABILITY

From the definition of the distribution of a point process, the void probability v_B can be attained. The void probability represents the probability of not having any point of the process in a given bounded region. It is therefore given as

$$\begin{aligned} v_B =& P(\Phi(B) = 0) \\ =& P(\Phi \cap B = \emptyset) \end{aligned} \tag{A.7}$$

From the definition of (A.6), the void probability of a PPP is given as

$$v_B = e^{-\Lambda(B)}. \tag{A.8}$$

A.1.6 CAMPBELL THEOREM

A common application in the theory of point processes is analysing the sum of a given real valued function $f(x)$ applied on all the points contained in a bounded region $B \in \mathbb{R}^d$. Given the fact that the number of points in a point process is a random variable, the sum itself is random depending on the number of points in each realization of the process. The expected value of the random sums in a point process can be obtained via Campbell theorem which states that

$$\mathbb{E}\left(\sum_{x_j \in \Phi} f(x_j)\right) = \int_B f(\mathbf{x}) \Lambda(d\mathbf{x}). \tag{A.9}$$

For a homogeneous point process (A.9) reduces to

$$\mathbb{E}\left(\sum_{x_j \in \Phi} f(x_j)\right) = \lambda \int_B f(\mathbf{x}) d\mathbf{x}. \tag{A.10}$$

A.1.7 GENERATING FUNCTIONAL

An analogy to a random variable probability generating function is the generating functional of a point process. It is defined for a function $f(\mathbf{x})$ applied to the points in the point process as

$$\begin{aligned} G(f) =& \mathbb{E}[f(x_1) f(x_2) \cdots] \\ =& \mathbb{E}\left[\prod_{x_j \in \Phi} f(x_j)\right]. \end{aligned} \tag{A.11}$$

When it comes to a Poisson Point Process (PPP) with intensity measure given as in

(A.4), the generating functional can be shown to be equal to

$$G(f) = \exp\left(-\int (1 - f(\mathbf{x}))\, \Lambda(d\mathbf{x})\right). \tag{A.12}$$

A.1.8 MARKED POINT PROCESS

Marked point processes are those in which a label is attached to each of the points in the process. Then a marked point process Φ can be considered as an ordinary point process in $\mathbb{R}^d \times \mathbb{M}$, where $\mathbb{M}$ constitutes the space or marks.

For a marked point process with marks $L \in \mathbb{M}$ the intensity measure is defined in a similar manner as an ordinary point process as

$$\Lambda(B \times L) = \mathbb{E}[\Phi(B \times L)]. \tag{A.13}$$

For a fixed value of L, the intensity measure transforms into

$$\Lambda(B \times L) = \lambda_L v_d(B). \tag{A.14}$$

A.1.9 THINNING

Thinning is an operation in which some points of a point process are removed according to a given rule $p(x)$. The resulting process is then called a thinned process. The intensity $\Lambda_p(B)$ of the resulting thinned process Φ_p in a given bounded region B is given as

$$\Lambda_p(B) = \int_B p(x)\Lambda(d\mathbf{x}) \tag{A.15}$$

where Λ is the intensity measure of the original point process before the thinning. It is straightforward that for a thinning rule independent of the point location ($p(x) = p$),

the expression in (A.15) transforms into

$$\Lambda_p(B) = p\Lambda(B). \tag{A.16}$$

A.1.10 SLIVNYAK'S THEOREM

It is very common in the study of point processes to obtain the statistics of an arbitrary typical point. The analysis of the properties of this typical point constitutes the Palm distribution theory. Palm probabilities are defined as the conditional probabilities of a given event in the point process given that the typical point is observed at a given location. In the particular case of PPP, Slivnyak's theorem state that the statistics of a typical point of the process do not change by adding a point at the origin o. This is expressed as

$$\mathbb{P}(\Phi \in Y || o) = \mathbb{P}(\Phi \cup \{o\} \in Y) \tag{A.17}$$

where Y is a given property of the point process.

B Appendix of Chapter 2

IN THIS APPENDIX:

The mathematical derivations and proofs of chapter 2 are presented.

B.1 Evaluation of $\mathcal{K}_i\left(s, R_i\right)$ in (2.10)

For the femtocell tier, the Laplace transform, is directly found in [28] as

$$\mathcal{L}_{I_{\Phi_f}}\left(sr_f^{\alpha_0}\right) = \exp\left(-\frac{\rho_f \lambda_f \pi^2 \delta_f}{\sin\left(\pi\delta_f\right)}\left(sr_f^{\alpha_0}\right)^{\delta_f}\right) \tag{B.1}$$

with $\delta_f = \frac{2}{\alpha_f}$. As was stated in the system model, the user is uniformly distributed in the area inside a radius R_f, and so we have

$$\begin{aligned}\mathcal{K}_f\left(s, r_f\right) =& \mathbb{E}_{r_f}\left[\mathcal{L}_{I_{\Phi_f}}\left(sr_f^{\alpha_0}\right)\right] \\ =& \int_0^{R_f} \frac{2r_f}{R_f^2}\, e^{-\frac{\rho_f \lambda_f \pi^2 \delta_f}{\sin\left(\pi\delta_f\right)}\left(sr_f^{\alpha_0}\right)^{\delta_f}}\, dr_f.\end{aligned} \tag{B.2}$$

By using the substitution $u = \frac{\rho_f \lambda_f \pi^2 \delta_f}{\sin\left(\pi\delta_f\right)}\left(sr_f^{\alpha_0}\right)^{\delta_f}$ and the definition of the lower

incomplete Gamma function $\gamma(a,x) = \int_0^x t^{a-1}e^{-t}dt$, we obtain

$$\mathcal{K}_f\left(s, r_f\right) = \frac{\gamma\left(\frac{\alpha_f}{\alpha_0}, R_f^{\frac{2\alpha_0}{\alpha_f}} \frac{\rho_f \lambda_f \pi^2 \delta_f}{\sin\left(\pi\delta_f\right)} s^{\delta_f}\right)}{R_f^2 \frac{\alpha_0}{\alpha_f}\left(\left(\frac{\rho_f \lambda_f \pi^2 \delta_f}{\sin\left(\pi\delta_f\right)}\right)^{\alpha_f} s^2\right)^{1/\alpha_0}}. \tag{B.3}$$

For the macro-cell tier, we have

$$\begin{aligned}
\mathcal{K}_m\left(s, r_m\right) =& \mathbb{E}_{r_m}\left[\mathcal{L}_{I_{\Phi_m}}\left(s r_m^{\alpha_m}\right)\right] \\
=& \mathbb{E}_{r_m}\left[\mathbb{E}_{I_{\Phi_m}}\left[e^{-s r_m^{\alpha_m} I_{\Phi_m}}\right]\right] \\
=& \mathbb{E}_{r_m}\left[\mathbb{E}_{\Phi_m, h_{j,0}}\left[e^{-s r_m^{\alpha_m} \sum\limits_{j \in I_{\Phi_m}} h_{j,0}\, l(r_{j,0})}\right]\right] \\
=& \mathbb{E}_{r_m}\left[\left[\mathbb{E}_{\Phi_m} \prod_{j \in I_{\Phi_m}} \mathbb{E}_h\left[e^{-s r_m^{\alpha_m} h\, (r_{j,0})^{-\alpha_m}}\right]\right]\right] \\
=& \mathbb{E}_{r_m}\left[\left[\mathbb{E}_{\Phi_m}\left[\prod_{j \in I_{\Phi_m}} \frac{1}{1 + s r_m^{\alpha_m}\ (r_{j,0})^{-\alpha_m}}\right]\right]\right].
\end{aligned} \tag{B.4}$$

Using the definition of the generating functional and the substitution $u = \left(\frac{r_{j,0}}{r_m s^{\frac{1}{\alpha_m}}}\right)^2$, the resulting expression can be written as [14]

$$\mathcal{K}_m\left(s, r_m\right) = \mathbb{E}_{r_m}\left[\exp\left(\frac{-\lambda_m \pi r_m^2}{N_S} \underbrace{s^{\delta_m} \int_{s^{-\delta_m}}^{\infty} \frac{du}{1 + u^{\frac{1}{\delta_m}}}}_{\zeta(s, \alpha_m)}\right)\right] \tag{B.5}$$

where $\delta_m = \frac{2}{\alpha_m}$. Now, the binomial negative series expansion is defined as

$$(a+x)^{-n} = \sum_{k=0}^{\infty} (-1)^k \binom{n+k-1}{k} x^k a^{-n-k}. \tag{B.6}$$

Applying the definition in (B.6) to $\zeta(s, \alpha_m)$ in (B.5), with $a = u^{\frac{1}{\delta_m}}$, $x = 1$ and $n = 1$, we obtain

$$\zeta(s, \alpha_m) = s^{\delta_m} \sum_{k=0}^{\infty} \int_{s^{-\delta_m}}^{\infty} (-1)^k \frac{(1)_k}{k!} \, u^{-\frac{(k+1)}{\delta_m}} du \tag{B.7}$$

where $(x)_k = \frac{\Gamma(x+k)}{\Gamma(x)} = x(x+1)...(x+k-1)$, is the Pochhammer symbol [93], and we used the property $(1)_k = k!$. Evaluating the integral in (B.7) we obtain

$$\begin{aligned} \zeta(s, \alpha_m) =& s^{\delta_m} \sum_{k=0}^{\infty} (-1)^k \frac{(1)_k}{k!} \, \frac{s^{k-\delta_m+1}}{\frac{k+1}{\delta_m} - 1} \\ =& s \, \delta_m \sum_{k=0}^{\infty} \frac{(1)_k}{k - \delta_m + 1} \, \frac{(-s)^k}{k!}. \end{aligned} \tag{B.8}$$

By noting that $\frac{(x)_k}{(x+1)_k} = \frac{x}{x+k}$, with $x = 1 - \delta_m$, then (B.8) can be expressed as

$$\zeta(s, \alpha_m) = \frac{s \, \delta_m}{1 - \delta_m} \sum_{k=0}^{\infty} \frac{(1)_k (1 - \delta_m)}{k - \delta_m + 1} \, \frac{(-s)^k}{k!}. \tag{B.9}$$

The summation in (B.9) corresponds to the general expression of the hypergeometric function given by ${}_2F_1(a, b; c; x) = \sum_{k=0}^{\infty} \frac{(a)_k (b)_k}{(c)_k} \, \frac{(x)^k}{k!}$, and so using this expression and substituting (B.9) into (B.5), we obtain

$$\mathcal{K}_m(s, r_m) = \mathbb{E}_{r_m} \left[e^{\frac{-\lambda_m \pi r_m^2 \, s \, \delta_m}{N_S (1 - \delta_m)} \, {}_2F_1(1, 1-\delta_m; 2-\delta_m; -s)} \right]. \tag{B.10}$$

Now, as previously stated, r_m is a random variable following the distribution of the closest neighbour, so obtaining the expected value in (B.10) with respect to the closest

neighbour, yields

$$\begin{aligned}
\mathcal{K}_m\,(s, r_m) &= \mathbb{E}_{r_m}\left[\exp\left(\frac{-\lambda_m \pi r_m^2}{N_S}\,\zeta(s, \alpha_m)\right)\right] \\
&= \int_0^\infty 2\lambda_m \pi r_m \left(e^{-\frac{\lambda_m \pi r_m^2}{N_S}\,\zeta(s,\alpha_m)}\, e^{-\lambda_m \pi r_m^2}\right) dr_m \\
&= \frac{1}{1 + \frac{\zeta(s,\alpha_m)}{N_S}} \\
&= \left(1 + \frac{s\,\delta_m}{N_S(1-\delta_m)}\,{}_2F_1(1, 1-\delta_m; 2-\delta_m; -s)\right)^{-1}. \qquad \text{(B.11)}
\end{aligned}$$

This concludes the evaluation of $\mathcal{K}_i\,(s, R_i)$).

C Appendix of Chapter 3

IN THIS APPENDIX:

The mathematical derivations and proofs of chapter 3 are presented.

C.1 Derivation of $\mathcal{P}^c(\beta, \phi_{tilt})$ in (3.15)

First, we derive two important expressions that will help to express the final value of $\mathcal{P}^c_m$. We take the general expression

$$\int_a^b \frac{y\, dy}{1 + \frac{1}{B}\left(\frac{y}{r}\right)^{\alpha_m}} \tag{C.1}$$

where B can be any function not dependant on y. We proceed to find an alternative expression for (C.1). Similar to the analysis in [14], we make use of the substitution $u = \left(\frac{r_j}{rB^{\frac{1}{\alpha_m}}}\right)^2$, and so

$$\int_a^b \frac{y\, dy}{1 + \frac{1}{B}\left(\frac{y}{r}\right)^{\alpha_m}} = \int_{\left(\frac{a}{rB^{1/\alpha_m}}\right)^2}^{\left(\frac{b}{rB^{\frac{1}{\alpha_m}}}\right)^2} \frac{\left(rB^{\frac{1}{\alpha_m}}\right)^2 du}{1 + u^{\frac{\alpha_m}{2}}}. \tag{C.2}$$

Now, the binomial negative series expansion is defined as

$$\begin{aligned}(c+x)^{-n} =& \sum_{k=0}^{\infty} \binom{-n}{k} x^k c^{-n-k} \\ =& \sum_{k=0}^{\infty} (-1)^k \binom{n+k-1}{k} x^k c^{-n-k}. \end{aligned} \tag{C.3}$$

Applying the definition in (C.3) to (C.2), with $c = u^{\frac{\alpha_m}{2}}$, $x = 1$ and $n = 1$, we obtain

$$\int_a^b \frac{y\, dy}{1 + \frac{1}{B}\left(\frac{y}{r}\right)^{\alpha_m}} = \frac{\left(rB^{\frac{1}{\alpha_m}}\right)^2}{2} \sum_{k=0}^{\infty} \int_{\left(\frac{a}{rB^{1/\alpha_m}}\right)^2}^{\left(\frac{b}{rB^{1/\alpha_m}}\right)^2} (-1)^k \frac{(1)_k}{k!}\, u^{-\frac{\alpha_m(k+1)}{2}} du \tag{C.4}$$

where $(x)_k = \frac{\Gamma(x+k)}{\Gamma(x)} = x(x+1)...(x+k-1)$, is the Pochhammer symbol [93], and we used the property $(1)_k = k!$. Evaluating the integral on the R.H.S. of (C.4) we obtain

$$\begin{aligned}\int_a^b \frac{y\, dy}{1 + \frac{1}{B}\left(\frac{y}{r}\right)^{\alpha_m}} =& \frac{\left(rB^{\frac{1}{\alpha_m}}\right)^2}{2} \left(\sum_{k=0}^{\infty} (-1)^k \frac{(1)_k}{k!} \frac{\left(\frac{a}{rB^{1/\alpha_m}}\right)^{-(1+k)\alpha_m+2}}{\frac{\alpha_m(k+1)}{2} - 1} \right. \\ & \left. - \sum_{k=0}^{\infty} (-1)^k \frac{(1)_k}{k!} - \frac{\left(\frac{b}{rB^{1/\alpha_m}}\right)^{-(1+k)\alpha_m+2}}{\frac{\alpha_m(k+1)}{2} - 1} \right) \\ =& r^{\alpha_m} B \left(a^{2-\alpha_m} \sum_{k=0}^{\infty} (-1)^k \frac{(1)_k}{k!} \frac{\left(\left(\frac{a}{rB^{1/\alpha_m}}\right)^{-\alpha_m}\right)^k}{\alpha_m - 2 + k} \right. \\ & \left. - b^{2-\alpha_m} \sum_{k=0}^{\infty} (-1)^k \frac{(1)_k}{k!} \frac{\left(\left(\frac{a}{rB^{1/\alpha_m}}\right)^{-\alpha_m}\right)^k}{\alpha_m - 2 + k} \right). \end{aligned} \tag{C.5}$$

By noting that $\frac{(x)_k}{(x+1)_k} = \frac{x}{x+k}$, with $x = \alpha_m - 2$, then (C.5) can be expressed as

$$\int_a^b \frac{y\,dy}{1+\frac{1}{B}\left(\frac{y}{r}\right)^{\alpha_m}} = \frac{r^{\alpha_m}B}{\alpha_m-2}\left(a^{2-\alpha_m}\sum_{k=0}^{\infty}\frac{(1)_k}{k!}\,\frac{(\alpha_m-2)\left(-\left(\frac{a}{rB^{1/\alpha_m}}\right)^{-\alpha_m}\right)^k}{\alpha_m-2+k}\right.$$
$$\left.-b^{2-\alpha_m}\sum_{k=0}^{\infty}\frac{(1)_k}{k!}\,\frac{(\alpha_m-2)\left(-\left(\frac{a}{rB^{1/\alpha_m}}\right)^{-\alpha_m}\right)^k}{\alpha_m-2+k}\right). \quad \text{(C.6)}$$

The summations in (C.6) correspond to the general expression of the hypergeometric function given by ${}_2F_1(a,b;c;x) = \sum_{k=0}^{\infty}\frac{(a)_k(b)_k}{(c)_k}\,\frac{(x)^k}{k!}$, and so using this expression we obtain

$$\int_a^b \frac{y\,dy}{1+\frac{1}{B}\left(\frac{y}{r}\right)^{\alpha_m}} = \frac{r^{\alpha_m}B}{\alpha_m-2}\left(a^{2-\alpha_m}\,{}_2F_1\left(1,1-\frac{2}{\alpha_m};2-\frac{2}{\alpha_m};-\left(\frac{a}{r}\right)^{-\alpha_m}B\right)\right.$$
$$\left.-b^{2-\alpha_m}\,{}_2F_1\left(1,1-\frac{2}{\alpha_m};2-\frac{2}{\alpha_m};-\left(\frac{b}{r}\right)^{-\alpha_m}B\right)\right). \quad \text{(C.7)}$$

In the special case in which $b=\infty$, (C.7) reduces to

$$\int_a^{\infty} \frac{y\,dy}{1+\frac{1}{B}\left(\frac{y}{r}\right)^{\alpha_m}} = \frac{r^{\alpha_m}B\,a^{2-\alpha_m}}{\alpha_m-2}\,{}_2F_1\left(1,1-\frac{2}{\alpha_m};2-\frac{2}{\alpha_m};-\left(\frac{a}{r}\right)^{-\alpha_m}B\right). \quad \text{(C.8)}$$

Note that the expressions in (C.7) and (C.8) only hold when B is not a function of y, in which case we cannot find a closed form expression for (C.1). Now, as was stated in Section 2.2, depending upon ϕ_{tilt}, we have two cases of antenna pattern expressions. For $\phi_{tilt} < \sqrt{A_{dB}/12}\,\phi_{3dB}$ we have the sum of two integrals expressed as

$$\mathcal{P}^c(\beta) = \int_0^{r_{th1}} 2\pi\lambda_m \exp\Big(-\lambda_m\pi\Big\{r^2 + \frac{2}{N_s}\left[\int_r^{r_{th1}} \frac{y\,dy}{1+\frac{1}{\beta}\left(\frac{y}{r}\right)^\alpha} + \int_{r_{th1}}^{\infty} \frac{y\,dy}{1+\frac{G^{-1}(y)}{100\,\beta}\left(\frac{y}{r}\right)^\alpha}\right]\Big\}\Big)\,dr + \int_{r_{th1}}^{\infty} 2\pi\lambda_m \exp\Big(-\lambda_m\pi\Big\{r^2 + \frac{2}{N_s}\int_r^{r_{th1}} \frac{y\,dy}{1+\frac{F^{-1}(ri)}{F^{-1}(r)\,\beta}\left(\frac{y}{r}\right)^\alpha}\Big\}\Big)\,dr. \quad \text{(C.9)}$$

And for the case of $\phi_{tilt} \geq \sqrt{A_{dB}/12}\,\phi_{3dB}$, we have 3 integrals expressed as

$$\begin{aligned}\mathcal{P}^c(\beta) = &\int_0^{r_{th1}} 2\pi\lambda_m r \exp\Big(-\lambda_m\pi\Big\{r^2 + \frac{2}{N_s}\left[\int_r^{r_{th1}} \frac{y\,dy}{1+\frac{1}{\beta}\left(\frac{y}{r}\right)^\alpha} + \int_{r_{th1}}^{r_{th2}} \frac{y\,dri}{1+\frac{F^{-1}(y)}{100\,\beta}\left(\frac{y}{r}\right)^\alpha} + \int_{r_{th2}}^{\infty} \frac{y\,dy}{1+\frac{1}{\beta}\left(\frac{y}{r}\right)^\alpha}\right]\Big\}\Big)\,dr \\ &+ \int_{r_{th1}}^{r_{th2}} 2\pi\lambda_m r \exp\Big(-\lambda_m\pi\Big\{r^2 + \frac{2}{N_s}\int_r^{r_{th2}} \frac{y\,dy}{1+\frac{F^{-1}(y)}{F^{-1}(r)\,\beta}\left(\frac{y}{r}\right)^\alpha} + \int_{r_{th2}}^{\infty} \frac{y\,dy}{1+\frac{1}{\beta}\left(\frac{y}{r}\right)^\alpha}\Big\}\Big)\,dr \\ &+ \int_{r_{th2}}^{\infty} 2\pi\lambda_m r\,\exp\left(-\lambda_m\pi\left\{r^2 + \frac{2}{N_s}\int_r^{\infty} \frac{y\,dy}{1+\frac{F^{-1}(y)}{F^{-1}(r)\,\beta}\left(\frac{y}{r}\right)^\alpha}\right\}\right)dr. \quad \text{(C.10)}\end{aligned}$$

Substituting the expressions (C.7) and (C.8) previously found into (C.9) and (C.10), we obtain the results in (3.15), which concludes the proof.

C.2 Proof of $\mathcal{L}_{I^m_{\Phi'_f}}(\eta s)$ in (3.23)

From (3.22), we have

$$\mathcal{L}_{I_{\Phi'_f}}(\eta s) = \exp\left(-\lambda_f\pi\left\{(\eta s)^{\delta_f}\underbrace{E_h\left[h^{\delta_f}\gamma\left(1-\delta_f, \eta s h R_c^{-\alpha_f}\right)\right]}_{\xi} - \frac{R_c^2\eta s}{\eta s + R_c^{\alpha_f}}\right\}\right). \quad \text{(C.11)}$$

By using the definition of the incomplete Gamma function in ξ, we have

$$\xi = \int_0^\infty h^{\delta_f} e^{-h} \int_0^{\eta s h R_c^{-\alpha_f}} e^{-t} t^{-\delta_f} dt\, dh. \tag{C.12}$$

By using the substitution $x = t^{-1}(\eta s h R_c^{-\alpha_f})$, we obtain

$$\begin{aligned}
\xi &= \left(\eta s R_c^{-\alpha_f}\right)^{1-\delta_f} \int_1^\infty x^{\delta_f - 2} \int_0^\infty h\, e^{-h\left(1+\frac{\eta s R_c^{-\alpha_f}}{x}\right)} dh\, dx \\
&= \left(\eta s R_c^{-\alpha_f}\right)^{1-\delta_f} \int_1^\infty \frac{x^{\delta_f - 2}}{\left(1+\frac{\eta s R_c^{-\alpha_f}}{x}\right)^2} dx \\
&= \left(\eta s R_c^{-\alpha_f}\right)^{1-\delta_f} \int_1^\infty \frac{x^{\delta_f}}{\left(x+\eta s R_c^{-\alpha_f}\right)^2} dx.
\end{aligned} \tag{C.13}$$

With the help of Maple, the integral can be evaluated in terms of the hypergeometric function, and so

$$\xi = \left(\eta s R_c^{-\alpha_f}\right)^{-\delta_f} \left(-\frac{1}{\eta s R_c^{-\alpha_f} + 1} + {}_2F_1\left(1, -\delta_f; 1-\delta_f; -\eta s R_c^{-\alpha_f}\right)\right). \tag{C.14}$$

Substituting the value of (C.14) into (C.11), and after some more algebra we obtain

$$\mathcal{L}_{I_{\Phi_f'}}(\eta s) = e^{-\lambda_f \pi R_c^2 \left({}_2F_1\left(1,-\delta_f;1-\delta_f;-\eta s R_c^{-\alpha_f}\right)-1\right)} \tag{C.15}$$

which concludes the evaluation.

References

[1] "Cisco visual networking index: Global mobile data traffic forecast update, 2011-2016," tech. rep., white paper by Cisco, February 2015. (Cited on page 1).

[2] "The zettabyte era-trends and analysis," tech. rep., white paper by Cisco, May 2015. (Cited on page 2).

[3] J. Andrews, S. Buzzi, W. Choi, S. Hanly, A. Lozano, A. Soong, and J. Zhang, "What will 5G be?," *IEEE Journal on Selected Areas in Communications*, vol. 32, pp. 1065–1082, June 2014. (Cited on page 2).

[4] "5G radio access: Requirements, concepts and technologies," tech. rep., white paper by NTT DOCOMO, INC, July 2014. (Cited on page 2).

[5] "Enhance mobile networks to deliver 1,000 times more capacity by 2020," tech. rep., white paper by NOKIA, 2015. (Cited on page 2).

[6] "The 1000x mobile data challenge more small cells, more spectrum, higher efficiency," tech. rep., white paper by Qualcomm, November 2013. (Cited on page 2).

[7] V. Chandrasekhar, J. G. Andrews, and A. Gatherer, "Femtocell networks: a survey," *IEEE Communications Magazine*, vol. 46, pp. 59 – 67, 2008. (Cited on pages 2, 3, 4, 5, 33).

[8] A. Damnjanovi, J. Montojo, Y. Wei, T. Ji, T. Luo, M. Vajapeyam, T. Yoo, O. Song, and D. Malladi, "A survey on 3GPP heterogeneous networks," *IEEE Wireless Communications*, vol. 18, pp. 10 – 21, June 2011. (Cited on pages 2, 10, 24, 64).

[9] C. Meinel and H. Sack, *Internetworking: Technological foundations and applications*. Springer Science & Business Media, 2013. (Cited on page 2).

[10] K. Iniewski, ed., *Internet Networks Wired, Wireless, and Optical Technologies*. 6000 Broken Sound Parkway NW, Suite 300. Boca Raton, FL.: CRC Press, 2010. (Cited on page 4).

[11] "Cisco universal small cell solution: A platform for service innovation," tech. rep., white paper by Cisco, 2015. (Cited on page 4).

[12] Z. Hasan, H. Boostanimehr, and V. K. Bhargava, "Green cellular networks: A survey, some research issues and challenges," *IEEE Communications Surveys and Tutorials*, vol. 13, no. 4, pp. 524 – 540, 2011. (Cited on pages 6, 24, 50).

[13] G. P. Fettweis, K.-C. Chen, and R. Tafazoli, "Green radio: Energy efficiency in wireless networks," *IEEE Journal of Communications and Networks*, vol. 12, pp. 99–102, April 2010. (Cited on page 6).

[14] J. G. Andrews, F. Baccelli, and R. Krishna, "A tractable approach to coverage and rate in cellular networks," *IEEE Transactions on Communications*, vol. 59,

pp. 3122 – 3134, November 2011. (Cited on pages 7, 26, 31, 34, 40, 65, 72, 78, 113, 121, 143, 148, 168, 171).

[15] H. S. Dhillon, R. Krishna, F. Baccelli, and J. G. Andrews, "Modeling and analysis of K-tier downlink heterogeneous cellular networks," *IEEE Journal on Selected Areas in Communications*, vol. 30, pp. 550 – 560, April 2012. (Cited on pages 7, 26, 65, 143).

[16] D. Stoyan, W. S. Kendall, and J. Mecke, *Stochastic Geometry and Its Applications*. WILEY, 2nd ed., 1995. (Cited on pages 9, 26, 77, 79, 84, 122, 125).

[17] M. Haenggi, J. G. Andrews, F. Baccelli, O. Sousse, and M. Franceschetti, "Stochastic geometry and random graphs for the analysis and design of wireless networks," *IEEE Journal on Selected Areas in Communications*, vol. 27, pp. 1029 – 1046, September 2009. (Cited on pages 9, 65).

[18] F. Baccelli and B. Blaszczyszyn, *Stochastic Geometry and Wireless Networks*, vol. 1. NOW, 2009. (Cited on page 9).

[19] M. Haenggi, *Stochastic Geometry for Wireless Networks*. Cambridge University Press, 2012. Cambridge Books Online. (Cited on pages 9, 115).

[20] H. ElSawy, E. Hossain, and M. Haenggi, "Stochastic geometry for modeling, analysis, and design of multi-tier and cognitive cellular wireless networks: A survey," *IEEE Communications Surveys & Tutorials*, vol. 15, no. 3, pp. 996–1019, 2013. (Cited on pages 9, 65).

[21] J. Zhang and G. de la Roche, *Femtocells Technologies and Deployment*. United Kingdom: Wiley, 2010. (Cited on page 10).

[22] J. Boccuzzi and M. Ruggiero, *Femtocells: Design & Application*. McGraw-Hill, 2011. (Cited on page 10).

[23] T. Zahir, K. Arshad, A. Nakata, and K. Moessner, "Interference management in femtocells," *IEEE Communications Surveys and Tutorials*, vol. PP, no. 99, pp. 1 – 19, 2012. (Cited on pages 10, 11).

[24] S. Cui, A. J. Goldsmith, and A. Bahai, "Energy-efficiency of MIMO and cooperative MIMO techniques in sensor networks," *IEEE Journal on Selected Areas in Communications*, vol. 22, pp. 1089 – 1098, August 2004. (Cited on page 24).

[25] D. Feng, G. Lim, L. J. Cimini, G. Feng, and G. Y. Li, "A survey of energy-efficient wireless communications," *IEEE Communications Surveys and Tutorials*, pp. 1 – 12, 2012. (Cited on page 24).

[26] W. C. Cheung, T. Q. S. Quek, and M. Kountouris, "Throughput optimization, spectrum allocation, and access control in two-tier femtocell networks," *IEEE Journal on Selected Areas in Communications*, vol. 30, pp. 561 –574, April 2012. (Cited on pages 25, 26, 65).

[27] T. Nakamura, S. Nagata, A. Benjebbour, Y. Kishiyama, T. Hai, S. Xiaodong, Y. Ning, and L. Nan, "Trends in small cell enhancements in lte advanced," *IEEE Communications Magazine*, vol. 51, no. 2, pp. 98–105, 2013. (Cited on page 25).

[28] F. Baccelli, B. Blaszczyszyn, and P. Muhlethaler, "Stochastic analysis of spatial and opportunistic Aloha," *IEEE Journal on Selected Areas in Communications*, vol. 27, pp. 1105 – 1119, September 2009. (Cited on pages 26, 167).

[29] S. Weber, J. G. Andrews, and N. Jindal, "The effect of fading, channel inversion, and threshold scheduling on ad hoc networks," *IEEE Transactions on Information Theory*, vol. 53, pp. 4127 – 4149, November 2007. (Cited on page 26).

[30] S. A. R. Zaidi, M. Ghogho, D. C. McLernon, and A. Swami, "Energy efficiency in large scale interference limited wireless ad hoc networks," *WCNC Workshop on Future Green Communications*, pp. 24 – 29, April 2012. (Cited on page 26).

[31] V. Chandrasekhar and J. G. Andrews, "Spectrum allocation in tiered networks," *IEEE Transactions on Communications*, vol. 57, pp. 3059 – 3068, October 2009. (Cited on pages 26, 34, 51, 72, 86).

[32] M. Wildemeersch, T. Q. S. Quek, C. H. Slump, and A. Rabbachin, "Cognitive small cell networks: Energy efficiency and trade-offs," *IEEE Transactions on Communications*, 2013. (Cited on page 26).

[33] T. M. Nguyen, Y. Jeong, T. Q. S. Quek, W. P. Tay, and H. Shin, "Interference alignment in a poisson field of MIMO femtocells," *IEEE Transactions on Wireless Communications*, vol. 12, pp. 2633–2645, June 2013. (Cited on pages 26, 28, 72, 108).

[34] T. M. Nguyen, H. Shin, and T. Q. S. Quek, "Network throughput and energy efficiency in mimo femtocells," *European Wireless Conference*, pp. 1 – 5, April 2012. (Cited on page 26).

[35] A. M. Hunter, J. G. Andrews, and S. Weber, "Transmission capacity of ad hoc networks with spatial diversity," *IEEE Transactions on Wireless Communications*, vol. 7, pp. 5058 – 5071, December 2008. (Cited on pages 26, 29, 30, 44).

[36] A. J. Fehske, F. Richter, and G. P. Fettweiss, "Energy efficiency improvements through micro sites in cellular mobile radio networks," *GLOBECOM Workshops*, pp. 1 – 5, November 2009. (Cited on pages 27, 38, 49, 51, 88, 137).

[37] H. Klessig, A. J. Fehske, and G. Fettweis, "Energy efficiency gains in interference-limited heterogeneous cellular mobile radio networks with random micro site deployment," *IEEE Sarnoff Symposium*, pp. 1 – 6, May 2011. (Cited on pages 27, 49, 88).

[38] F. Cao and Z. Fan, "The tradeoff between energy efficiency and system performance of femtocell deployment," *International Symposium on Wireless Communication Systems*, pp. 315 – 319, September 2010. (Cited on page 27).

[39] T. Q. S. Quek, W. C. Cheung, and M. Kountouris, "Energy efficiency analysis of two-tier heterogeneous networks," *Wireless Conference - Suistainable Wireless Technologies*, pp. 1 – 5, April 2011. (Cited on pages 28, 49, 108).

[40] J. Rao and A. O. Fapojuwo, "Energy efficiency of outage constrainted two-tier heterogeneous cellular networks," *IEEE Wireless Communications and Networking Conference (WCNC)*, pp. 146–151, 2013. (Cited on pages 28, 49, 108).

[41] R. Hernandez-Aquino, D. McLernon, M. Ghogho, and S. A. R. Zaidi, "Energy efficiency in MIMO large scale two-tier networks with beamforming and adaptive modulation," in *2013 Proceedings of the 21st European Signal Processing Conference (EUSIPCO)*, pp. 1–5, IEEE, 2013. (Cited on page 29).

[42] F. Héliot, M. A. Imran, and R. Tafazolli, "On the energy efficiency-spectral efficiency trade-off over the mimo rayleigh fading channel," *IEEE Transactions on Communications*, vol. 60, no. 5, pp. 1345–1356, 2012. (Cited on page 29).

[43] S. A. R. Zaidi, M. Ghogho, and D. C. McLernon, "Achievable spatial throughput in multi-antenna cognitive underlay networks with multi-hop relaying," *IEEE Journal on Selected Areas in Communications*, pp. 1 – 16, 2012. (Cited on pages 29, 46, 47).

[44] 3GPP, "TR36.814 v9.0.0.: Further advancements for E-UTRA physical layers aspects (release 9)," technical report, 3GPP, March 2010. (Cited on pages 32, 73, 79).

[45] Z. Chen, C.-X. Wang, X. Hong, J. S. Thompson, S. A. Vorobyov, X. Ge, H. Xiao, and F. Zhao, "Aggregate interference modeling in cognitive radio networks with power and contention control," *IEEE Transactions on Communications*, vol. 60, pp. 456–468, February 2012. (Cited on page 33).

[46] M. Haenggi, "Mean interference in hard-core wireless networks," *IEEE Communications Letters*, vol. 15, pp. 792–794, August 2011. (Cited on pages 33, 86).

[47] E.C.R., "Energy efficiency for network equipment: Two steps beyond greenwashing," tech. rep., Energy Consumption Rating Initiative, August 2008. (Cited on pages 34, 138).

[48] M. Deruyck, D. D. Vulder, W. Joseph, and L. Martens, "Modelling the power consumption in femtocell networks," *WCNC Workshop on Future Green Communications*, pp. 30 – 35, April 2012. (Cited on pages 38, 49, 88).

[49] A. Goldsmith, *Wireless Communications*. 40 West 20th Street, New York: Cambridge University Press, 2005. (Cited on pages 37, 39).

[50] A. J. Grant, "Performance analysis of transmit beamforming," *IEEE Transactions on Communications*, vol. 53, pp. 738 – 744, April 2005. (Cited on page 46).

[51] C. Khatri, "Distribution of the largest or the smallest characteristic root under null hypothesis concerning complex multivariate normal populations," *The Annals of Mathematical Statistics*, vol. 35, no. 4, pp. 1807 – 1810, 1964. (Cited on page 47).

[52] F. Richter, A. J. Fehske, and G. P. Fettweis, "Energy efficiency aspects of base station deployment strategies for cellular networks," *IEEE Vehicular Technology Conference*, pp. 1 – 5, September 2009. (Cited on pages 49, 137).

[53] Y. S. Soh, T. Q. S. Quek, M. Kountouris, and H. Shin, "Energy efficient heterogeneous cellular networks," *IEEE Journal on Selected Areas in Communications*, vol. 31, pp. 840–850, May 2013. (Cited on pages 49, 50).

[54] W. Cheng, H. Zhang, L. Zhao, and Y. Li, "Energy efficient spectrum allocation for green radio in two-tier cellular networks," *Global Telecommunications Conference (GLOBECOM 2010)*, pp. 1 – 5, December 2010. (Cited on page 49).

[55] D. Halperin, B. Greenstein, A. Sheth, and D. Wetherall, "Demystifying 802.11n power consumption," *Proceedings of the 2010 international conference on Power aware computing and systems*, pp. 1 – 5, October 2010. (Cited on page 49).

[56] Y. Li, H. Celebi, M. Daneshmand, C. Wang, and W. Zhao, "Energy-efficient femtocell networks: challenges and opportunities," *IEEE Wireless Communications*, vol. 20, pp. 99–105, December 2013. (Cited on page 50).

[57] O. G. Aliu, A. Imran, M. A. Imran, and B. Evans, "A survey of self organisation in future cellular networks," *IEEE Communications Surveys and Tutorials*, vol. 15, pp. 336–361, First Quarter 2013. (Cited on page 64).

[58] O. Yilmaz, S. Hamalainen, and J. Hamalainen, "Comparison of remote electrical and mechanical antenna downtilt performance for 3GPP lte," in *Vehicular Technology Conference Fall (VTC 2009-Fall), 2009 IEEE 70th*, pp. 1–5, IEEE, 2009. (Cited on pages 64, 66).

[59] "Optimizing small cells and the heterogeneous network (HetNet)," March 2013. (Cited on page 65).

[60] R. W. Heath, M. Kountouris, and T. Bai, "Modeling heterogeneous network interference using poisson point processes," *IEEE Transactions on Signal Processing*, vol. 61, no. 16, pp. 4114–4126, 2013. (Cited on pages 65, 81).

[61] B. Blaszczyszyn, M. Karray, and H. Keeler, "Using Poisson processes to model lattice cellular networks," in *2013 Proceedings IEEE INFOCOM*, pp. 773–781, April 2013. (Cited on page 65).

[62] A. Guo and M. Haenggi, "Spatial stochastic models and metrics for the structure of base stations in cellular networks," *IEEE Transactions on Wireless Communications*, vol. 12, pp. 5800–5812, November 2013. (Cited on page 65).

[63] A. Imran, M. A. Imran, R. Tafazolli, *et al.*, "Distributed spectral efficiency optimization at hotspots through self organisation of bs tilts," in *2011 IEEE GLOBECOM Workshops (GC Wkshps)*, pp. 570–574, IEEE, 2011. (Cited on page 66).

[64] A. Imran, M. A. Imran, A. Abu-Dayya, and R. Tafazolli, "Self organization of tilts in relay enhanced networks: A distributed solution," *IEEE Transactions on Wireless Communications*, vol. 13, no. 2, pp. 764–779, 2014. (Cited on page 67).

[65] W. Guo, S. Wang, Y. Wu, J. Rigelsford, X. Chu, and T. O'Farrell, "Spectral-and energy-efficient antenna tilting in a hetnet using reinforcement learning," in *2013 IEEE Wireless Communications and Networking Conference (WCNC)*, pp. 767–772, IEEE, 2013. (Cited on page 67).

[66] A. Imran, M. Bennis, and L. Giupponi, "Use of learning, game theory and optimization as biomimetic approaches for self-organization in macro-femtocell coexistence," in *2012 IEEE Wireless Communications and Networking Conference Workshops (WCNCW)*, pp. 103–108, IEEE, 2012. (Cited on page 67).

[67] H. Wang and M. C. Reed, "Tractable model for heterogeneous cellular networks with directional antennas," in *2012 Australian Communications Theory Workshop (AusCTW)*, pp. 61–65, IEEE, 2012. (Cited on pages 68, 70).

[68] J. Wildman, P. H. J. Nardelli, M. Latva-aho, and S. Weber, "On the joint impact of beamwidth and orientation error on throughput in wireless directional poisson networks," *CoRR*, vol. abs/1312.6057, 2013. (Cited on pages 68, 70).

[69] T. Bai and R. Heath, "Coverage and rate analysis for millimeter-wave cellular networks," *IEEE Transactions on Wireless Communications*, vol. 14, pp. 1100–1114, Feb 2015. (Cited on pages 68, 70).

[70] M. Di Renzo, "Stochastic geometry modeling and analysis of multi-tier millimeter wave cellular networks," *IEEE Transactions on Wireless Communications*, vol. 14, pp. 5038–5057, Sept 2015. (Cited on page 68).

[71] W. Lu and M. Di Renzo, "Stochastic geometry modeling of cellular networks: Analysis, simulation and experimental validation," *arXiv preprint arXiv:1506.03857*, 2015. (Cited on pages 69, 70).

[72] 3GPP, *Further Advancements for E-UTRA Physical Layers Aspects (Release 9)*. 3GPP, Sophia, Antipolis, France, March 2010. Tech. Rep. TR36.814 V9.0.0. (Cited on page 70).

[73] H.-S. Jo, P. Xia, and J. G. Andrews, "Downlink femtocell networks: Open or closed?," *IEEE International Conference on Communications (ICC)*, pp. 1 – 5, June 2011. (Cited on page 72).

[74] S. Chen, H. Jin, Y. Li, and M. Peng, "Performance analysis of two-tier femtocell networks in Nakagami-m fading channels," in *2013 International Conference on Wireless Communications & Signal Processing (WCSP)*, pp. 1–5, IEEE, 2013. (Cited on page 72).

[75] 3GPP, *Evolved Universal Terrestrial Radio Access (E-UTRA); Further advancements for E-UTRA Physical layer aspects*. 3GPP, Sophia, Antipolis, France, May 2014. Tech. Rep. TR 36.814 V1.7.0. (Cited on page 73).

[76] S.-M. Cheng, W. C. Ao, F.-M. Tseng, and K.-C. Chen, "Design and analysis of downlink spectrum sharing in two-tier cognitive femto networks," *IEEE Transactions on Vehicular Technology*, vol. 61, pp. 2194 – 2207, June 2012. (Cited on page 81).

[77] M. Haenggi and K. Ganti, *Interference in Large Wireless Networks*. NOW, 2009. (Cited on page 83).

[78] Kathrein Inc., "800 10510v01 antenna specifications." (Cited on page 92).

[79] Alliance corporation, "Andrew® tri-band antenna tbxlhb-6565a-vtm specifications," 2015. (Cited on page 92).

[80] 4G Americas, *MIMO and Smart Antennas for Mobile Broadband Systems*. 4G Americas, October 2012. White paper. (Cited on page 92).

[81] CommScope Inc., "Andrew® metrocell antenna specifications," 2015. (Cited on page 92).

[82] V. Olsbo, *Spatial Analysis and Modelling Motivated by Nerve Fiber Patterns*. Chalmers University of Technology, 2008. (Cited on pages 107, 111, 114).

[83] R. Hernandez Aquino, S. Zaidi, D. McLernon, and M. Ghogho, "Energy efficiency analysis of two-tier MIMO diversity schemes in Poisson cellular networks," *IEEE Transactions on Communications*, vol. pp, no. 99, pp. 1–16, 2015. (Cited on page 108).

[84] M. Haenggi, "A versatile dependent model for heterogeneous cellular networks," *arXiv preprint arXiv:1305.0947*, 2013. (Cited on page 109).

[85] H. Wang, X. Zhou, and M. Reed, "Coverage and throughput analysis with a non-uniform small cell deployment," 2014. (Cited on pages 109, 110, 132).

[86] N. Deng, W. Zhou, and M. Haenggi, "A heterogeneous cellular network model with inter-tier dependence,Ť," in *IEEE Global Communications Conference (GLOBECOMŠ14)*, 2014. (Cited on page 110).

[87] M. Haenggi, "On distances in uniformly random networks," *IEEE Transactions on Information Theory*, vol. 51, no. 10, pp. 3584–3586, 2005. (Cited on page 114).

[88] J.-S. Ferenc and Z. Néda, "On the size distribution of poisson voronoi cells," *Physica A: Statistical Mechanics and its Applications*, vol. 385, no. 2, pp. 518–526, 2007. (Cited on page 119).

[89] T. Bai and R. W. Heath, "Location-specific coverage in heterogeneous networks," *IEEE Signal Processing Letters*, vol. 20, no. 9, pp. 873–876, 2013. (Cited on page 122).

[90] S. Singh, H. S. Dhillon, and J. G. Andrews, "Offloading in heterogeneous networks: Modeling, analysis, and design insights," *IEEE Transactions on Wireless Communications*, vol. 12, no. 5, pp. 2484–2497, 2013. (Cited on page 134).

[91] EARTH, "D.2.3 energy efficiency analysis of the reference systems, areas of improvements and target breakdown," January 2012. (Cited on pages 136, 137, 139).

[92] F. Richter, A. J. Fehske, P. Marsch, and G. Fettweis, "Traffic demand and energy efficiency in heterogeneous cellular mobile radio networks," *IEEE Vehicular Technology Conference*, pp. 1 – 6, May 2010. (Cited on page 137).

[93] I. Gradshteyn and I. Ryzhik, *Table of Integrals, Series, and Products*. MA, USA: Elsevier Academic Press, seventh ed., 2007. (Cited on pages 169, 172).